

A study of Tunable Filters Technology in RF/ microwave Engineering

Hassan Jubran Mohammed Alaqil

Submitted for the degree of Doctor of Philosophy

Heriot-Watt University

School of Engineering and Physical Sciences

February 2018

The copyright in this thesis is owned by the author. Any quotation from the thesis or use of any of the information contained in it must acknowledge this thesis as the source of the quotation or information.

Due to increasing demand for wireless communication systems, and because of the stringent requirements of the congested RF-frequency spectrum, reconfigurable/tunable filters have advanced significantly in recent years. Tunable filters can be tuned to different frequency bands constituted a qualitative shift in the field of civil and military communications because of their great potential to minimise the size, complexity, power consumption and cost of traditional filter banks. At the same time, high performance is becoming increasingly important to meet the modern communication systems' specifications.

Against this background, this dissertation provides a study of tunable filters technology in RF/microwave Engineering. In order to accomplish this study, several tunable filters using different tuning approaches have been presented in this dissertation.

A mechanically tuned lowpass filter is presented achieving a good tuning range over the filter's passband. The suspended substrate stripline (SSS) topology has been utilized to obtain a high-quality response while the generalized Chebyshev responses has been applied to obtain flexible transmission zeros in terms of controlling their locations. Tuning was achieved by using a fabricated mechanical structure to tune a set of five SSS resonators synchronously. A systematic numerical design of this type of filters has been offered with full equations' derivations and consequentially manufactured samples are validated experimentally and presented in this work.

A novel design of a narrow tunable bandwidth bandpass filter with two transmission zeros has been developed. In this project, two different structures were combined containing the microstrip structure to simplify the integration with other system parts and the SSS structure to obtain high quality response. Moreover, it introduces two transmission zeros at both sides of the filter's passband without the need of using the conventional cross coupling method. Furthermore, two different tuning approaches have been used, one for tuning the bandwidth and the two transmission zeros while the second one was for fine tuning. An extensive design methodology and a numerical

design example for both, the fixed and tunable filters have been presented and consequentially the proposed design has been proven experimentally.

A new cascaded bandpass filter is presented offering an outstanding response with relatively small number of cascaded elements. This filter utilizes the characteristics of the Step Impedance resonators (SIR) in terms of their flexibility of controlling the spurious response and the insertion loss by changing the ratio of the filter's high to low impedance. In addition, it offers high quality responses by using SSS structures. The filter's design methodology is presented, extensively illustrated with a numerical example and proven experimentally.

A tuning feasibility of the cascaded SSS filter has been introduced where the electrical tuning has been used to tune the lower side of the passband while the upper side is mechanically tuned. The proposed tuning approach has been simulated by using an EM full-wave simulation software and presented whereas the manufacturing was unfortunately postponed due to the end of the research time.

Dedication

To the soul of my mother
To my father and to my family for their great and ever-lasting love and support

Acknowledgements

I would like to express my deep appreciation to my supervisor, Professor Jia-Sheng Hong, for his expert guidance throughout my PhD studies. His contributions, suggestions and insight have been invaluable. Without his kindest help and encouragement, completing my research work would not have been possible.

my special thanks to my country the kingdom of Saudi Arabia which gave me this opportunity and sent me to study in the United Kingdom as an extension of all efforts and great offers provided to the ambitious Saudi youth wishing to participate in the renaissance of the homeland.

I also extend my sincere thanks to the Saudi ministry of defence which gave me the confidence and nominated me for scholarship and to the Saudi cultural bureau in London for all services and help have given to me.

Special thanks go to Dr Ross Aitken, Dr Wenxing Tang, Dr Jia Ni, for all their time and assistance and to my friends, Ibrahim Alotaibi, Khaled and Zhou Zhou for their help and assistance.

I am grateful for the support of my institution, the Department of Electrical, Electronic and Computer Engineering at Heriot-Watt University.

Most importantly, I would like to thank my family, especially my father, family and my brothers and sisters, for giving me their great and everlasting lasting love and support

ACADEMIC REGISTRY
Research Thesis Submission

Name:	Hassan Jubran Mohammed Alaqil		
School:	Engineering and Physical Science		
Version: <i>(i.e. First, Resubmission, Final)</i>	Final	Degree Sought:	PhD in Microwave Engineering

Declaration

In accordance with the appropriate regulations I hereby submit my thesis and I declare that:

- 1) the thesis embodies the results of my own work and has been composed by myself
- 2) where appropriate, I have made acknowledgement of the work of others and have made reference to work carried out in collaboration with other persons
- 3) the thesis is the correct version of the thesis for submission and is the same version as any electronic versions submitted*.
- 4) my thesis for the award referred to, deposited in the Heriot-Watt University Library, should be made available for loan or photocopying and be available via the Institutional Repository, subject to such conditions as the Librarian may require
- 5) I understand that as a student of the University I am required to abide by the Regulations of the University and to conform to its discipline.
- 6) I confirm that the thesis has been verified against plagiarism via an approved plagiarism detection application e.g. Turnitin.

* *Please note that it is the responsibility of the candidate to ensure that the correct version of the thesis is submitted.*

Signature of Candidate:	Hassan Alaqil	Date:	11/05/2018
-------------------------	---------------	-------	------------

Submission

Submitted By <i>(name in capitals)</i> :	HASSAN JUBRAN ALAQIL
Signature of Individual Submitting:	Hassan Alaqil
Date Submitted:	11/05/2018

For Completion in the Student Service Centre (SSC)

Received in the SSC by (<i>name in capitals</i>):	
Method of Submission (<i>Handed in to SSC; posted through internal/external mail</i>):	
E-thesis Submitted (mandatory for final theses)	
Signature:	Date:

Table of Contents

Chapter1

Introduction to tunable microwave filters	1
1.1 Motivation	1
1.2 Tuning technologies of RF/microwave filters	3
1.2.1 Electrical tuning.....	4
1.2.2 Electromechanical tuning.....	6
1.2.3 Mechanical tuning.....	6
1.3 Literature survey on tuning techniques of the substrate dependent shielded microwave filters	8
1.4 Aims and Objective	12
1.5 Organization of the thesis.....	12

Chapter 2

Suspended Substrate Stripline Filters	14
2.1 Introduction to RF/Microwave Filters topologies.....	14
2.2 Suspended Substrate Stripline transmission lines analysis.....	17
2.2.1 Introduction	17
2.2.2 Structure of the Suspended Substrate stripline filters	19
2.2.3 Characteristic impedance of the broadside-coupled SSS.....	25
2.2.4 Characteristic impedance of the edge-coupled SSS.....	29

2.3 Conclusion	36
Chapter 3	
Mechanically Tuned Suspended Substrate Stripline Lowpass Filter	37
3.1 Introduction.....	37
3.2 Suspended substrate stripline Lowpass filter analysis and Synthesis	38
3.3 Generalized Chebyshev lowpass filter design example.....	43
3.3 Tuning analysis and synthesis of the generalized Chebyshev lowpass filter. 47	
3.4 Conclusion:.....	51
Chapter 4	
Tunable combined Microstrip (MS) and Suspended Substrate Stripline (SSS) comblin bandpass filter with two transmission zeros	53
4.1 Introduction	53
4.2 Design methodology of the Four-Pole Combined MS and SSS Comblin filter with two transmission Zeros BP Filter.	54
4.3 The extraction method for the mutual coupling ($M_i, i + 1$) and external quality factor (Q_{en}) of the combined MS and SSS BPF	56
4.3.1 External coupling extraction	58
4.3.2 Mutual coupling extraction.....	61
4.4 Transmission zeros extraction method.....	62
4.5 Design Example of the fixed frequency combined MS and SSS comblin BPF with two transmission zeros.	64
4.6 Results and discussion of the Simulated and measured responses of the fixed frequency combined MS and SSS bandpass filter	74
4.7 Tunable combined MS and SSS filter.....	76
4.7.1 Methodology of the bandwidth tuning	76
4.7.2 Design Example of the narrow bandwidth tunable combined MS and SSS comblin BPF with two transmission zeros.....	80

4.7.3	Measured results and discussion of the fabricated filter	84
4.7.4	Conclusion	88
Chapter 5		
Study of Tunable Cascaded Suspended Stripline Bandpass Filter		89
5.1	Introduction	89
5.2	Designing and implementing of a fixed-frequency cascaded BPF	90
5.2.1	Lowpass filter design	93
5.2.2	The design method for the proposed highpass filter	96
5.2.3	HPF design example.....	102
5.3	Feasibility of tuning the cascaded SSS BPF	109
5.4	Conclusion	116
Chapter 6		
Conclusion and future work		117
6.1	Conclusion	117
6.2	Future work	120
Appendix A.....		121
Appendix B.....		124
References		128

List of Tables

TABLE 1.1 COMPARISON TUNING TECHNOLOGIES OF RF/MICROWAVE FILTERS[2].	7
TABLE 2.1 COMPARISON OF TRANSMISSION LINES' CHARACTERISTICS [51].	19
TABLE 3.2 THE OPTIMIZED DIMENSIONS OF THE FILTER ELEMENTS	45
TABLE 4.2 SIMULATED READINGS OF THE EXTERNAL COUPLINGS	69
TABLE 4.3 THE EXTRACTED DISTANCE OF THE COUPLING COEFFICIENTS AND EXTERNAL COUPLING	70
TABLE 4.4 THE PROCESSED DATA OF THE UPPER AND LOWER TRANSMISSION ZEROS	73
TABLE 4.5 FILTER DISTRIBUTED ELEMENTS' DIMENSIONS IN (MM) [80]	80
TABLE 4.6 FILTER ELEMENTS COUPLING DISTANCES IN (MM) [80]	80
TABLE 4.7 A LIST OF THE USED TUNING VARACTOR DIODES [80]	83
TABLE 4.8 THE TUNABILITY OF THE PROPOSED FILTER VERSUS TUNING ELEMENTS [80]	84
TABLE 4.9 A LIST OF THE USED TUNING VARACTOR DIODES.	86
TABLE 4.10 THE MEASURED TUNABILITY OF THE FILTER.	86
TABLE 5.1 THE DESIGN PARAMETERS OF THE PROPOSED CASCADED BANDPASS FILTER.	92
TABLE 5.2 THE DESIGN PARAMETERS OF THE PROPOSED CASCADED BANDPASS FILTER.	92
TABLE 5.3 PROTOTYPE FILTER ELEMENT VALUES AND THEIR TRANSFORMED VALUES [87]	93
TABLE 5.4 LOWPASS FILTER ELEMENTS' DIMENSIONS (MM)	95
TABLE 5.5 THE CALCULATED CHARACTERISTICS AND DIMENSIONS OF THE SIR.	103
TABLE 5.6 THE OBTAINED PARAMETERS OF THE PARALLEL COUPLED RESONATORS METHOD.	103
TABLE 5.7: THE OPTIMISED PHYSICAL DIMENSIONS OF THE PROPOSED STOPBAND LOWPASS FILTER IN MM	112
TABLE 5.8 A LIST OF THE USED TUNING VARACTOR DIODES [80]	113

List of Figures

FIGURE 1.1 SYSTEM ARCHITECTURE FOR MULTIBAND HSDPA/WEDGE DIVERSITY RADIO SUBSYSTEM [1].....	2
FIGURE 1.2 TUNABLE RF-SYSTEM FRONT END [2].....	2
FIGURE 1.3 VARICAP (A) GENERAL STRUCTURE (A) NARROW DEPLETION REGION AT LOWER BIAS VOLTAGE, HIGH CAPACITANCE (B) WIDE DEPLETION REGION AT HIGH BIAS VOLTAGE, LOWER CAPACITANCE [2].....	4
FIGURE 1.4 PIN DIODE STRUCTURE [9].....	5
FIGURE 2.1 COMMON TYPES OF FILTER STRUCTURES (A) MICROSTRIP (B) STRIPLINE (C) COPLANAR (D) COAXIAL (E) WAVEGUIDE [45].....	16
FIGURE 2.2 THE COMMON PRINTED TRANSMISSION LINES AND THEIR MODIFICATIONS [51].....	18
FIGURE 2.3 SUSPENDED SUBSTRATE STRAPLINE [53].	20
FIGURE 2.4 EFFECT OF THE ENCLOSURE GROOVES ON CHARACTERISTIC IMPEDANCE FOR DIFFERENT SUBSTRATE THICKNESSES AND CONSTANT HEIGHT FOR THE ENCLOSURE (A) 13MM, 0.5 MM (B) 13MM, 3MM.....	21
FIGURE 2.5 EFFECT OF THE ENCLOSURE GROOVES ON THE CHARACTERISTIC IMPEDANCE FOR DIFFERENT ENCLOSURE HEIGHTS AND SUBSTRATE THICKNESSES (A) 20MM, 0.5MM (C) 20MM, 3MM.	22
FIGURE 2.6 THE CALCULATED AND SIMULATED CHARACTERISTIC IMPEDANCE OF A SSS TRANSMISSION LINE	25
FIGURE 2.7 A CROSS-SECTIONAL VIEW OF A BROADSIDE-COUPLED SSSL [46].....	26
FIGURE 2.8 THE CALCULATED AND SIMULATED CHARACTERISTIC IMPEDANCE OF THE SSS BROAD-SIDE COUPLED TRANSMISSION LINES.....	28
FIGURE 2.9 A CROSS-SECTIONAL VIEW OF AN EDGE COUPLED SSSL [59].....	29
FIGURE 2.10 ODD MODE EXCITATION AND EDGE-COUPLED SSS.....	29
FIGURE 2.11 EVEN MODE EXCITATION AND EDGE-COUPLED SSS.....	30
FIGURE 2.12 THE CALCULATED AND SIMULATED CHARACTERISTIC IMPEDANCE OF THE SSS EDGE-COUPLED TRANSMISSION LINES.....	36
FIGURE 3.1 GENERALIZED CHEBYSHEV LOWPASS FILTER [69].....	38
FIGURE 3.2 RICHARD'S TRANSFORMATION LUMPED ELEMENT RESONATOR TO DISTRIBUTED OPEN STUB [70]	39

FIGURE 3.3 STATIC CAPACITANCE OF SINGLE SUSPENDED TRANSMISSION LINE [55].	41
FIGURE 3.4 EQUIVALENT CIRCUIT OF A LENGTH OF TRANSMISSION LINE.	42
FIGURE 3.5 GENERALIZED CHEBYSHEV LOWPASS FILTER CIRCUIT MODEL RESPONSE.	45
FIGURE 3.6 LAYOUT OF THE GENERALIZED CHEBYSHEV LOWPASS FILTER CIRCUIT WITH THE CALCULATED PERIODIC ELEMENTS.....	46
FIGURE 3.7 EM FULL-WAVE SIMULATION RESPONSE OF THE DESIGNED GENERALIZED CHEBYSHEV LOWPASS FILTER [73].....	46
FIGURE 3.8 MEASURED AND SIMULATED RESPONSES OF THE GENERALIZED CHEBYSHEV LOWPASS FILTER.....	47
FIGURE 3.9 EQUIVALENT ELECTRICAL CIRCUIT OF THE PROPOSED TUNING METHOD.....	48
FIGURE 3.10 EQUIVALENT ELECTRICAL CIRCUIT OF THE PROPOSED TUNING METHOD.....	48
FIGURE 3.11 SIMULATED TUNING PERFORMANCE OF THE FILTER (A) S11 (B) S21 [73]	49
FIGURE 3.12 SIMULATED TUNING PERFORMANCE OF THE FILTER (A) S11 (B) S21 [73]	50
FIGURE 3.13 THE MANUFACTURED MECHANICALLY TUNED SSS LOWPASS FILTER (A) SIDE VIEW	51
(B) PROSPECTIVE VIEW	51
FIGURE 4.1 CONVECTIONAL EQUIVALENT CIRCUIT OF (A) COMBLINE FILTER (B) J- INVERTER	54
FIGURE 4.2 THE COMBINED MS AND SSS BPF (A) CIRCUIT MODEL (B) SIMULATED RESPONSE.	56
FIGURE 4.3 COUPLING RELATIONS BETWEEN FILTER'S COMPONENTS	57
FIGURE 4.4 PHASE RESPONSE OF S11 [40].....	59
FIGURE 4.5 GROUP DELAY OF A BANDPASS FILTER.....	60
FIGURE 4.6 TYPICAL RESPONSE OF THE COUPLED RESONATOR [40]	62
FIGURE 4.7 ALUMINIUM ENCLOSURE OF THE FILTER (A) FRONT CROSS SECTION VIEW (B) TOP VIEW (C) RIGHT CROSS SECTION VIEW.....	66
FIGURE 4.8 METHODOLOGY LAYOUT OF THE COUPLING COEFFICIENT EXTRACTION.	68
FIGURE 4.9 EXTERNAL COUPLING EXTRACTION METHODOLOGY LAYOUT.	68

FIGURE 4.10 DESIGN CURVES OF THE FILTER (A) INTERNAL COUPLING COEFFICIENT (B) EXTERNAL COUPLING FACTOR.....	70
FIGURE 4.11 COMBINED SSS AND MS CHEBYSHEV COMBLINE FILTER (A) FILTER CIRCUIT (B) FILTER RESPONSE [77]	71
FIGURE 4.12 COMBINED SSS AND MS CHEBYSHEV INCLUDING THE RESONATORS OF THE TRANSMISSION ZERO [77]	72
FIGURE 4.13 THE PROCESSED DESIGN GRAPHS OF TRANSMISSION ZERO EXTRACTORS.....	73
(A) LOWER TRANSMISSION ZERO GAP (S1) (B) UPPER TRANSMISSION ZERO GAP (S2)	73
FIGURE 4.14 SIMULATED COMBINED SSS AND MS CHEBYSHEV BANDPASS FILTER WITH TWO TRANSMISSION ZEROS.....	74
FIGURE 4.15 SIMULATED AND MEASURED RESPONSES OF THE COMBINED SSS AND MS CHEBYSHEV BANDPASS FILTER WITH TWO TRANSMISSION ZEROS [77]....	75
FIGURE 4.16 USED GROUNDING STRUCTURE	76
FIGURE 4.17 THE COUPLING REDUCER SUBNETWORK AT (A) BANDWIDTH CONTROL SUBNETWORK (B) $Y_{BW} \rightarrow 0$ (C) $Y_{BW} \rightarrow \infty$ [79].....	77
FIGURE 4.18 CIRCUIT MODEL OF THE COMBLINE FILTER WITH COUPLING REDUCER	78
FIGURE 4.19 FINE TUNING SCREWS [80].....	79
FIGURE 4.20 THE TUNABLE DESIGNED FILTER (A) CIRCUIT MODEL (B) SIMULATED RESPONSE	81
FIGURE 4.21 THE LAYOUTS OF THE TUNABLE COMBINED MICROSTRIP AND SSL FILTER (A) TOP LAYER (B) BOTTOM LAYER (C) 3D VIEW INCLUDING TUNING SCREWS. [80].....	82
FIGURE 4.22 SIMULATION RESULT OF THE PROPOSED FILTER AT DIFFERENT VARACTOR VALUES (A) INSERTION LOSS (S21) IN DB (B) RETURN LOSS S11 IN DB [80]	83
FIGURE 4.23 MEASURED RESULT OF THE PROPOSED FILTER AT DIFFERENT VARACTOR VALUES: (A) INSERTION LOSS (S21) IN DB (B) RETURN LOSS S11 IN DB [80].....	85
FIGURE 4.24 FABRICATED PROTOTYPE OF THE FILTER AND BIASING CIRCUIT.....	86
FIGURE 5.1 THE DESIGNED CASCADED BANDPASS FILTER: (A) AWR FILTER LAYOUT (B) AWR SIMULATION OF THE FILTER [87].....	91

FIGURE 5.2 CIRCUIT MODEL OF THE PROPOSED GENERALISED LOWPASS CHEBYSHEV FILTER [87]	93
FIGURE 5.3 LOWPASS FILTER CIRCUIT MODEL RESPONSE [87].....	94
FIGURE 5.4 RICHARD'S TRANSFORMATION OF THE PROPOSED GENERALISED LOWPASS CHEBYSHEV FILTER.....	95
FIGURE 5.5 THE FILTER'S PROPOSED MECHANICAL STRUCTURE.....	96
FIGURE 5.6 GENERALISED LOWPASS FILTER (A) DISTRIBUTED CIRCUIT (B) EM FULL-WAVE SIMULATION OF THE FILTER [87]	96
FIGURE 5.7 THE EQUIVALENT CIRCUIT MODEL OF THE PROPOSED FILTER.....	97
FIGURE 5.8 THE DISTRIBUTED AND LUMPED ELEMENT CIRCUIT OF THE SIR (A) FOR $k > 1$ (B) FOR $k < 1$	98
FIGURE 5.9 THE RESONANCE CONDITION OF THE SIRS	100
FIGURE 5.10 SIR SPURIOUS FREQUENCIES AND TRANSMISSION POLES AGAINST THE IMPEDANCE RATIO (K)	101
FIGURE 5.11 PARALLEL COUPLED LINE AND ITS EQUIVALENT CIRCUIT [2].....	102
FIGURE 5.12 HPF CIRCUIT MODEL RESPONSE	104
FIGURE 5.13 THE PROPOSED MECHANICAL STRUCTURE OF THE FILTER	105
FIGURE 5.14 THE COUPLING IMPEDANCES DESIGN GRAPH	105
FIGURE 5.15 THE DESIGNED HIGHPASS FILTER (A) THE DISTRIBUTED CIRCUIT (B) THE FULL-WAVE EM SIMULATED RESPONSE [87].....	106
FIGURE 5.16 THE FINAL CIRCUIT LAYOUT OF THE CASCADED SSS BPF FILTER [87]	107
FIGURE 5.17 THE DESIGNED CASCADED SSS BPF FILTER (A) THE DISTRIBUTED CIRCUIT (B) THE FULL-WAVE EM SIMULATION [87].....	107
FIGURE 5.18 THE MEASUREMENT OF THE FABRICATED CASCADED BANDPASS FILTER AND ITS EM SIMULATED RESPONSE [87].....	108
FIGURE 5.19 THE MANUFACTURED CASCADED SSS BANDPASS FILTER	108
FIGURE 5.20 THE FULL-WAVE CIRCUIT LAYOUT OF THE TUNABLE CASCADED SSS BANDPASS FILTER.....	110
FIGURE 5.21 THE CIRCUIT MODEL OF THE PROPOSED STOPBAND LOWPASS FILTER	111
FIGURE 5.22 THE CIRCUIT MODEL OF THE PROPOSED STOPBAND LOWPASS FILTER	111
FIGURE 5.23 STOPBAND LOWPASS FILTER BASED ON SIR.....	112

FIGURE 5.24 EM FULL-WAVE SIMULATION OF THE STOPBAND LOWPASS FILTER BASED ON SIR.....	112
FIGURE 5.25 EM FULL-WAVE SIMULATION OF THE INTEGRATED LOWPASS FILTER'S MECHANICAL TUNING (A) RETURN LOSS (B) INSERTION LOSS	114
FIGURE 5.26 EM FULL-WAVE SIMULATION OF THE INTEGRATED HIGHPASS FILTER'S ELECTRONIC TUNING (A) RETURN LOSS (B) INSERTION LOSS.....	115
FIGURE B.1 LUMPED ELEMENTS' RICHARD'S TRANSFORMATION.....	125
FIGURE C1 THE SIR BASIC STRUCTURES (A) $\lambda_g/4$ (B) $\lambda_g/2$ (C) λ_g [92].....	126
FIGURE C2 ADVANCED STRUCTURES OF SIR RESONATORS (A) MULTISTEPPEDED (B) TAPERED [92]	127

List of Publications by the Candidate

A- Conference Papers

- 1- H. Alaqil and J. Hong, "Combined microstrip and suspended substrate stripline combline bandpass filter with two transmission zeros," *Mediterr. Microw. Symp.*
- 2- H. Alaqil and J. Hong, "Mechanical Tuning of Suspended Substrate Stripline Lowpass Filter," in *Proceedings of the Eighth Saudi Students Conference in the UK*, 2016, pp. i–xxiii.

B- Journal Papers

- 3- H. Alaqil and H. Jiasheng, "Tunable Narrow Bandwidth of a Bandpass Filter combined Microstrip and Suspended substrate stripline," *Microw. Opt. Technol. Lett.*, 2017.

C- Submitted Papers

- 4- H. Alaqil and J. Hong, "Cascaded Suspended Stripline Bandpass Filter," *Submitt. to Microw. Opt. Technol. Lett.*, p. 12.

Introduction to tunable microwave filters

1.1 Motivation

Given the continued high demand for modern wireless communication methods, tunable filters attract the interest of scientists around the world as they work towards an optimal use of the limited and consumable frequency band. There are several civilian and military applications for tunable filters, for instance mobile phones, satellite applications and radars. These applications make it more urgent to improve wireless systems' functionality, performance and frequency spectrum elasticity, and to minimise size and reduce production costs. Although designers have made huge progress in the architecture of wireless systems, the challenge of producing more advanced integrated systems requires more research. As an example of one model, the block diagram of the HSDPA/WEDGE multiband diversity radio subsystem is shown in Figure 1.1. The complexity of such a system, comprising a considerable number of active devices as well as the passive components which occupy a wide proportion of the surface area, prevent the required level of integration. Moreover, the use of such conventional filter banks (i.e. cascaded lumped element filters) may represent a weak point in modern communication systems due to their rapid consumption of the limited, valuable frequency spectrum. Moreover, their high-power consumption and the size of their occupied area may limit how portable these systems can be. In contrast, the level of complexity of the fully tunable system depicted in Figure 1.2 has been significantly reduced. The use of tunable devices such as tunable matching networks and tunable filters could play a key role in overcoming the critical disadvantages of conventional communication systems, and may increase their flexibility as well as reducing the cost of materials, which may decline significantly.

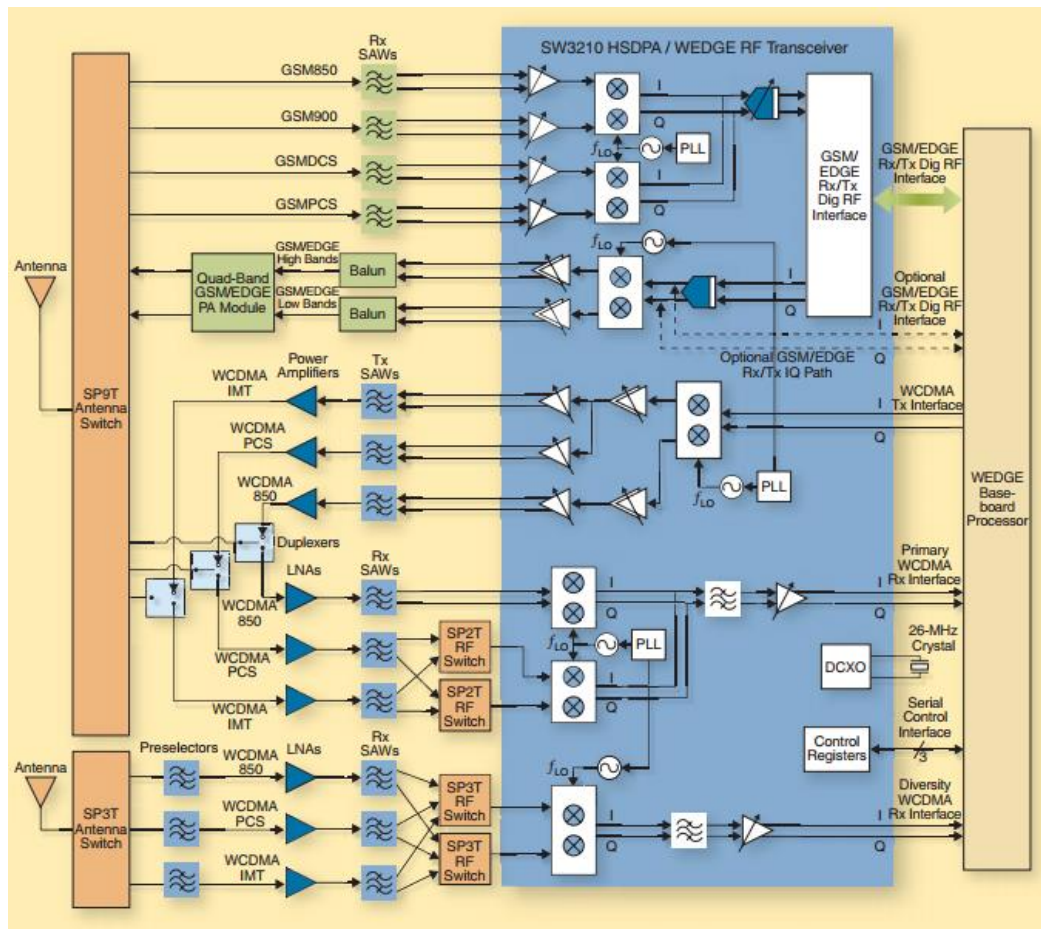


Figure 1.1 System architecture for multiband HSDPA/WEDGE diversity radio subsystem [1]

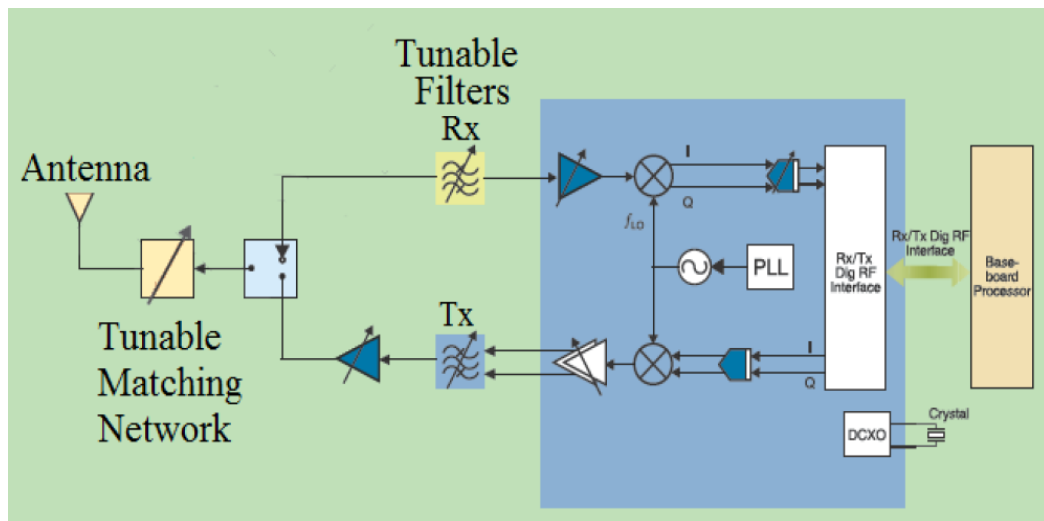


Figure 1.2 Tunable RF-System front end [2]

1.2 Tuning technologies of RF/microwave filters

Tunable filters' design is subject to stringent requirements to fulfil its purpose and to save the limited consumable frequency band. The quality factor and tuning method are two key factors greatly affecting performance. The quality factor is defined as the ratio between the average energy stored in a resonant structure to the energy lost per second, so, it is desirable to keep that ratio as high as possible. Furthermore, it has a strong relationship with the chosen filters' design topology and the tuning method. In other words, the topology used to design the filters has a significant effect on quality factor. For instance, although Microstrip filters are relatively easy to design compared to other topologies, their losses reduce the quality factor compared with other design techniques, such as stripline, suspended substrate microstrip line, suspended substrate stripline and waveguide tunable filters. On the other hand, the tuning process, which can be defined as the operation enabling the filter to pick up the required frequency or frequency band/bands, and which rejects unwanted frequencies, may affect operational quality. Since the filter's working environment is the congested medium, the tuning process is critical to tunable filters' function in separating different signals to prevent interference between different them, or to choose the required working band.

Tuning elements are another issue, in that they may cause an increase in the filter's losses, resulting in a decrease in its performance. Therefore, the tuning method must be chosen very accurately together with the various design factors. The tuning of reconfigurable filters can be classified in two categories, as follows:

- 1- Continuous tuning
- 2- Discrete tuning

These two categories are achieved using various techniques. The methods used for continuous and discrete tuning are classified according to the devices used, in three categories, which are:

- 1- Electrical tuning
- 2- Electromechanical tuning
- 3- Mechanical tuning

The advantages and disadvantages of these tuning methods are explained briefly in the following sections.

1.2.1 Electrical tuning

Electrical tuning is the most common tuning method. The electronic continuous tuning method can be achieved using different types of electronic devices, such as varactors and PIN diodes [3]. There are several types of varactors, for instance, diode varactors [3] and Barium Strontium Titanite (BST) oxide- based varactors [4]. However, the basic principle of all varactors is the same. All varactors are based on a PN junction in the reverse bias, as shown in Figure 1.3 (a). The voltage alteration on either port of the diode will, accordingly, change the width of the varactor diode's depletion region, leading to a change in varactor capacitance [5], as seen in Figures 1.3 (b) and (c).

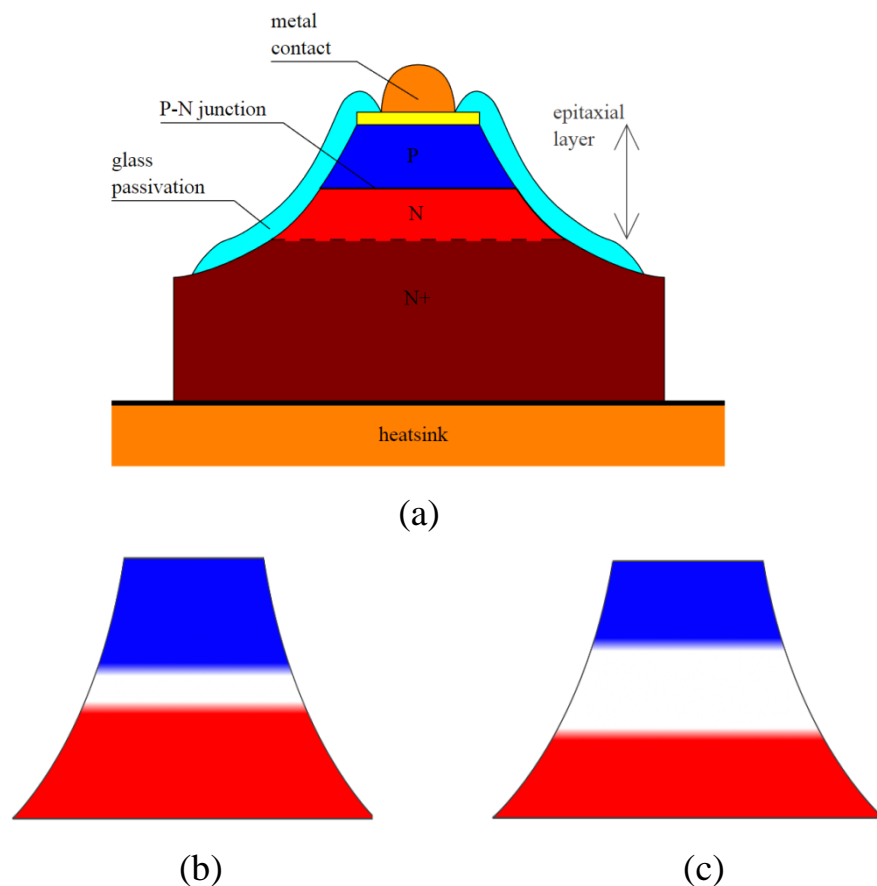


Figure 1.3 Varicap (a) General structure (a) Narrow depletion region at lower bias voltage, high capacitance (b) Wide depletion region at high bias voltage, lower capacitance [2]

Thus, the capacitance of the varactor changes as soon as the applied voltage is varied. Moreover, other materials are frequently used for continuous tuning, for example, ferroelectric and ferromagnetic materials [3] and Piezoelectric Transducers (PETs) [4]. This kind of tuning is the most popular centre frequency tuning technique

because of its limited biasing circuits, compact size and fast tuning time. Despite this, electronic tuning provides high insertion and return losses and low power handling.

λ. Further, varactors have a limited life cycle [4] and [7]. Equally, ferroelectric materials have the disadvantage of a high tangent loss, reducing the resonator's unloaded quality factor [4]. Ferromagnetic materials such as YIG have drawbacks including their biasing circuit complexity, low tuning speed and high power consumption [4]. However, ferroelectric and ferromagnetic materials have some advantages, including high integration, high tuning speeds for ferroelectric materials and a high unloaded quality factor, high power handling and good linearity for ferromagnetic substances [8].

On the other hand, PIN diodes are considered to be continuous tuning elements. The main difference between PIN diodes and varactors is that a PIN diode has three layers, the P and N layers plus an intrinsic layer between them [9], as shown in Figure 1.4. On the forward bias, the level of the charge carriers becomes very high and moves deeply into the intrinsic layer, resulting in a faster movement of charge from P to the N region with help of the electric field [9].

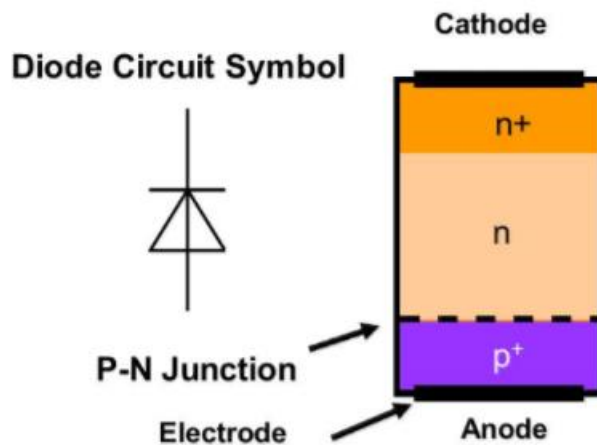


Figure 1.4 PIN Diode structure [9]

PIN diodes have become an attractive tuning method because of their advanced technological improvements [10], which enhance loss level and RF signal distortion compared with varactors as an electronic device. Furthermore, Miller & Alexander [11] argue that PIN diodes are more favourable for wide tuning in applications of a wide and ultra-wide tuning range. Nevertheless, PIN diodes require a high biasing current for good linearity [12].

1.2.2 Electromechanical tuning

Electromechanical Systems (MEMS) are miniature devices comprising microscopic mechanical parts and electronic circuits [13]. There are many applications for MEMS, including sensors and actuators.

The use of RF MEMS is a developing field in the arena of commercial MEMS technology. These devices are used in many communication systems including radars, GPS, filters and steerable Antennae. They can be used for both continuous tuning with MEMS capacitors and as a discrete tuning method with the use of MEMS switches. In fact, MEMS are classified as unique because of their structure. Golio and Golio [14] state that “MEMS are integrated circuit devices that combine both electrical and mechanical components to achieve both frequency selectivity and switching”. This type of tuning has better characteristics compared with other techniques. It has the advantages of very low power consumption, a miniaturized filter, low weight, high power handling in tunable networks and a high quality factor in the range of 50-400 at 2-400 GHz [12]. These characteristics make this tuning technique an excellent solution for designing miniaturised reconfigurable filters.

Another advantage of using RF-MEMS as a tuning method is its usefulness in designing packaged tunable filters. However, the packaging process involves expensive equipment. Furthermore, high switching times compared with PIN diodes, and short life cycles for switching ([7], [15] and [11]) are the major drawbacks of MEMS tuners. Garro and Brito [16] indicate that a mixed tuning tunable filter can be built by consolidating a discrete tuning device such as a diode and continuous tuning devices such as varactors at the same reconfigurable filter.

1.2.3 Mechanical tuning

In contrast with electrical tuning, the mechanical method is a discrete tuning process using several tuning devices such as stepper and piezoelectric motors for precise control of the coupled tuning elements, such as screws. However, Shen, Kawthar and Chi [7] reveal in their study that the tuning range for such metallic screws is very small, so they are more appropriate for fine-tuning. They added that the metallic disks are more effective in achieving a wide tuning range, albeit causing an expected degradation of the unloaded quality factor [7]. This mechanism has various critical

advantages such as a high-quality factor, linearity and the ability to handle high power such as that found in mechanically tuned waveguide filters. In contrast with other tuning methods, mechanical tuning could be used with different filter technologies from planar to waveguide filters. The disadvantages of this method include its bulky size and its tuning speed [7], even though these characteristics may be required in many microwave applications.

Table 1.1 Comparison tuning technologies of RF/Microwave filters[2].

Tuning technology	Mech.	YIG	PIN diode	Vacator diode	BST	RF MEMS
Unload Q	> 1000	> 500	$R_s = 1-4 \Omega$	30-50 ^b	30-50 ^b	50-400
Tuning speed	>10 μ s	ns	ns	ns	ns	μ s
Bias	>100 V	N/A	10-40mA	< 30V	< 30V	20-100V
Linearity (IIP3: dBm)	high	< 30	> 33	10-35	10-35	> 60
Power handling	high	2W	~mW	~mW	~mW	1-2 W
Power consumption	high	high	medium	low	negligible	negligible
Size	large	large	small	small	small	small
Cost	high	high	low	low	low	medium
Integration	difficult	difficult	good	good	good	good

Table 1.1 shows a comparison between different tuning technologies. An obvious variation can be noticed in their parameters, so that none of them is perfect [2] and choosing based on the application and the specification of the system.

1.3 Literature survey on tuning techniques of the substrate dependent shielded microwave filters

In this survey, the shielded tunable planar microwave filters are highlighted according to the used tuning technology and design method. In general, the aim of the tuning process is to tune the resonant frequency or control the filter's passband. Moreover, a higher selectivity could be achieved by controlling the locations of the transmission zeros. There are several shielded tunable planar filters which have been designed and implemented over the past few years. But despite these filters' remarkable performance, to the best of my knowledge, there is a lack of tuning works for this category of planar filters. This might be due to these filters' substantial size, and the difficulty of achieving an adequate grounding level. However, different tuning techniques have been applied to these filters, for instance, the works in [17]–[21] are tuned mechanically. On the other hand, other works have investigated the electrical tuning of shielded structures by continuous tuning methods using varactors, as presented in [22]–[29], or used a discrete tuning approach by exploiting MEMS and PIN diodes, such as in [15], [30]–[34].

In [17], Saeedi et al. used piezoelectric actuators to tune a high quality factor Evanescent-Mode cavity filter. This comprised cascaded Bandpass and Bandstop (BP-BS) filters integrated on a single layer substrate. The tuning technique controls the bandwidth of the filter as well as synchronous and asynchronous controlling of the transmission zeros at both sides of the passband [17]. The measured loss was as low as 0.9 dB with a tuning range of 600 MHz. The cascaded structure's spurious response was eliminated by adding extra resonators to BSF to control the phase relationship between the filters [17]. Similarly, according to Fermin et al. [17] and [21], a substrate integrated wave guide (SIW) resonator and a (SIW) based oscillator, were tuned by using the same concept of an electromagnetic perturbation method adopting a different approach. The method involves introducing a metallised via on the cavity of the waveguide and slightly deviated from the centre of the substrate. Additionally, an open-loop slot at the top of the metallic layer surrounds the via hole. As well as that, the inclusion of a metal contact to connect the via to the surrounding open loop slot provides electromagnetic field distribution, and moves the resonance frequency between the two positions of the contact at $\Phi=0^\circ$ and $\Phi=180^\circ$. The tuning range and

the quality factor change according to the position and orientation of that slot. The resonant frequency of the measured resonator is changed from 6.85 GHz to 7.42 GHz, and from 12.1 GHz to 12.4 GHz, with tuning ranges of 8% and 2.5% respectively. The unloaded quality factor varied from 94-100 for both experiments. Furthermore, the authors used the previous principle of tuning to design and fabricate a SIW tunable bandpass filter [20]. They implemented three different designs of tunable four-pole Chebyshev filters, with the functions of trimming, frequency tuning and bandwidth tuning. The responses achieved showed excellent trimming, resonance frequency tuning of 10% and 100% of passband tuning, respectively[20]. Another approach of the mechanical tuning is presented by Kurudere and Erturk [19], who applied the mechanical tuning technique to a planar-printed circuited bandpass filter. In this filter, the conventional rod tuning screws were replaced by a combination of a printed circuit and tuning screws [19]. Furthermore, a microstrip feeding was used instead of a conventional rod-type combined filter. The tuning screws of this filter perform two functions simultaneously, they are used as a tuning screw through the movable part and as a resonating rod via the stable section. However, both sections could be considered as a tuning rod of variable length. The tuning process involves moving the movable parts vertically above the opposite printed microstrip structure. This produces a variable capacitor between the tip of the rod and the printed circuit, which in turn leads to the retuning the resonance frequency of the filter's response. The measured tuning response showed a tuning range of 10% of the centre frequency, with a constant bandwidth and a minimum return loss of 10 dB.

For electrical tuning of the substrate-dependent shielded filters, several topologies of the microwave filters were tuned electrically and extensively investigated by a number of researchers. In terms of discrete electrical tuning, El-Tanani and Rebeiz proposed RF-MEMS tuned resonant frequency wideband and narrow band bandpass filters with constant bandwidths [15]. These filters comprise two symmetrical sections of coupled-pair transmission lines, which in turn are linked using interdigital coupling. The authors claimed that the high quality factor obtained, and the analogue and digital tuning capabilities, were provided by fabricating the RF MEMS tuning network on the same substrate [15]. Moreover, the importance of the availability of this agile tuning technique lies in its ability to provide equal loading capacitance for all resonators,

particularly in narrowband filters. The tuning range of the filter was from 1.5 to 1.5 GHz with a respective insertion loss of 1.9 to 2.2 dB. Similarly, Schulte et al. [33], used similar tuning device, i.e. RF-MEMS switches. In this work, an LTCC technology was used to fabricate a two Evanescent Mode Cavity filters which employ a capacitive and inductive coupling methods for the RF-MEMS tuning elements. The measured tuning responses were 4% and 6% respectively. In [33] and [34], the authors used RF-MEMS tuning elements to tune two different filters' topologies, designed and implemented on a suspended substrate stripline structure (SSS). In [32], Reines et al. propose a three-pole, centre frequency tunable SSS combline filter. The tuning range of this filter is between 1.6 and 2.4 GHz with a measured unloaded quality factor (Q_u) range, insertion loss and 3-dB bandwidth equivalent to 50-150, 1.34-3.03 dB and 201-279 MHz respectively. However, it can be seen from the filter's response that the design needs more effort regarding the transmission zero's tunability to increase overall selectivity. In [31], the centre frequency and bandwidth of a two-pole filter were tuned using an RF-MEMS capacitive tuning network. The proposed filter comprised $\lambda/2$ suspended-substrate stripline ring resonators, therefore the ground connection was not required. The measured centre frequency tuning range was 3.7-5.95 GHz, while the bandwidth is tuned at any frequency from 90 to 515MHz. As with the previous research [32], this work suffers from a low selectivity at the upper stopband edge. As well as MEMS, PIN diodes are considered to be discrete tuning elements, as mentioned above. In [31] and [35], a PIN diode switching element is used to tune the centre frequency and the bandwidth of two different designs of a Substrate Integrated Waveguide (SIW) filter. In [34], a bandpass filter is tuned digitally using a three-bit capacitive switchable loading PIN diode tuning network. The tuning process of this filter produced eight almost equally spaced frequency-tuned responses from 4.03-4.36 GHz. Another work focusing on the frequency and bandwidth SIW PIN diode tuned filter is presented in [30]. The tuning approach to the proposed SIW cavities relies on the connecting/disconnecting the perturbing VIA posts to or from the cavity's top metal layer. This tuning method resulted in six states within the tuning range of 25%, i.e. from 1.55 – 2 GHz, whereas the ranges of the fractional bandwidth are between 2.3% and 3%.

On the other hand, several researches investigated the electrical continuous tuning of the shielded substrate-dependent microwave filters. In [27]–[29], three suspended substrate stripline filters were tuned using varactors. Zahirovic et al. [29] propose a two-pole tunable filter, the centre frequency of the filter was tuned by varying the electrical length of the resonators. Alternatively, in [28], Renedo et al. discussed a tunable bandpass filter in which the centre frequency and bandwidth were changed continuously. The main contribution of that work is the use of tunable coupling reducers between resonators to control the filter's bandwidth. Furthermore, S. Kumar [27] a tunable filter which was realised as a suspended substrate stripline filter. The tuning method depends on two coupled ring resonators, tuned by using GaAs Varactor.

Other works discussed the use of varactor tuning devices with SIW. In, [22],[23]–[25] the authors presented a tunable SIW filter exploiting a continuous tuning method. In [22], a SIW bandstop resonator was tuned using a varactor tuning device and an open-end stub to electrically create a short-circuit condition on both sides of the cavity. The combination of the varactor and the stub are fed initially by the cavity. But when the electrical length of the open-end stub equals $\lambda/4$, the short-circuit occurs, leading to the SIW cavity closure [22]. In another work [23]. The authors designed and fabricated a SIW tunable combline filter. This filter comprised two capacitively loaded posts, each one surrounded by two ring gaps at the cavity top wall. Tuning was done using surface-mounted varactors, which change those gaps [23]. The tuning range of the proposed filter is from 0.56 to 1.18 GHz, or the equivalent of an octave of the frequency band. Similarly, Akash Anand and Xiaoguang Liu [24] proposed a two-pole SIW filter. The composition of the proposed filter is very similar to that put forward in [23], except for the parts of the feeding lines designed at both sides of the cavity's top part as coplanar waveguides to provide the external coupling. This similarity extends to the technique of connecting the tuning elements which are put on the gaps of the rings over the capacitively loaded cavity resonators. Consequently, the tuning process of the centre frequency used the same method as [23]. The cavity resonators are coupled through two different paths, both of which have different coupling levels. Bandwidth tuning is achieved using a varactor element along the weak coupling path to change the coupling coefficient between the two cavity resonators. This tuning

method is similar to the previous work presented in [23], in which Chen et al. [25] presented a tunable dual-band SIW filter. This filter comprises two capacitive loading resonators. The resonant frequencies of these bands are tuned independently by controlling the external and internal couplings of the capacitive loadings of the evanescent-mode cavity resonators.

1.4 Aims and Objective

Following the motivation and literature survey presented above, the main aim of this thesis is to develop new filter technology in terms of design, tuning methods, concepts and configuration.

The filter is constructed around the following objectives:

- 1- To develop a tunable generalized Chebyshev lowpass suspended substrate filter, mechanically tuned method is to be used to achieve the objective.
- 2- To develop a combine bandpass filter. This filter combines two different structures those are microstrip and SSS. The objectives of this structure are to facilitate the integration of the filter through the microstrip section, introduce a high-quality bandpass filter through the SSS combine structure and to introduce a new method of generating the transmission zeros rather than the conventional cross-coupling method.
- 3- To develop a tunable combined bandpass filter of high-quality response and flexible transmission zeros allocating.
- 4- To develop a new cascaded bandpass filter of high selectivity.
- 5- To study the visibility of tuning the designed cascaded bandpass filter.

1.5 Organization of the thesis

This project is divided into six chapters:

1- Chapter 2: This chapter presents a detailed overview of the suspended-substrate stripline structure (SSS), including analysis and synthesis equations of the suspended stripline, broadside coupled SSS and edge-coupled SSS. It also includes a theoretical analysis of the effect of the enclosure grooves on the characteristic impedance for different enclosure heights and substrate thicknesses. The study was

completed using full electromagnetic (EM) simulation software, namely SONNET ® [36].

2- Chapter 3: This chapter is divided into two parts. The first section addresses in detail the full design procedures for the generalised Chebyshev low-pass filter using a (SSS) structure. A circuit model and complete analysis and synthesis equations for the proposed filter are presented. A detailed design example with distributed circuit realisation and full-wave simulation are also offered. Finally, the measured implemented filter is shown with an excellent agreement between the measurements and simulated results.

The second phase of this chapter focuses on the tuning technique for the proposed filter. Firstly, the filter was mechanically tuned and simulated using full EM simulation software, and the simulated results are given. Next, a suggested geometric diagram for the structure of the tuning screws is presented. Finally, the measurements of the fabricated and mechanically tuned lowpass filter were carried out, and are also discussed.

3- Chapter 4: introduces a novel structure of a combined bandpass filter. it is divided into seven sections, first one is an introduction followed by the second section which presents the design methodology of the proposed filter including circuit model, the simulated result of the circuit model is provided. Third section introduces the extraction method of the external quality factor and mutual couplings. Fourth section presents a numerical example including Full-wave EM simulation and the measured of the implemented filter.

4- Chapter 5: in this chapter a tunable cascaded bandpass filter has been presented in three sections, the first one is for introduction. The second section is customized to explain the designing procedures of the fixed frequency cascaded bandpass filter including a detailed explanation of the design process of its constituent filters, those filters are generalised Chebyshev lowpass filter and step impedance resonator highpass filters. The third section is for presenting the tuning process of the filter with different simulated and measured responses.

5- Chapter 6: presents the conclusion of the thesis and future work.

Suspended Substrate Stripline Filters

2.1 Introduction to RF/Microwave Filters topologies

RF/Microwave filter design utilizes several technological methods which are able to design a resonator due to the fact that these filters are predominantly implemented on the basis of the coupled resonators. These methods have several advantages such as light weight and small size and low power consumption. On the other hand, their disadvantages are related to many factors, for instance, the high sensitivity to external boundaries and low power handling, depending on the circuit elements and the structure of the filter.

The Lumped Elements Filters topology is the simplest form of filters because it depends on a parallel combination of inductors and capacitors known as an LC tank resonator circuit. These are mainly used in low frequencies applications. The main disadvantage of such filters is their high loss, which can lead to weak performance because of the resonators' low quality, and their frequency band limitations, not to mention their low immunity to internal, external, thermal and electromagnetic noises. However, Lumped Elements Filters have several advantages including their compact size, wide tuning bandwidth and low cost.

Alternatively, Planar Filters, also known as distributed element filters, are considered the mainstay of the new RF/Microwave filters. They are based on the planar transmission line on a dielectric substrate with a ground plane [37] [38]. Several structures have been investigated to create planar filters, including Microstrip, Coplanar Waveguide (CPW), Stripline and Suspended Substrate stripline (SSS) filters [39] [38]. Furthermore, numerous topologies have been created to obtain different responses from planar filters including Compline bandpass filters, Quasi- lumped Elements low-pass filters, interdigital bandpass filters, Hairpin Line Bandpass Filters [40] and various types of planar filters. As with the lumped elements filters, the planar filters' power handling capacity is low. However, in contrast to the lumped elements technology, planar filters' performance is generally better due to their relatively high-quality factor, low power consumption and wide frequency band.

Several factors may affect planar filters' performance, including manufacturing technique and dielectric substrate. It has been found, for example, that the Suspended Substrate stripline filters' quality factor is much higher than that of the Microstrip filters [41]. However, the dielectric substrate's high dielectric loss tangent is a significant factor, causing high power loss. Similarly, the resistivity of transmission lines plays a key role in the filter's performance [38].

Coaxial filters are another RF/Microwave filter technology. These kinds of non-dispersive, transverse electromagnetic (TEM) modes' filters are generally used in high-performance applications, because the coaxial transmission line's quality factor is higher than that of the planar transmission lines. Their structures can be described in two ways: as wave guidance since there are two concentric conductors with a guided wave between them, or as a transmission line when the conductors' currents and their nested voltage are highlighted [38].

Waveguide filters are another type of bulky filter structure. They're designed with a rectangular or circular metal cavity to confine and direct the signal to a specific path and couple the resonators to pass the required frequency band while rejecting others. In contrast to the planar filters, they're generally used for higher-frequency bands since they can handle high power with considerable low return and insertion losses. However, the cost of producing them and their bulky body are major disadvantages for these filters' technology. Additionally, planar technology can also be used to design coaxial and waveguide filters [42] and [43].

There are other technologies, such as Cavity, Dielectric and Electroacoustic filters. These filters' methods have high quality factors and reasonable selectivity. Acoustic and cavity filters have the advantage of a small size, but the size of the dielectric filters can also be minimised by increasing their dielectric constant. Lay's study of the phase and group delay of S-band reveals that cavity filters have the further advantage of significant selectivity even under high power loads [44]. Figure 2 depicts some common types of filters.

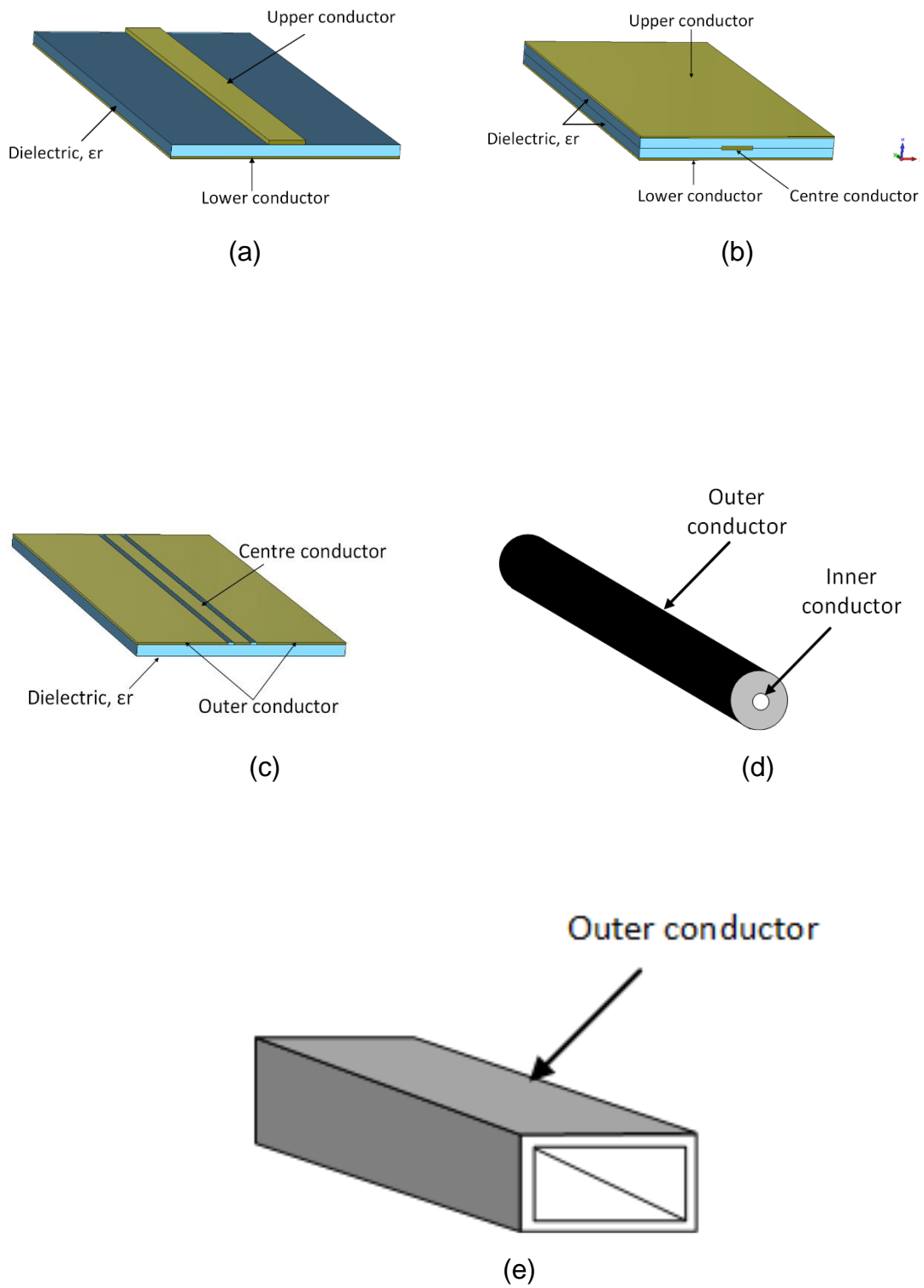


Figure 2.1 Common types of filter structures (a) Microstrip (b) Stripline (c) Coplanar (d) Coaxial (e) Waveguide [45]

Bearing in mind the previous brief presentation of microwave topologies, it was essential to develop a new way of designing such filters which combined the different topologies' distinctive features.

The Suspended Substrate Stripline (SSS) is one of the transmission lines that has been developed, and it's used in the modern filter design. This type of transmission line has several advantages such as large tolerance of fabrication, lower attenuation [46] and the immunity against the external influences. These advantages make SSS an excellent choice for researchers and developers of microwave filters, leading to several methods and mathematical formulae for the design and manufacture of the suspended substrate stripline (SSS).

2.2 Suspended Substrate Stripline transmission lines analysis

2.2.1 Introduction

The importance of microwave technology has grown, and it became one of the major applications in modern electronic and communications engineering.

The high demand for this technology made it more important to study the transmission medium for transporting the wave between clients to ensure a rapid, efficient exchange of information. To achieve this aim, many microwave transmission media have been studied and analysed to address various aspects which may affect their performance.

Many types of printed transmission lines have been developed and applied in different microwave systems. The structures of the most commonly printed transmission lines and their related modifications are shown in Figure 2.2. These transmission lines have different standards of performance and manufacturing, as described in Table 2.1.

A suspended substrate stripline transmission line is an important transmission medium which has many benefits such as low transmission loss, as well as the larger fabrication tolerance compared with the microstrip line. Many formulae have been developed to calculate the transmission line parameters. Some of these approaches are very complicated and need sophisticated mathematical derivation, for instance [47] and [48], whereas others are suitable for the suspended microstrip line in which the enclosure remains open, meaning there is no cover or side walls, as in [49]. Given this persistent need to develop new approximations for such lines, several

mathematical approaches appropriate for the SSS have been presented, for example in [50], and [46]. In this section, a detailed numerical analysis of the SSS transmission line is presented. It includes the mathematical formulae for the characteristic impedance, effective dielectric constant and coupled lines' parameters.

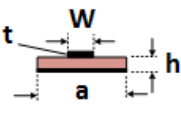
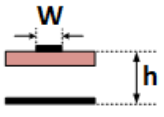
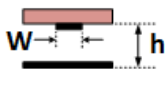
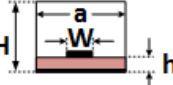
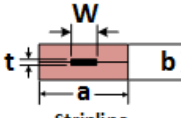

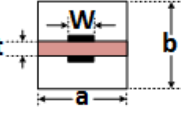
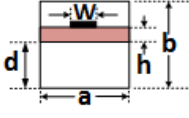
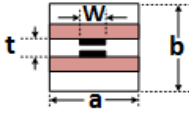
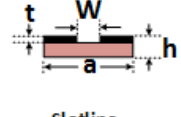
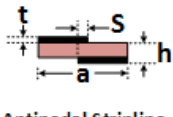
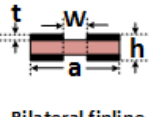
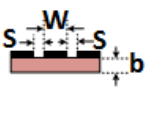
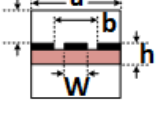
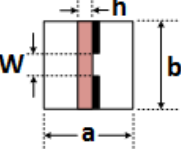
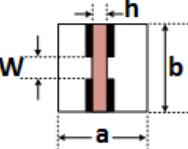
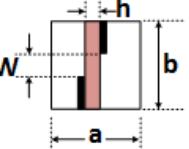
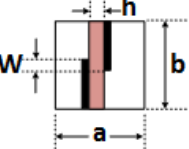
	Basic Lines	Modifications		
Microstrip line	 Microstrip line	 Suspended MS Line	 Inverted MS line	 Shielded MS line
Stripline	 Stripline	 Double conductor stripline		
Suspended Stripline	 Suspended HQ SL	 Shielded Suspended SL	 Shielded suspended Double Substrate SL	
Slotline	 Slotline	 Antipodal Stripline	 Bilateral finline	
Coplanar waveguide	 Symmetrical coplanar line	 Shielded coplanar waveguide		
Finline	 Finline	 Bilateral slotline	 Antipodal finline	 Antipodal overlapping finline

Figure 2.2 The common printed transmission lines and their modifications [51]

Table 2.1 Comparison of transmission lines' characteristics [51].

Transmission line	Q-factor	Radiation	Dispersion	Impedance range	Clip mounting
Microstrip (dielectric) (GaAs, Si)	250	Low High	Low	20 to 200	Difficult for shunt, easy for series
Stripline	400	Low	None	35 to 250	Poor
Suspended Stripline	500	Low	None	40 to 150	Fair
Slotline	100	Medium	High	60 to 200	Easy for shunt, difficult for series
Coplanar Waveguide	150	Medium	Low	20 to 250	Easy for series and shunt
Finline	500	None	Low	10 to 400	Fair

2.2.2 Structure of the Suspended Substrate stripline filters

Suspended substrate stripline (SSS) is a structure in which a transmission line is etched out of a dielectric substrate and the whole structure is suspended inside a metallic box so the circuit exists between two air layers, as shown below in Figure 2.3. The SSS has many advantages, including lower passband loss, a high quality factor, lower spurious radiation, more temperature stability and lower manufacturing tolerance [52].

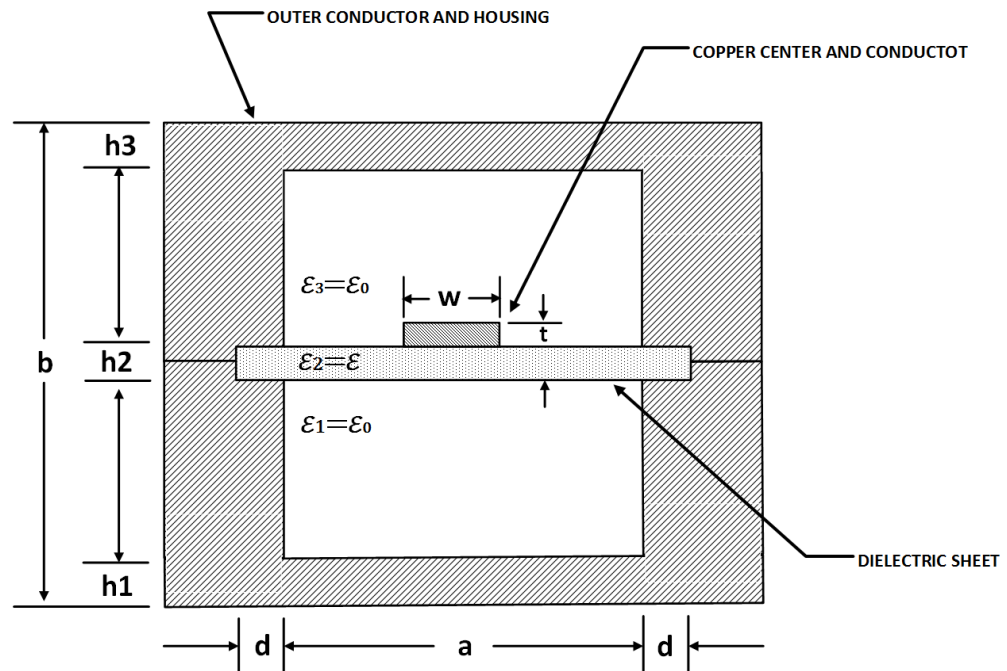


Figure 2.3 Suspended Substrate Stripline [53].

According to this structure, a few of the electric and magnetic fields extend to the dielectric substrate, whereas the majority encounter the surrounding air. This feature in addition to the used thin substrate of a small dielectric constant, will lead to a low passband loss [52] and a high unloaded quality factor that is almost equal to an air dielectric substrate stripline [54]. Moreover, the existence of the circuit in a closed conductive housing forms a TEM propagation mode and low dispersion [52]. However, both TE and TM modes can be excited in the box structure[55]. Furthermore, it has been revealed that this structure makes the SSS less dependent on the temperature variation of the dielectric substrate [56] compared with microstrip and stripline structures. This decrease occurred because the design's resonant sections are suspended and surrounded by air, which mitigates the effect of temperature variance. As well as the aforementioned advantages, the SSS has less sensitivity to manufacturing's tolerance due to relatively large elements sizes compared to conventional structures of microwave filters such as microstrip and stripline. Crucially, the mechanical design of the metallic box has a significant effect on the circuit's performance, for example, spurious TE and TM modes excited in the box can affect the filters stopband performance negatively. It has been found that the side walls of the enclosure and the grooves which are used to support the substrate mechanically as shown in Figure 2.3, affect characteristic impedance and the

wavelength's reduction factor to some extent. According to [53], the authors carried out a numerical analysis of a transmission line with sidewall grooves and a TEM mode approximation. They found that the characteristic impedance (Z_o) and the wavelength reduction factor (λ/λ_o) are increased rapidly as the depth of the grooves increased to a certain depth, afterwards, they become steady without change. They also found that this steadiness was because the groove's effect is significant at small ranges of their depth d . Furthermore, they stated that these effects could be avoided by minimising the height of the sidewalls. To prove the effect of the enclosure grooves on the characteristic impedance of the transmission line, a single SSS transmission line was simulated. The testing enclosure had a height of 13mm, while the length and width were 100mm and 30mm, respectively. The experiment was performed at different frequencies for different groove's depth and enclosure's height of equals 13mm. Two substrates were used for this experiment, both of them were Roger's substrate 3003 [57], see Appendix A, with a dielectric constant of 3, but with different thickness of 0.5mm and 3mm. The simulated result is for d/b against characteristic impedance, where d is the groove depth and b is the internal height of the enclosure. Figure 2.4 (a) and (b), shows that the variation in characteristic impedance is more obvious for the substrate of 0.5mm thickness, this oscillation could be decreased by increasing either the groove's depth or thickness of the dielectric substrate or both of them at the same height of the enclosure.

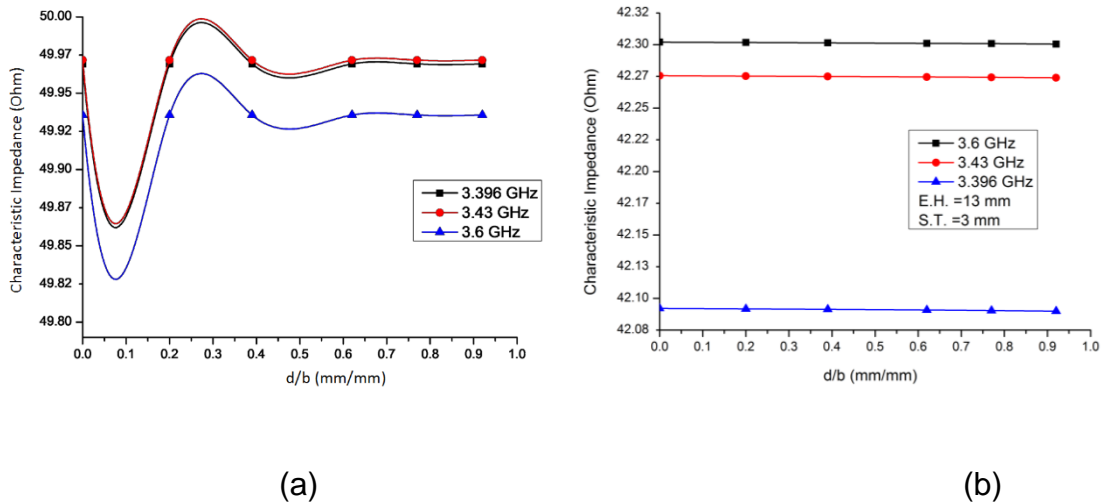


Figure 2.4 Effect of the enclosure grooves on characteristic impedance for different substrate thicknesses and constant height for the enclosure (a) 13mm, 0.5 mm (b) 13mm, 3mm

However, the enclosure's height increase would decrease significantly the variation of the characteristic impedance regardless of the depth of the groove or the substrate thickness as shown in Figure 2.5 (a) and (b). Here, the same substrates have been used with an enclosure has a height of 20mm,

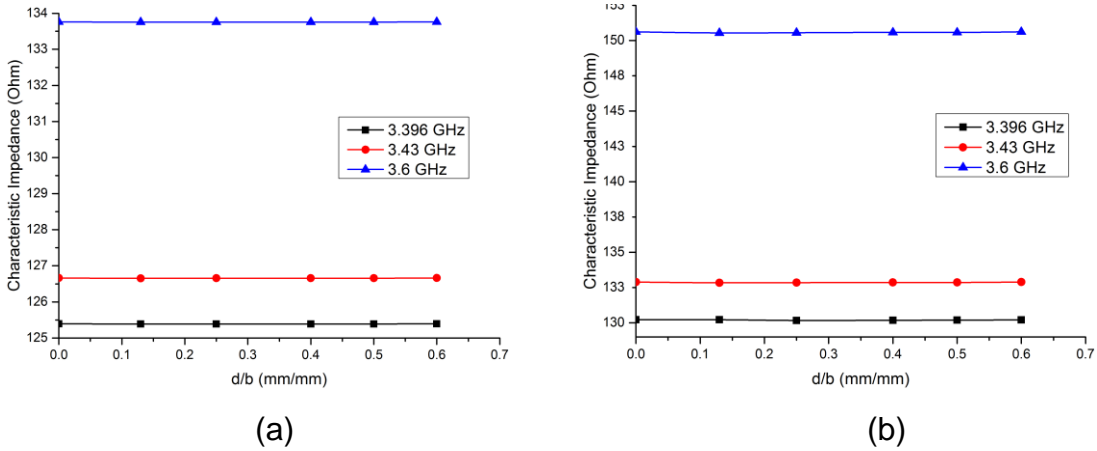


Figure 2.5 Effect of the enclosure grooves on the characteristic impedance for different enclosure heights and substrate thicknesses (a) 20mm, 0.5mm (c) 20mm, 3mm.

According to the previous study, it is believed that deep change of the characteristic impedance which is shown in figure 2.4 (a) was due to introducing of a new TE₁₀ wave guide that it can be revealed that the characteristic impedance can be controlled by choosing the right enclosure height and a suitable substrate thickness.

2.2.2 Derivation of the SSS characteristic impedance and effective dielectric constant

Suspension of the transmission line significantly affects both the characteristic impedance and the relative dielectric constant. The air layers above and below the dielectric substrate reduce the effective dielectric constant, resulting in a wider strip conductor. Knowing that the concept of the effective dielectric constant can be described physically as the mean field in a randomly inhomogeneous medium [58]. In other words, the effective dielectric constant is defined as the squared ratio between the squared speed of light to the phase velocity of the travelling wave in a certain dielectric substrate [39]. In [46], the characteristic impedance of the suspended transmission line presented in Figure1 is analysed, and can be expressed mathematically as:

$$z = \frac{z_0}{\sqrt{\epsilon_e}} \quad 2.1$$

Where, Z_0 and ϵ_e are the characteristic impedance and the effective dielectric constant of the SSL, which is placed in an air-filled enclosure with identical dimensions. It has been clarified that the modified expressions are valid within the following condition, $1 \leq \frac{a}{b} \leq 2.5$, $1 < \epsilon_r < 4$, $0.1 < \frac{h_2}{b} < 0.5$.

The effective dielectric constant ϵ_e of SSL has also been analysed, and can be expressed as follows:

$$\sqrt{\epsilon_e} = \left[1 + \left((E - F) * \ln\left(\frac{w}{b}\right) * \ln\left(\frac{1}{\sqrt{\epsilon_r}}\right) \right) \right]^{-1} \quad 2.2$$

According to [46], the variable parameters E and F have two cases, the first case is for $1 < w < a/2$, Thus:

$$E = 0.2077 + 1.2177 * \left(\frac{h_2}{b}\right) - 0.08364 * \left(\frac{a}{b}\right) \quad 2.3$$

$$F = 0.03451 - 0.1031 * \left(\frac{h_2}{b}\right) - 0.01742 * \left(\frac{a}{b}\right) \quad 2.4$$

The second case is for $a/2 < w < a$, thus:

$$E = 0.4640 + 0.9647 * \left(\frac{h_2}{b}\right) - 0.2063 * \left(\frac{a}{b}\right) \quad 2.5$$

$$F = 0.03451 - 0.1031 * \left(\frac{h_2}{b}\right) - 0.02411 \left(\frac{a}{b}\right) \quad 2.6$$

The second part of this mathematical analysis resolves the characteristic impedance of the suggested transmission line. The authors [46] assumed two conditions defining the limits of this analysis. The first condition is for $0 < w < a/2$, hence:

$$Z_0 = \frac{\eta_0}{2\pi} \left[(v + R) * \ln \left(\frac{6}{w/b} + \sqrt{1 + \frac{4}{(w/b)^2}} \right) \right] \quad 2.7$$

where:

$$\eta_0 = 120\pi \quad 2.8$$

$$V = -1.7866 - 0.2035 \frac{h_2}{b} + 0.4750 \frac{a}{b} \quad 2.9$$

$$R = 1.0835 + 0.1007 \frac{h_2}{b} + 0.09457 \frac{a}{b} \quad 2.10$$

The second condition is for $a/2 < w < a$, then:

$$z_0 = \eta_0 \left\{ (v + R) \left[\frac{w}{b} + 1.3930 + 0.6670 * \ln \left(\frac{w}{b} + 1.444 \right) \right]^{-1} \right\} \quad 2.11$$

where:

$$V = -0.6301 - 0.07082 \frac{h_2}{b} + 0.2470 \frac{a}{b} \quad 2.12$$

$$R = 1.9492 + 0.1553 \frac{h_2}{b} + 0.5123 \frac{a}{b} \quad 2.13$$

This method is accurate within a margin of error of $\pm 2\%$ for $0 < w < a/2$ and $\pm 3\%$ for $a/2 < w < a$. Given that use of the mathematical analysis above is limited to particular dimensions, as explained, it can only be considered as an initial starting point for those designs which have dimensions outside the ranges mentioned, and it needs to be followed by an optimisation process using full-wave electromagnetic simulation software (EM) to obtain the required response. To verify the need for further optimisation by using EM full-wave simulations, the characteristic impedance of a SSS structure has been calculated by using the offered closed form equations and simulated for different transmission line width. The dimensions of the metal box and the dielectric substrate were chosen carefully to meet the limitations of equations,

therefor, the box dimensions were as follows: $b=10\text{mm}$, and $a=10\text{mm}$, While the width of the transmission line is being changed from $w=4$ to 5 mm on a step of 0.1 mm and the dielectric constant of the substrate $\epsilon_r=3$ and thickness $(h)=0.5\text{ mm}$. The results are shown on Figure 2.6.

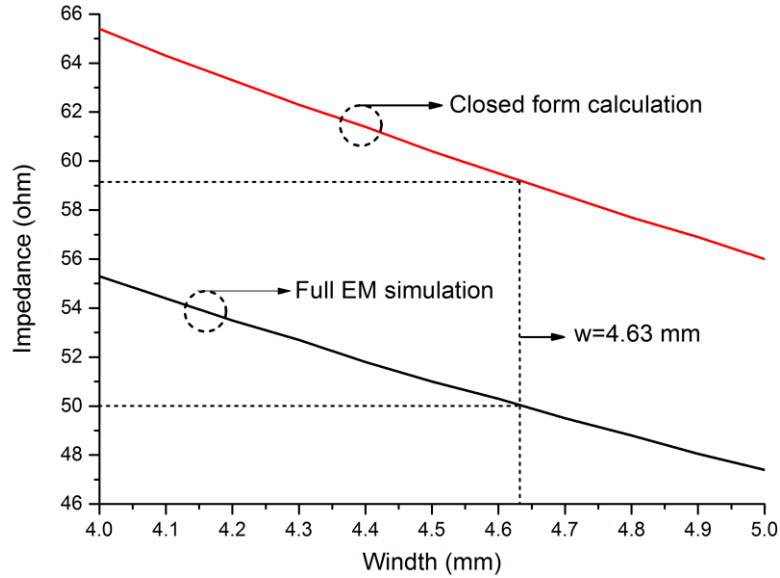


Figure 2.6 The calculated and simulated characteristic impedance of a SSS transmission line

It is obvious that the difference between the simulated and calculated results is about 10%, this difference could be due to the excluding of the parasitic effect, loss tangent of the substrate and the conductor loss which are included in the simulated result. Those excluded parameters could play a key role in increasing of unwanted susceptance and reactance to the transmission line which might be the reason of the calculated difference [39]. However, the closed form equations could form a good approach to start any design especially at the absence of the expensive simulation software.

2.2.3 Characteristic impedance of the broadside-coupled SSS

In the previous section, the effect of the electrical circuit suspension on the characteristic impedance of the transmission line was discussed and framed in specific equations to calculate the suspended line's characteristic impedance.

This section highlights the effects of shielding on the suspended coupled lines. Coupling structure is an essential way of building microwave circuits, and is used extensively to implement microwave structures. There are different approaches for

different coupling structures. In [46], Shu et al. developed a numerical method for calculating the characteristic impedance of the broadside-coupled transmission lines, as shown in Figure 2.7:

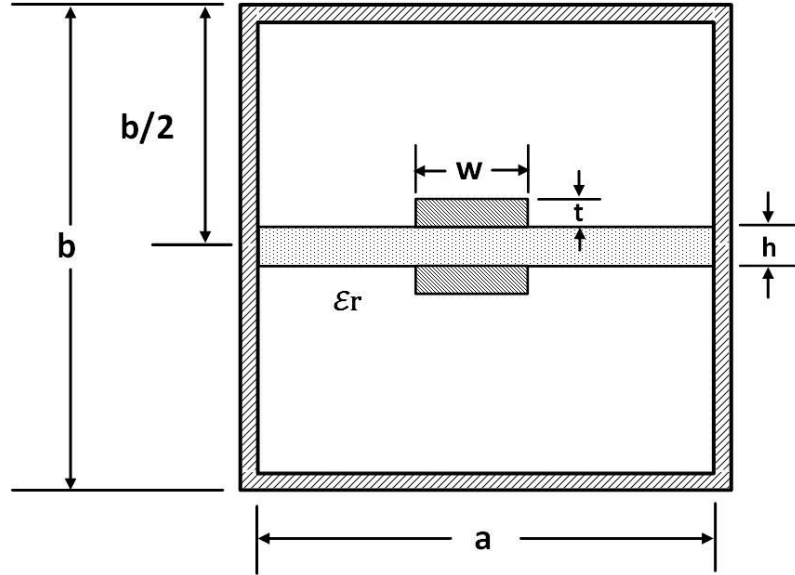


Figure 2.7 A cross-sectional view of a broadside-coupled SSSL [46]

The coupled-line structures are defined by two main factors: coupling coefficient (k) and characteristic impedance (Z_0). These parameters are calculated by applying the following formulae [46]:

$$K = \frac{Z_{oe} - Z_{oo}}{Z_{oe} + Z_{oo}} \quad 2.14$$

$$Z_o = \sqrt{Z_{oe}Z_{oo}} \quad 2.15$$

where Z_{oo} and Z_{oe} are the odd and even modes characteristic impedances, respectively. The first step in finding those factors is addressing their odd and even mode impedances. From (1), the odd mode impedance (Z_{oo}) can be expressed as [46]:

$$Z_{oo} = \frac{Z_{oo}^0}{\sqrt{\epsilon_{00}}} \quad 2.16$$

where:

$$\frac{1}{\sqrt{\epsilon_{oo}}} = 1 + 0.5 \left(H - P \ln \left(\frac{w}{b} + \sqrt{\left(\frac{w}{b} \right)^2 + 1} \right) \left(\ln \frac{1}{\sqrt{\epsilon_r}} + \frac{1}{\sqrt{\epsilon_r}} - 1 \right) \right) \quad 2.17$$

and:

$$H = 0.7210 - 0.3568 \frac{h}{b} + 0.02132 \frac{a}{b} \quad 2.18$$

$$P = -0.3035 + 0.3743 \frac{h}{b} + 0.07274 \frac{a}{b} \quad 2.19$$

On the other hand:

$$Z_{oo}^o = \frac{\eta_o}{2} \left[S + T \ln \left(\frac{0.2}{w/b} + \sqrt{1 + \frac{0.23}{(w/b)^2}} \right) \right] \quad 2.20$$

where:

$$S = -0.1073 + 1.67080 \frac{h}{b} + 0.007484 \frac{a}{b} \quad 2.21$$

$$T = 0.4768 + 2.1295 \frac{h}{b} - 0.01278 \frac{a}{b} \quad 2.22$$

In the case of the even mode characteristic impedance:

$$Z_{oe} = \frac{Z_{oe}^o}{\sqrt{\epsilon_{oe}}} \quad 2.23$$

Similarly, the even-mode dielectric constant has been expressed in [46] as:

$$\frac{1}{\sqrt{\epsilon_{oe}}} = 1 + \left(H - P \ln \frac{w}{b} \right) * \ln \frac{1}{\sqrt{\epsilon_r}} \quad 2.24$$

So:

$$H = 0.2245 + 0.7192 \frac{h}{b} + 0.1022 \frac{a}{b} \quad 2.25$$

$$P = 0.001356 + 0.06590 \frac{h}{b} + 0.01951 \frac{a}{b} \quad 2.26$$

Next, the formula for the identical even-mode characteristic impedance is considered as follows:

$$Z_{oe}^o = \frac{\eta_o}{2\pi} \left[S + T \ln \left(\frac{12}{w/b} + \sqrt{1 + \frac{16}{(w/b)^2}} \right) \right] \quad 2.27$$

where:

$$S = -2.6528 + 0.9452 \frac{h}{b} + 0.4531 \frac{a}{b} \quad 2.28$$

$$T = 1.4793 - 1.1903 \frac{h}{b} - 0.04511 \frac{a}{b} \quad 2.29$$

A comparison experiment in terms of the characteristic impedance has been established to justify the accuracy of these equations, this study used the offered closed form equations and a simulation software. The dimensions of the metal box and the dielectric substrate were chosen carefully to meet the limitations of equations, therefore, the box dimensions were as follows: $b=10\text{mm}$, and $a=10\text{mm}$ while the widths of the coupled transmission lines $w=4\text{ mm}$ and the dielectric constant of the substrate $\epsilon_r=3$ and thickness $(h)=0.5\text{ mm}$. The result of the experiment is depicted in figure 2.8. the difference between the experiment's outcomes could be due to not being used the parasitic capacitance, the loss tangent and the loss of the conductor in the closed form equation.

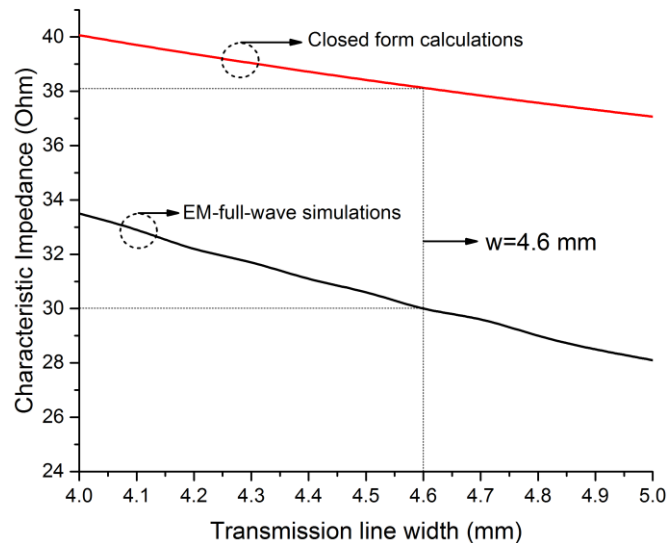


Figure 2.8 The calculated and simulated characteristic impedance of the SSS broad-side coupled transmission lines.

2.2.4 Characteristic impedance of the edge-coupled SSS

Edge or parallel coupled lines have a different structure to coupled transmission lines in that their internal edges are coupled, as shown in Figure 2.9. As with the broadside coupling, this coupling structure supports two full-TEM coupling modes, i.e. the odd and even coupling ones. For the odd mode excitation, the coupled conductors carry opposite sign charges or so-called negative and positive charges, leading to the formation of an electric wall between the coupled conductors, as shown in Figure 2.10.

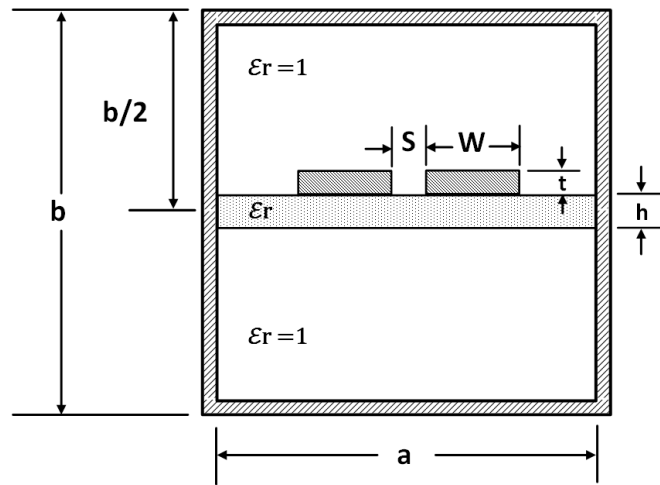


Figure 2.9 A cross-sectional view of an edge coupled SSSL [59]

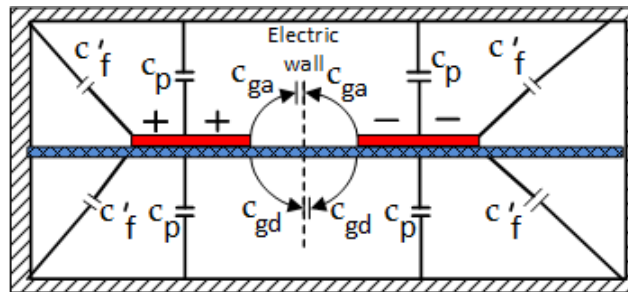


Figure 2.10 Odd mode excitation and edge-coupled SSS

In contrast, in the even mode excitation, both conductors carry the same charge whether positive or negative, which in turn leads to the formation of a magnetic wall between the coupled conductors [40], as shown in Figure 2.11.

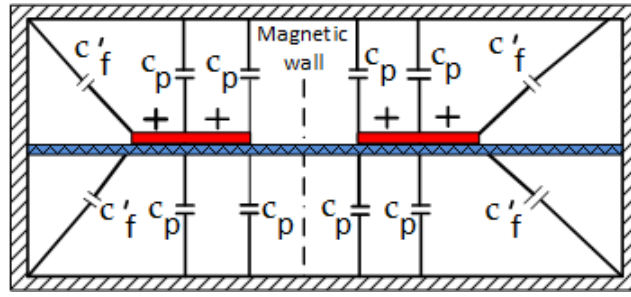


Figure 2.11 Even mode excitation and edge-coupled SSS

Several analytical techniques are applied to investigate the characteristic impedance of the suspended substrate stripline edge-coupled transmission lines, such as those described in [60]–[62]. According to [59], the most commonly used approach is the spectral domain technique, however, as mentioned, the problem of this method lies in the complexity of its mathematical procedures, as well as the difficulty of selecting the basis function. Therefore, a new method called the method of lines is proposed. This is based on a closed-form equation to analyse and synthesise the coupled lines' characteristic impedance. The authors stated in [59] that the proposed technique's analytical accuracy is about 3.5%, while it is the equivalent of around 5% for synthesis. However, this technique can be a first step in finding the odd and even characteristic impedances of the coupled lines, after which an optimisation technique can be used to obtain the optimal values. This approach is divided into two phases, the first of which involves addressing the equations for obtaining the effective dielectric constant, while the second phase involves calculating the characteristic impedance of both excitation modes.

In the odd mode, the effective dielectric constant equation can be expressed as follows:

$$\frac{1}{\sqrt{\epsilon_{ro}}} = 1 - E \left(\ln \frac{s}{a} - F \right) * \left(\ln \frac{w}{a} - G \right) * \ln \epsilon_r * \epsilon_r^{0.03} \quad 2.30$$

where:

$$s = 10^{-4} \left\{ 7.7291 \left[\frac{b}{a} + 6.9924 * \left(9.5 * \left(\frac{h}{a} \right)^2 - 1 \right) \right] * \left[\ln \frac{h}{a} + 2.1657 \right] + 561.62 * \left(\frac{h}{a} \right)^2 - 6.7772 * \left(\frac{h}{a} \right) \right\} \quad 2.31$$

$$F = 60.4762 \left[\left(\frac{b}{a} - 6 * \frac{h}{a} \right)^2 * \left(1 + 2 \frac{h}{a} \right) - 1.6012 * \left(1 - 8 * \left(\frac{h}{a} \right)^2 \right) \right] \\ * \left(e^{\frac{h}{a}} - 1.04684 \right) + 1721.61 * \left(\frac{h}{a} \right)^2 + 19.027 * \left(\frac{h}{a} \right) \quad 2.32$$

$$G = 0.05154 * \left[- \left(\frac{b}{a} - 0.8 \right)^2 + 0.3653 * \left(1 - 8 * \left(\frac{h}{a} \right)^2 \right) \right] \\ * \left[e^{\frac{h}{a}} + 54.554 \right] + 9551.53 * \left(\frac{h}{a} \right)^3 + 34.76 * \left(\frac{h}{a} \right) \quad 2.33$$

It is shown in [59] that the accuracy of the odd effective dielectric approximation falls within an margin of error of about 2%. Moreover, the general formula of the even effective dielectric constant is presented as:

$$\frac{1}{\sqrt{\epsilon_{re}}} = 1 - \left(D \frac{S}{a} + H * \ln \left(\frac{W}{a} \right) + R \right) * \ln(\epsilon_r) * \epsilon_r^{0.06} * \left(\frac{\epsilon_r}{2.8} \right)^{\frac{(b-a-0.4)}{3}} \quad 2.34$$

where:

$$D = K_{11} \left(\frac{h}{a} \right)^3 + K_{12} \left(\frac{h}{a} \right)^2 + K_{13} \left(\frac{h}{a} \right) + K_{14} \quad 2.35$$

$$K_{11} = -28794 \left(\frac{b}{a} \right)^2 + 29.958 \left(\frac{b}{a} \right) + 52.861 \quad 2.36$$

$$K_{12} = 0.92658 \left(\frac{b}{a} \right)^2 + 2.2713 \left(\frac{b}{a} \right) - 20.653 \quad 2.37$$

$$K_{13} = -1.5075 \left(\frac{b}{a} \right)^2 + 1.8914 \left(\frac{b}{a} \right) + 75778 \quad 2.38$$

$$K_{14} = -0.25477 \left(\frac{b}{a} \right)^3 + 0.60480 \left(\frac{b}{a} \right)^2 - 0.48538 \left(\frac{b}{a} \right) \\ + 0.16713 \quad 2.39$$

$$H = K_{21} \left(\frac{h}{a}\right)^3 + K_{22} \left(\frac{h}{a}\right)^2 + K_{23} \left(\frac{h}{a}\right) + K_{24} \quad 2.40$$

$$K_{21} = -11.459 \left(\frac{b}{a}\right)^2 + 18.744 \left(\frac{b}{a}\right) - 17.109 \quad 2.41$$

$$K_{22} = 7.4499 \left(\frac{b}{a}\right)^2 - 11.927 \left(\frac{b}{a}\right) + 74606 \quad 2.42$$

$$K_{23} = -0.33432 \left(\frac{b}{a}\right)^2 + 0.552 \left(\frac{b}{a}\right) - 37.211 \quad 2.43$$

$$K_{24} = 0.014317 \left(\frac{b}{a}\right)^2 + 0.030418 \left(\frac{b}{a}\right) - 0.0314 \quad 2.44$$

$$R = K_{31} \left(\frac{h}{a}\right)^2 + K_{32} \left(\frac{h}{a}\right) + K_{33} \quad 2.45$$

$$K_{31} = -48.729 \left(\frac{b}{a}\right)^2 + 115.45 \left(\frac{b}{a}\right) - 92.939 \left(\frac{b}{a}\right) + 22.5953 \quad 2.46$$

$$K_{32} = 1.4237 * \ln \left(\frac{b}{a} + 3.2411\right) - 11.927 \left(\frac{b}{a}\right) + 74606 \quad 2.47$$

$$K_{33} = 0.014478 * \ln \left(\frac{b}{a} + 0.23568\right) - 0.024308 \quad 2.48$$

It is clarified in [59] that the accuracy of the presented even dielectric constant analysis falls within a margin of error of around 2.5%. Similarly, odd and even characteristic impedance has been analysed using the same technique, namely the line method.

However, it is expected that both even and odd modes of the effective dielectric constants of broadside and parallel coupled lines are equal, because the dominant media is air in the presence of a very thin substrate.

The odd and even characteristic impedances of the edge-coupled transmission lines Z_{oo}, Z_{oe} are introduced as follows [59]:

$$Z_{oo} = Z_o / \sqrt{\epsilon_{ro}} \quad 2.49$$

$$Z_{oe} = Z_e / \sqrt{\epsilon_{re}} \quad 2.50$$

By assuming $\epsilon_{ro} = \epsilon_{re} = 1$, It can be seen from the above equation that both odd and even characteristic impedances of the SSS are equal to those of the excitation modes.

The odd mode characteristic impedance Z_o is written as [59]:

$$Z_o = 60\pi^2 / \ln \left(2 * \frac{1 + \sqrt{K'_1}}{1 - \sqrt{K'_1}} \right) \quad 2.51$$

where:

$$K'_1 = \sqrt{1 - K_1^2} \quad 2.52$$

Also:

$$K_1 = \frac{\varphi'_1}{\varphi'_2} \quad 2.53$$

where:

$$\varphi'_1 = Q_1 * \tan^{-1} \left(\frac{2w + s}{b} * Q_2 \right) + Q_3 \quad 2.54$$

$$\varphi'_2 = Q_1 * \tan^{-1} \left(\frac{s}{b} * Q_2 \right) + Q_3 \quad 2.55$$

$$\begin{aligned} Q_1 &= 0.0361168 * \exp(5.12k) + 1.4404 \\ Q_2 &= 0.0316177 * \exp(3.947k) + 1.07319 \\ Q_3 &= 0.15988K^3 - 0.0895K^2 + 0.02535K + 0.002311 \end{aligned} \quad 2.56$$

$$K = \sqrt{1 - \left(\frac{e^{\pi a/b} - 2}{e^{\pi a/b} + 2} \right)^4} \quad 2.57$$

The accuracy of the odd characteristic impedance falls within a margin of error of around 3% [59].

Meanwhile, the even characteristic impedance is expressed mathematically as [59]:

$$Z_e = 60\pi^2 / \ln \left(2 * \frac{1 + \sqrt{K'_2}}{1 - \sqrt{K'_2}} \right) \quad 2.58$$

where:

$$K'_2 = \sqrt{1 - K_2}$$

$$K_2 = \sqrt{\frac{1 + t_g^2 * \varphi'_2}{1 - t_g^2 * \varphi'_1}} \quad 2.59$$

Knowing that, φ'_1 and φ'_2 are equivalent to those in equations (31a) and (31b).

The next phase of this approach is to address the equations for synthesis. These aim to find the ratio between the physical width of the stripline and the metallic enclosure, making it easier to determine the stripline's dimensions. A formulation for this ratio is developed in [59] as:

$$\frac{w}{a} = \exp \left(\frac{t_2 + \sqrt{t_2^2 - 4t_1 * t_2}}{2t_1} \right) \quad 2.60$$

where:

$$t_1 = HB_1 \left(\frac{\epsilon_r}{2.8} \right)^{\frac{b/a-0.4}{3}} / \epsilon^{0.02}$$

$$t_2 = B_1 + p_1 * E \left(\ln \frac{S}{a} - F \right) - (B_1 \left(D \frac{S}{a} + R \right) + HB_2 \left(\frac{\epsilon_r}{2.8} \right)^{\frac{b/a-0.4}{3}} / \epsilon^{0.02}) \quad 2.61$$

$$t_2 = B_1 + p_1 * E \left(\ln \frac{S}{a} - F \right) - (B_1 \left(D \frac{S}{a} + R \right) + HB_2 \left(\frac{\epsilon_r}{2.8} \right)^{\frac{b/a-0.4}{3}} / \epsilon^{0.02})$$

$$B_1 = d_1\left(\frac{s}{a}\right)^4 + d_2\left(\frac{s}{a}\right)^3 + d_3\left(\frac{s}{a}\right)^2 + d_4\left(\frac{s}{a}\right) + d_5 \quad 2.62$$

$$\begin{aligned} d_1 &= 49228.93\left(\frac{b}{a}\right)^3 - 86515.93\left(\frac{b}{a}\right)^2 + 50484.33\left(\frac{b}{a}\right) - 9992.325 \\ d_2 &= -29055.1\left(\frac{b}{a}\right)^3 + 51037.57\left(\frac{b}{a}\right)^2 - 29730.67\left(\frac{b}{a}\right) + 5949.112 \\ d_3 &= 5949.73\left(\frac{b}{a}\right)^3 - 10436.34\left(\frac{b}{a}\right)^2 + 6087.17\left(\frac{b}{a}\right) - 1236.955 \\ d_4 &= -489.14\left(\frac{b}{a}\right)^3 + 849.65\left(\frac{b}{a}\right)^2 - 495.616\left(\frac{b}{a}\right) + 104.9031 \\ d_5 &= 11.9172\left(\frac{b}{a}\right)^3 - 20.3952\left(\frac{b}{a}\right)^2 + 11.8292\left(\frac{b}{a}\right) - 2.8858 \end{aligned} \quad 2.63$$

$$\begin{aligned} B_2 &= m_1 + \ln\left(\frac{s}{a} + m_2\right) + m_3 \\ m_1 &= 16.132\left(\frac{b}{a}\right)^3 - 27.578\left(\frac{b}{a}\right)^2 + 14.6088\left(\frac{b}{a}\right) - 2.74812 \\ m_2 &= -15.443\left(\frac{b}{a}\right)^3 + 27.658\left(\frac{b}{a}\right)^2 - 16.409\left(\frac{b}{a}\right) + 3.2731 \\ m_3 &= 12.9051\left(\frac{b}{a}\right)^3 - 20.6769\left(\frac{b}{a}\right)^2 + 10.0935\left(\frac{b}{a}\right) - 0.6533 \end{aligned} \quad 2.64$$

Knowing that p is equal to:

$$p = \frac{Z_{oe} - Z_{oo}}{Z_{oe} + Z_{oo}} \quad 2.65$$

And:

$$p_1 = Z_{oe}/Z_{oo} \quad 2.66$$

Despite the limited conditions in which this approach can be used, it is considered a starting point for further optimisation to obtain the required dimensions of the edge-coupled SSS transmission lines. These limitations are addressed as follows:

$$2.22 \leq \epsilon_r \leq 3.8, 0.05 \leq \frac{w}{a} \leq 0.2, 0.054 \leq \frac{s}{a} \leq 0.26, 0.4 \leq \frac{b}{a} \leq 0.85 \text{ and } 0.04 \leq \frac{h}{a} \leq 0.12$$

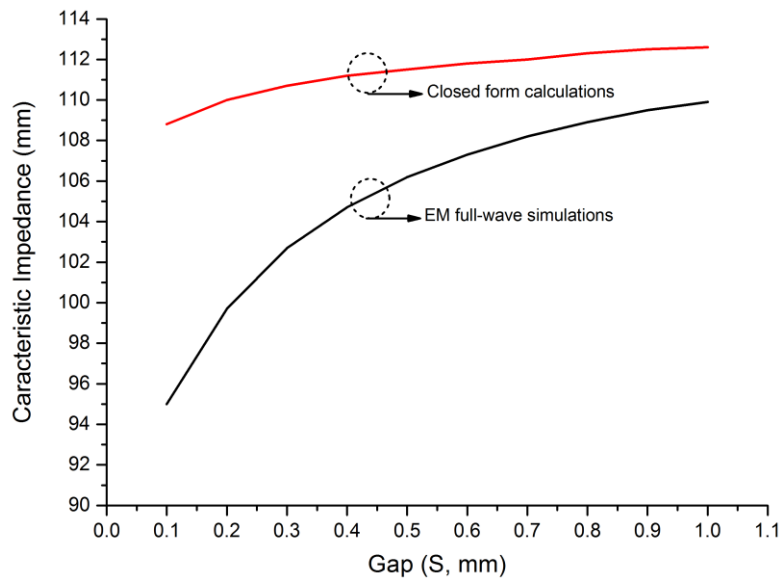


Figure 2.12 the calculated and simulated characteristic impedance of the SSS edge-coupled transmission lines.

A comparison experiment in terms of the characteristic impedance has been established to justify the accuracy of these equations, this study used the offered closed form equations and a simulation software. The dimensions of the metal box and the dielectric substrate were chosen carefully to meet the limitations of equations, therefore, the box dimensions were as follows: $b=10\text{mm}$, and $a=10\text{mm}$ while the widths of the coupled transmission lines $w=1.5\text{ mm}$ and the dielectric constant of the substrate $\epsilon_r=3$ and thickness $(h)=0.5\text{ mm}$. The result of the experiment is depicted in Figure 2.12. The difference between the experiment's outcomes could be due to not being used the parasitic capacitance, the loss tangent and the loss of the conductor in the closed form equation.

2.3 Conclusion

In this chapter the suspended substrate stripline has been highlighted briefly where some of the topics related to the subject of the research were discussed. A comparison table between different topologies has been presented, the effect of the grooves on the characteristic impedance has been investigated and the mathematical derivation of the different SS coupling structures has been introduced. Although these mathematical equations are associated with some application limitations, yet they provide very good approximation approaches. These approaches are then followed by multiple optimization procedures to achieve the optimal response.

Mechanically Tuned Suspended Substrate Stripline Lowpass Filter

3.1 Introduction

Lowpass filters play a significant role in the wireless communication systems. They are commonly placed between the base stations and transceiver to uproot undesired harmonics and spurious signals that are produced in the RF nonlinear mixing subsystems [2]. Recently, due to the high demand of the tunable devices because of the growing consumption of the frequency band, the importance of the lowpass filter extended further to become a key factor of developing the RF Reconfigurable devices. Tunable low pass filters present a wide tuning range in some tuning techniques and progressing suppression capabilities in their stopband. Furthermore, lowpass filter could be cascaded with other structures such as highpass or bandstop filter leading to a sophisticated bandpass or bandstop filters which have attractive characteristic in terms of centre frequency and bandwidth tuning. There are few works concerning the tuning of the lowpass filter have been published [63]–[68]. However, they fabricated as microstrip filters and utilized the electronic components for tuning continuously or in discrete manner.

In this chapter, a different discrete tuning method is presented rather than using lossy electronic components. However, the chapter is divided into many sections, in 3.2, a full presentation of the analysis and synthesis equations of the suspended lowpass filter is introduced, in 3.3 a detailed design example is presented with full simulated and measured results followed by a discussion of the obtained results, in section 3.4 the tuning mechanism is discussed, supported by a complete presentation of the tuning elements and their arrangement as well as the simulated and measured results, in 3.5 the work is summarized and an entire comparison with similar works is offered.

3.2 Suspended substrate stripline Lowpass filter analysis and Synthesis

The design procedure of this filter starts by choosing the appropriate lumped lowpass prototype model. According to [69], The generalized Chebyshev prototype lowpass filter is used to design a SSS filter. The generalized Chebyshev lowpass filter circuit model is illustrated below in Figure 3.1.

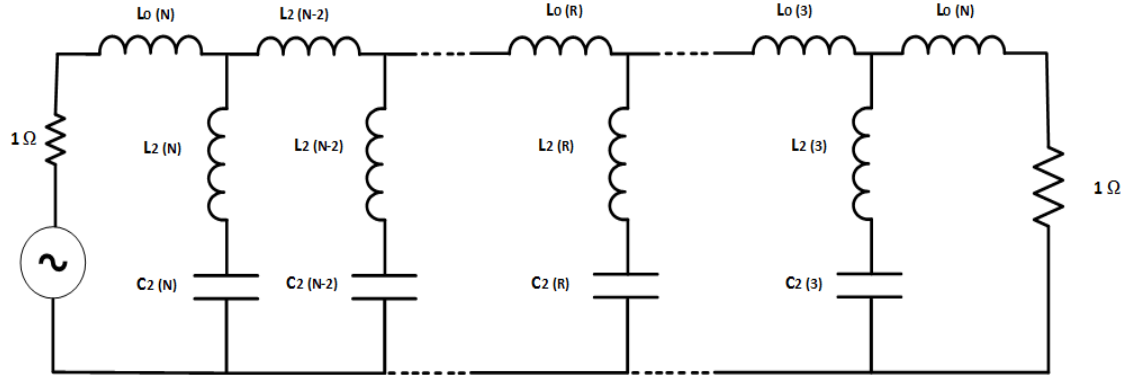


Figure 3.1 Generalized Chebyshev Lowpass Filter [69]

This model then transformed to its equivalent distributed lowpass filter by applying Richards's transformation [69] as follows,

Since, the admittances of the shunt elements of lowpass prototype filter equals

$$Y = j \frac{C\omega}{1 - LC\omega^2} \quad 3.1$$

Knowing that, $LC = \omega_0^{-2}$, at resonance and $p = j\omega$, then

$$Y = j \frac{Cp}{1 + \frac{p^2}{\omega_0^2}} \quad 3.2$$

Richard's transformation leads to

$$p \rightarrow \alpha \tanh(a_L p) \quad 3.3$$

Where p is the complex frequency variable, α is a constant which controls the band covered by the first stopband so that the band becomes broader as α becomes smaller [56] and a_L is the ratio of the length of the basic commensurate transmission line element to the phase velocity of the wave in such a line element [39]. More explanation on Richard's transformation is provided in appendix B. Therefore, the admittance of the distributed lowpass filter becomes [69]

$$Y = \frac{\omega_o \cdot C_2(R)}{2} \tanh(2a_L p) \quad 3.4$$

Which is also can be expressed as

$$Y = j \frac{\omega_o \cdot C_2(R)}{2} \tan(2a_L \omega) \quad 3.5$$

Since the admittance of the open circuited stub has a general form, that is

$$Y = jY_o \cdot \tan\left(\frac{\omega l}{v}\right) \quad 3.6$$

Then, by equating (4) and (5)

$$jY_o \cdot \tan\left(\frac{\omega l}{v}\right) = j \frac{\omega_o \cdot C_2(R)}{2} \tan(2a_L \omega) \quad 3.7$$

From (3.7), it could be deduced that the lumped elements resonator can be realized as a distributed shunt open stub as shown below in figure 3.2.

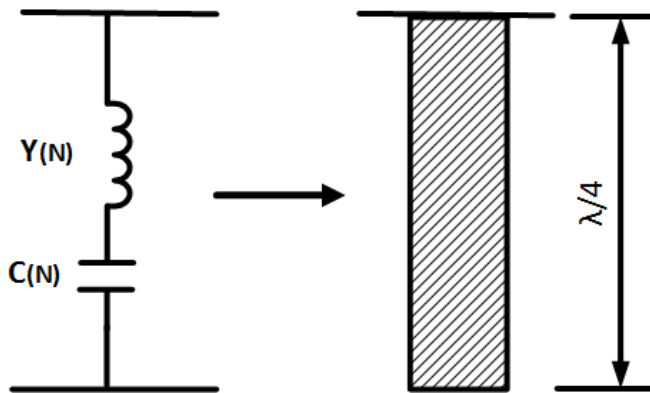


Figure 3.2 Richard's transformation Lumped element resonator to distributed open stub [70]

Furthermore, the normalized characteristic impedance [69] of the distributed open stub can be expressed as

$$Z_o = \frac{2}{\omega_o * C_2(R)} \quad 3.8$$

Moreover, from the hyperbolic arguments it can be found that

$$a_L = \frac{l}{2v} \quad 3.9$$

Where, l and v indicate the length of the shunt open stub and the speeds of light in free space, respectively. It is known that the length of the open stop is equal to $\frac{\lambda}{4}$ at

the resonance frequency (f_o). As reported by [69], the centre stopband frequency occurs when the length of the stub equals $\frac{\lambda}{2}$, this requires

$$f_{sb} = 2 * f_o \quad 3.10$$

Therefore

$$l = \frac{v}{4 * f_o} \quad 3.11$$

From equation (3.3)

$$\omega = \omega_o * \tan(a_L * 2\pi f) \quad 3.12$$

Then

$$a_L * 2\pi f = \tan^{-1}\left(\frac{\omega}{\omega_o}\right) \quad 3.13$$

From (3.9) and (3.11) it can be realized that

$$a_L = \frac{1}{8f_o} \quad 3.14$$

Substituting (3.14) in (3.13), therefore

$$f_o = \frac{4f}{\pi * \tan^{-1}\left(\frac{\omega}{\omega_o}\right)} \quad 3.15$$

Since, the prototype cut-of frequency $\omega=1$ at the bandage, a stub physical length equal to

$$l = \frac{v}{\pi * f_{bl}} * \tan^{-1}\left(\frac{1}{\omega_o}\right) \quad 3.16$$

Referring to [69] and [55], the lossless strip characteristic impedance can be expressed arithmetically as follows

$$Z_o * \sqrt{\epsilon_r} = \frac{\eta}{C/\epsilon} \quad 3.17$$

Where, ϵ_R is traveling wave medium relative dielectric constant, η is the free space impedance which is equal to 377.6Ω and $\frac{C}{\epsilon}$ is the static capacitance per unit length

which is a ratio between the conductor carrying the wave and the dielectric medium permittivity as illustrated below in figure 3.3.

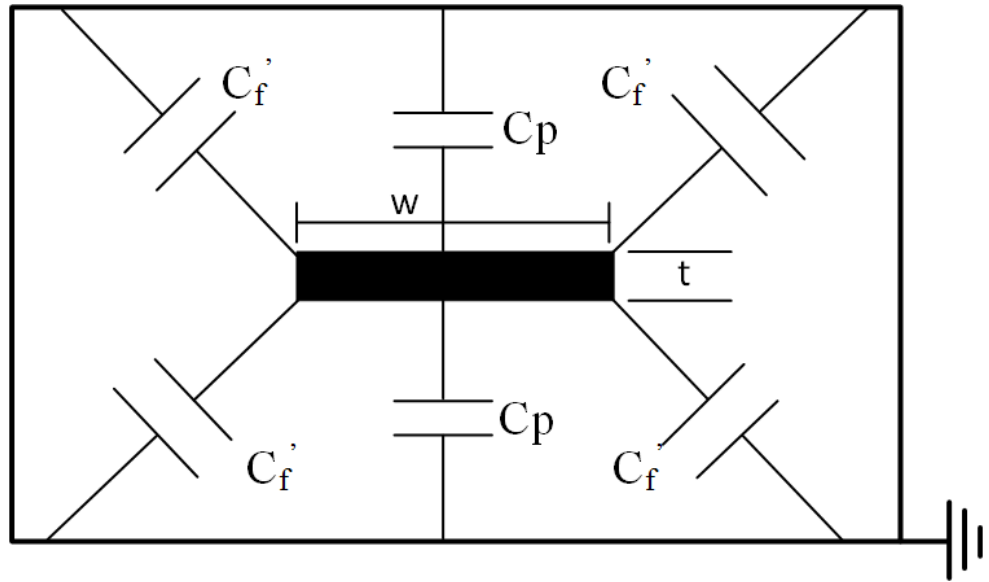


Figure 3.3 Static capacitance of single suspended transmission line [55].

It can be seen that the total static capacitance between the suspended conductor and the ground planes surrounding are given by [55]

$$\frac{C}{\epsilon} = 2 * C_p + 4 * \frac{C_f'}{\epsilon} \quad 3.18$$

Knowing that, C_p is the capacitance between the top and bottom of the conductor and C_f' is the fringing capacitance between the edges of strip conductor both to the nearest ground plane. According to [55], the total parallel capacitance C_p can be written as

$$C_p = \frac{2w}{b - t} \quad 3.19$$

Furthermore, the thickness of the transmission line of the printed circuit board can be assumed as zero, by using figure 5 in [71] then $\frac{C_f'}{\epsilon} = 0.46$, by substituting equation (3.19) into (3.18) then

$$\frac{C}{\epsilon} = \frac{4w}{b} + 1.84 \quad 3.20$$

By equating $\frac{C}{\epsilon}$ of equations (17) and (20) then

$$W = \frac{b}{4} * \left(\frac{377.6}{Z_o * \sqrt{\epsilon_r}} - 1.84 \right) \quad 3.21$$

By substituting equation (3.19) into (3.18) and normalizing Z_o to 50Ω termination, then,

$$W = \frac{b}{4} * \left(\frac{3.767 * \omega_o * C_2(R)}{\sqrt{\epsilon_r}} - 1.84 \right) \quad 3.22$$

Referring to Richard's transformation, the series lumped inductors also transformed into a high impedance transmission line. According to [39], [69] the distributed transmission line can be approximated electrically as a π -network as illustrated in figure 3.4.

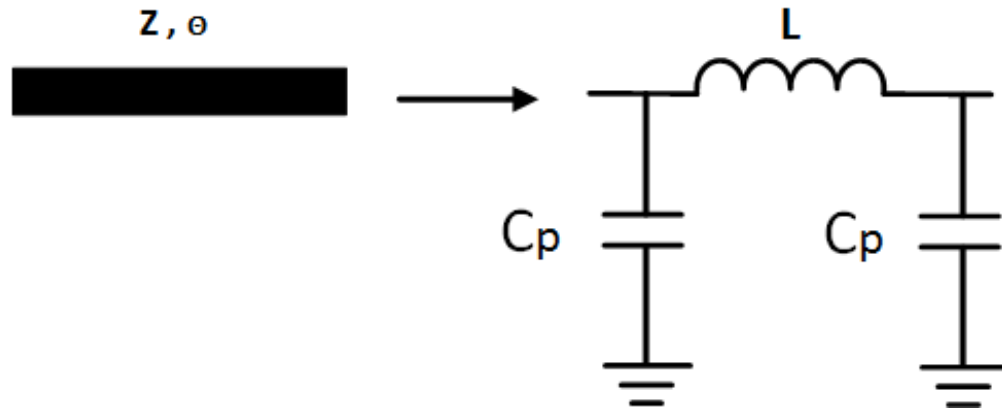


Figure 3.4 Equivalent circuit of a length of transmission line.

Where, C_p is the parasitic capacitance between the between the line and the ground planes. It is reported by [70] that these elements contributes the third transmission zero at infinity. The author affirmed that the series elements corresponds to the shunt circuited stubs because of the Richard's transformation, therefore they produce infinite admittance at $2f_o$ when the electrical length equals $\lambda/4$. In contrast, the open circuited stubs which don't contribute at this frequency. However, he emphasized, that due to the difficulty of the realization of the series short stubs on the printed circuit board, they can be realized as short transmission line to provide the inductive effect like the series short stubs at an electrical length below the quarter wave length. The obtainment of short series stub physical length can be achieved by using the following equation [72]

$$l = \frac{v}{\omega_c} \sin^{-1} \left(\frac{L_r}{Z_o} \right) \quad 3.23$$

Where, L_r is an inductor value of the prototype lumped element circuit.

Where, Z_L is the normalized impedance which equals [69]

$$Z_L = \omega * L_r \quad 3.24$$

As shown, the value of the width should be chosen carefully so that the manufacturing resolution of such short transmission lines becomes higher and to decrease the deviation of the fabrication tolerances that could occurs during implementation. However, the designing process could be followed by an optimization phase to obtain the required response of the filter.

Next section will discuss a real design example of the suspended substrate stripline generalized Chebyshev low pass filter. The details of the design procedures will be introduced in addition to the simulated and measured results.

3.3 Generalized Chebyshev lowpass filter design example

Assume that a Chebyshev filter has been constructed on a Roger Substrate with relative dielectric constant =3, substrate height = 0.5mm, copper thickness=0.017mm and dielectric loss tangent= 0.0031. The proposed filter order is 11 with cut-off frequency equals 1.784GHz. The minimum return loss and stopband insertion loss equal to -20 dB and -60 dB, respectively. The porotype filter elements' values which are correspond to the angular frequencies of $\omega_o=1.29479$ rad/s and $\omega_1=1.13086$ rad/s are chosen from [70]

The design process starts by composing the circuit model of the filter using Microwave office (AWR) designing software as shown above in figure 3.1. The next step is the transformation the prototype lumped element to lowpass filter with a termination impedance of 50Ω at the predefined cut-off frequency. The transformation process is achieved by applying the following equations [39]

$$L = \left(\frac{\Omega_c}{\omega_c} \right) * Z_o * L_r \quad 3.25$$

$$C = \left(\frac{\Omega_c}{\omega_c} \right) * \frac{C_r}{Z_o} \quad 3.26$$

Where Z_0 is the filter characteristic impedance and equal to 50Ω , ω_c is the filter's the filter's angular cutoff frequency and the lowpass prototype filter cutoff frequency $\Omega_c=1$, while L_r and C_r are the inductors and capacitors, values of the prototype lumped element circuit respectively.

The selected elements of the prototype generalized Chebyshev filter [70] and their transformed values are shown in table 3.1.

Table 3.1 Prototype filter element values and their optimized transformed values

R	Element	Prototype value	Transformed value	Unit
11	$L_o(11)$	0.50507	2.252926	nH
	$L_2(11)$	0.782383	3.489914	nH
	$C_2(11)$	0.762399	1.360309	pf
9	$L_o(9)$	1.27764	5.699067	nH
	$L_2(9)$	0.557858	2.488393	nH
	$C_2(9)$	1.06925	1.907807	pf
7	$L_o(7)$	1.33125	5.938201	nH
	$L_2(7)$	0.545154	2.431725	nH
	$C_2(7)$	1.09416	1.952253	pf
5	$L_o(5)$	1.33125	5.938201	nH
	$L_2(5)$	0.557858	2.488393	nH
	$C_2(5)$	1.06925	1.907807	pf
3	$L_o(3)$	1.27764	5.699067	nH
	$L_2(3)$	0.782383	3.489914	nH
	$C_2(3)$	0.762399	1.360309	pf
1	$L_o(1)$	0.50507	2.252926	nH

The next step of the filter design is the lumped element lowpass filter realization. The realization phase is initiated by calculation the dimensions of the distributed elements. Knowing that the characteristic impedance of the short transmission lines is chosen to be 150Ω which is related to the width of 2mm to simplify the fabrication process and obtain a good resolution quality. The simulated result of the proposed filter circuit model is presented in figure 3.5.

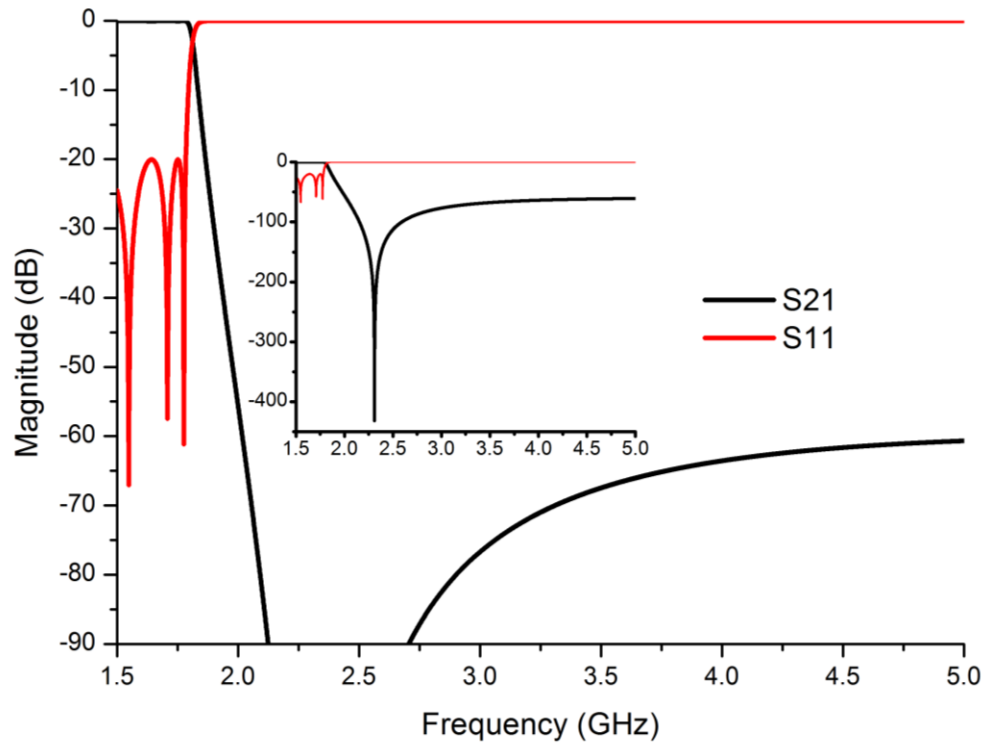


Figure 3.5 Generalized Chebyshev lowpass filter circuit model response.

The calculated and optimized dimensions of the filter elements are tabulated in tables 3.2.

Table 3.2 The optimized dimensions of the filter elements

	Lengths (mm)		Width		
	Short transmission lines	l_1	0.9	2.1	W1 w3
L_3		3.4	W5 W7		
L_5		1	2.1	W9 W11	
L_7		1		Wrs1 Wrs5	
First and Fifth resonators		$Res_{1,}$ Res_5	32.3	12.2	Wrs3
		Res_3	36.3	8.5	Wrs2 Wrs4
Second and Fourth resonators	Res_2 Res_4	36.2			

The circuit of the filter has been built and simulated by using the commercial full wave simulation software, namely Sonnet®. The layout of the filter's distributed circuited and its related EM simulated response are shown in figures 3.6 and 3.7, respectively.

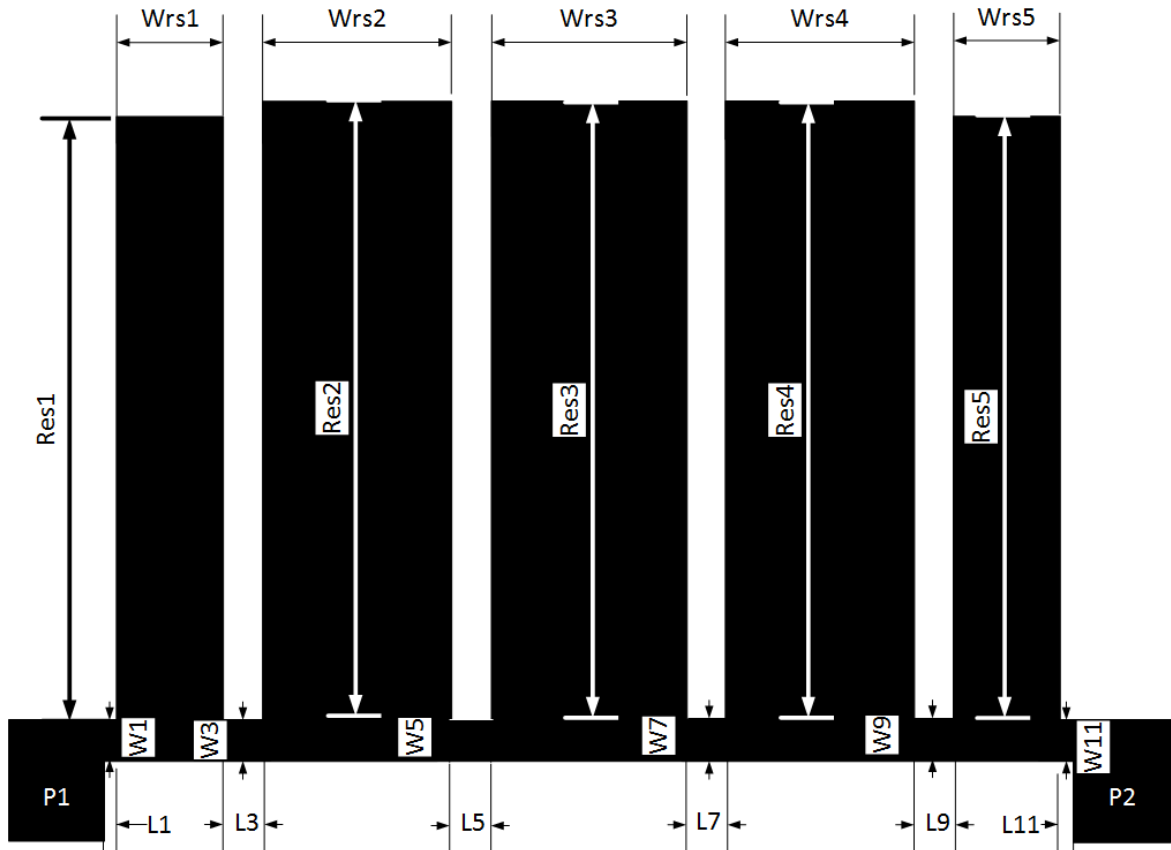


Figure 3.6 Layout of the generalized Chebyshev lowpass filter circuit with the calculated periodic elements.

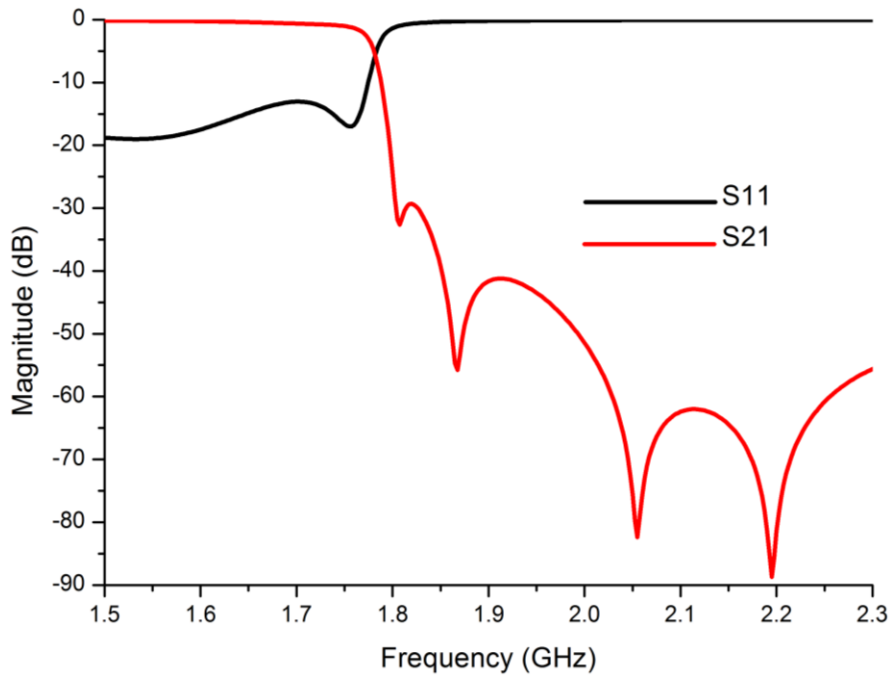


Figure 3.7 EM full-wave simulation response of the designed generalized Chebyshev lowpass filter [73]

The proposed suspended substrate stripline lowpass filter has been fabricated and placed in a metallic box with the dimensions of 12 mm, 53 mm and 70 mm for height, width and length, respectively. The measured and simulated responses of the filter are presented in figure 3.8.

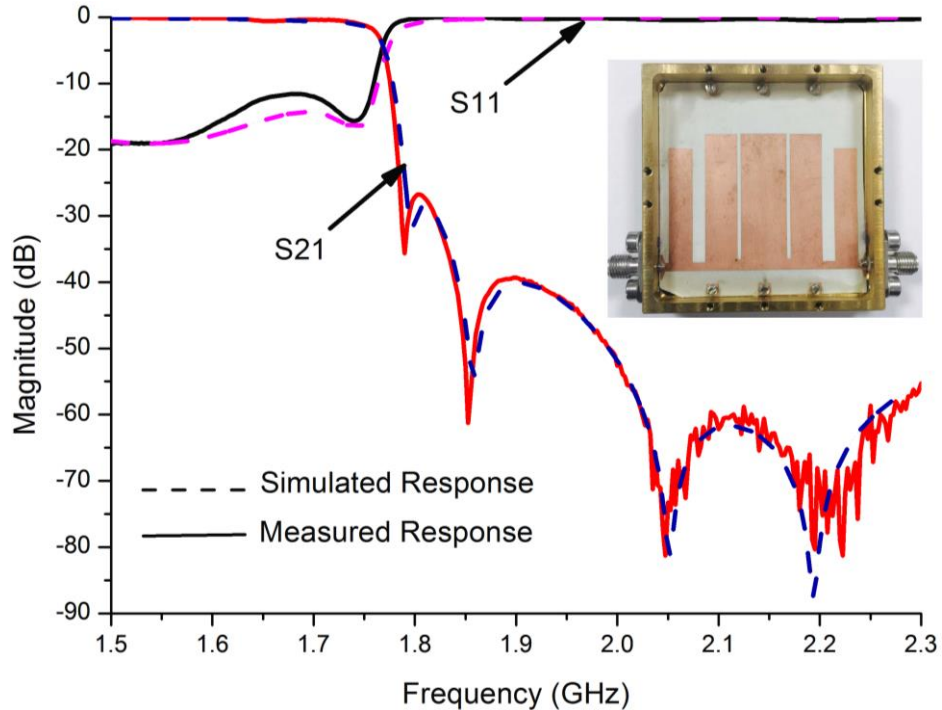


Figure 3.8 Measured and simulated responses of the generalized Chebyshev lowpass filter.

An excellent agreement between the measured and simulated performance can be noticed. However, the slight difference in term of the return loss could be due to manufacturing tolerance of filter's circuit.

Next section will highlight the synthesis procedures of the tunable filter and introduce the measured and simulated responses. A new manual tuning structure will be introduced as the first work of its kind applied on suspended substrate stripline, to my best knowledge.

3.3 Tuning analysis and synthesis of the generalized Chebyshev lowpass filter.

As being discussed previously, there are many tuning means have been used with different structures and methods of the microwave filters. It has been noticed that most works have been tuned electronically despite its negative impact on the levels

of the filter losses. However, the diversity shortage of the tuning techniques that have been used with the planar lowpass filters led to propose the mechanical tuning method to be used with this filter. Moreover, the vast development of the small-size servomotors manufacturing motivated us to put more effort on the high-quality mechanical tuning method so that they can be integrated for automatic tuning capability. Moreover, the large width of the resonators which requires tuning varactors of very small values was another reason of choosing the mechanical tuning method. The tuning process of this filter is achieved by using a developed structure of the screws which are arranged together to move up/down, synchronously. These screws are placed at the top end of the resonators to tune the filter capacitively. The equivalent electrical circuit of the proposed tuning method is illustrated in figure 3.9 and the mechanical structure of the screw is shown in figure 3.10.

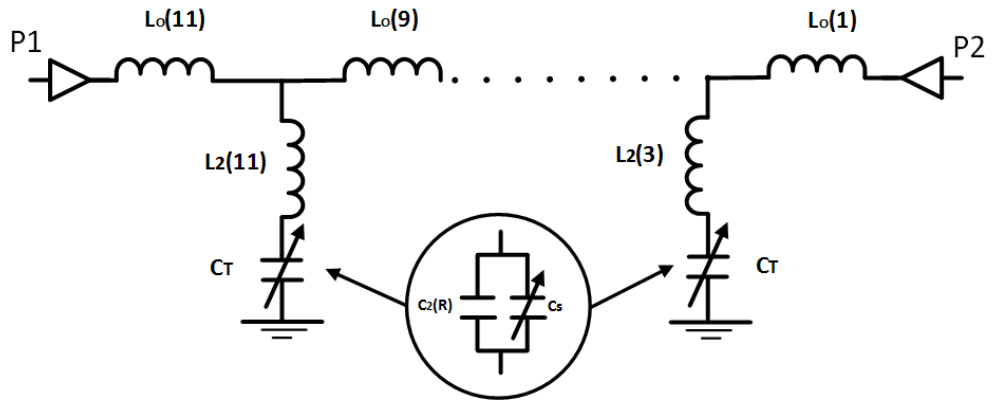


Figure 3.9 Equivalent electrical circuit of the proposed tuning method.

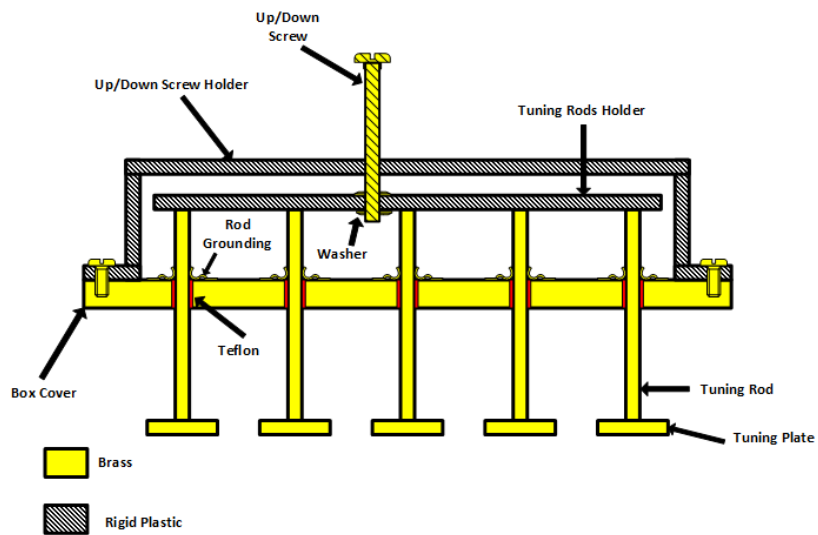


Figure 3.10 Mechanical structure of the proposed tuning method.

By moving a screw down, the distance between the positive plate which is in our design the resonator that is facing the screw, and the ground plate which is the moving plate of the screw, decreases, hence the capacitance increased and vice versa. The relation between the capacitance value and the separation distance between the plates of the capacitor is as follow

$$C_s = \frac{\epsilon * A}{d} \quad 3.27$$

Where, A is the area of the corresponding plates, ϵ is the dielectric constant which for this case equals 1 and d is the distance between the plates of the capacitor. According to this principle, the movement of the tuning screws toward or far from the top end of the resonators causes the increasing or decreasing the stray capacitance C_s between the resonator and the top ground as shown in above in figure 3.3.1, this leads to the retune the resonance frequency of the resonators, subsequently, retuning the cut-off frequency of the filter. To perform the capacitive tuning, an EM simulation carried out by using SONNET software for different gap levels. The simulated tuning result of the generalized Chebyshev lowpass filter is shown in figure 3.11 (a) and (b).

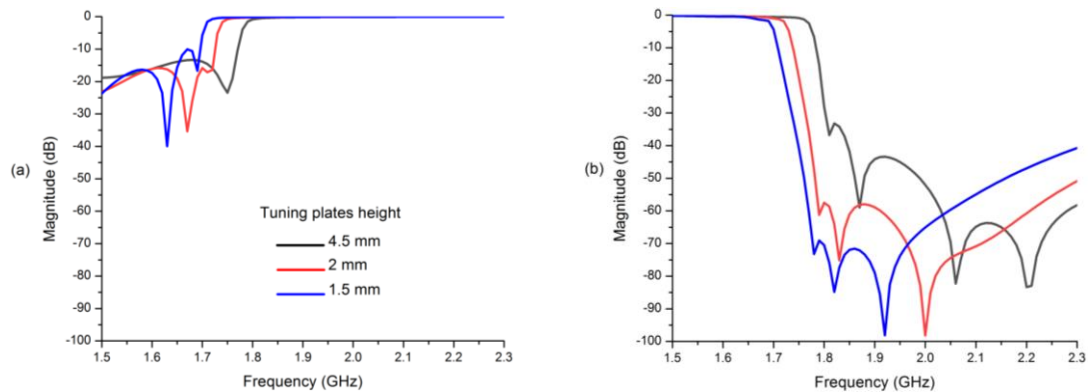


Figure 3.11 Simulated tuning performance of the filter (a) S11 (b) S21 [73]

The tuning range equals 109MHz that is from 1.675 GHz to 1.784 GHz, while the return and insertion loss vary from -10 dB to -16.5 dB and from -32 dB to -70 dB, respectively.

The measurement process has been realized by fixing the proposed tuning structure to the filter's containing box as shown in Figure 3.13. The measured responses of the

implemented suspended substrate stripline generalized Chebyshev lowpass filter is shown in figure 3.12 (a) and (b).

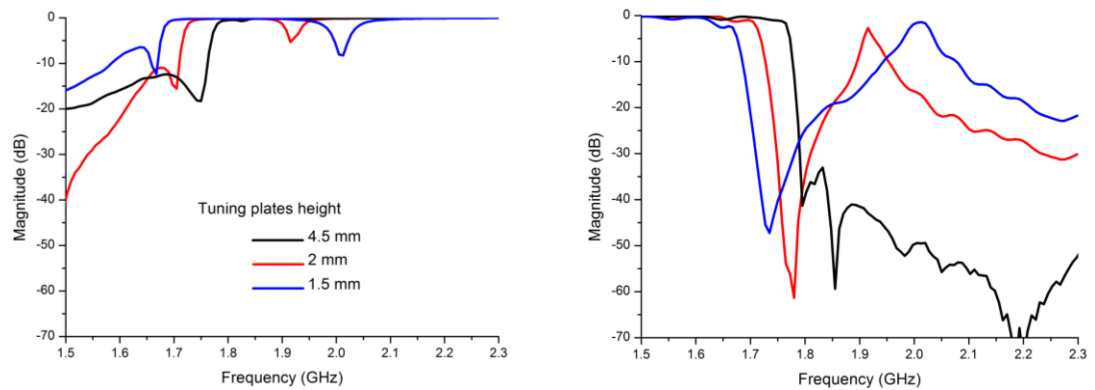
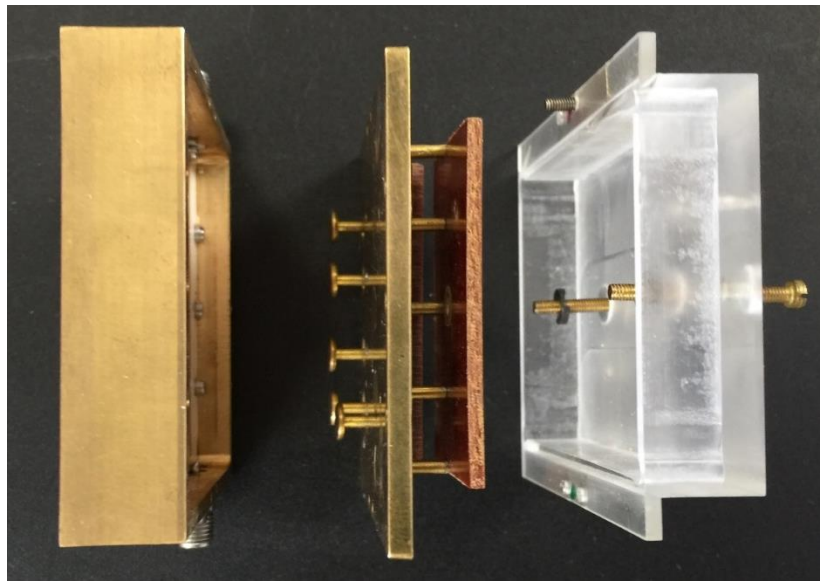


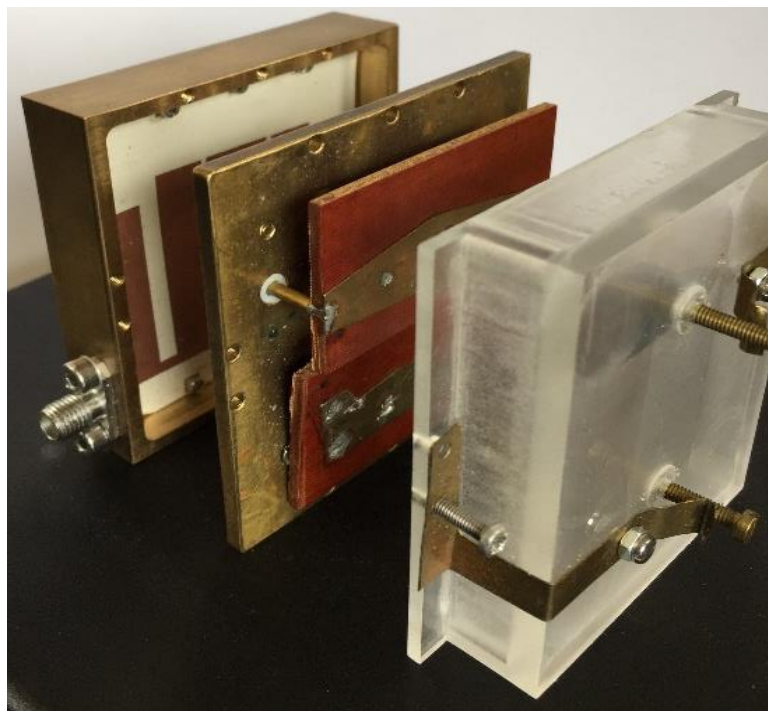
Figure 3.12 Simulated tuning performance of the filter (a) S11 (b) S21 [73]

The measured tuning range equals 109b MHz that is from 1.675 GHz to 1.784 GHz, while the return and insertion loss vary from -7 dB to -13 dB and from -50 dB to -20 dB, respectively.

It is clearly noticed that the insertion loss of both simulated and measured responses increases as the cut-off frequency decreases, however, it is lower in the simulated response. Meanwhile, the return loss of the simulated filter presents a slight difference during the tuning process, in contrast to that, the return loss of the measured filter suffers from the unwanted spurious responses is the bad grounding of the tuning screws in the stopband of the filter. It is believed that the reason of these spurious responses may return to the low grounding of the tuning screws. In more details, the use of the Teflon plugs which are shown in figure 3.3.2 causes a weak contact with the common ground circuit although they were attached to the ground through grounded washer and pins. The second suspected reason is the leakage of the electromagnetic field through the holes surrounding the rods of the screws. So, the fields are contained under the metallic cover which holds the main screw that control the movement of all tuning screws, this in turn may influence the characteristic impedances of the filter elements.



(a)



(b)

Figure 3.13 The manufactured mechanically tuned SSS lowpass filter (a) Side View
(b) Prospective View

3.4 Conclusion:

A shielded suspended substrate stripline generalized Chebyshev lowpass filter is designed and implemented. This project is achieved in two phases, the first one is the designing and implementing the fixed frequency lowpass filter with cut off frequency of 1.784GHz with superb selectivity. The second phase is the tuning of the implemented filter. A mechanical tuning structure is designed, fabricated and used to tune the proposed SSS Filter as the first work of its kind used to tune suspended substrate stripline planar lowpass filter. Despite the slight difference between the simulated and measured results that may have been occurred due to a fault in the designed tuning mechanism, the main objective of this project has been achieved. However, better compatibility between the measured and simulated responses can be obtained by more modification of the tuning structure. In addition to that, the tuning technique can be automated by adding modern servo motors to obtain more accurate results, however, this equipment is very expensive and need high budget to buy them.

Tunable combined Microstrip (MS) and Suspended Substrate Stripline (SSS) combine bandpass filter with two transmission zeros

4.1 Introduction

Given the recent high demand for modern communication methods, and the crowded marketplace for wireless communications, bandpass filters perform various functions in instrumentation subsystems, radio communications and radars, for instance searching receivers and detection devices. Moreover, this filter is suited for the S band applications covering the frequency range from 2-4 GHz where communications satellites as well as surface ship and weather radars are all potential applications.

Different methods are applied to design bandpass filters, including the lowpass prototype filter transformation method and the image method. Furthermore, several topologies have been used to design SSL [1], such as interdigital filters [2] and [3], capacitive gap filters [4]–[6], combline filters [7] and cascaded filters [8]. However, it is claimed that the short-circuited transmission lines may increase the filter losses [1]. In this chapter, a new structure for a microstrip and suspended substrate stripline (SSS) combination will be introduced. The proposed filter is composed of a combline filter, which is designed as an SSS, and two microstrip transmission zero extractors on either side of the filter. Such a diverse design provides two important characteristics – high-Q resonators and integration simplicity with other devices of a system. Moreover, using coupling reducers between the resonators contributed greatly to reducing the size of the filter, and effectively controlling the coupling between the adjacent resonators [9]. Equally, the transmission zero extracting method selected provides a simple way to tune both the upper and lower zeros, rather than the traditional method, namely cross-coupling. The combline filter topology has been chosen due to its distinguishing features, including its relatively small size and broad stopband.

This chapter is divided into six sections, with the first one explaining the combined bandpass filter's design methodology. This section addresses the design of proposed filter as a lumped element circuit in detail. Next, the internal and external couplings of this structure are highlighted in the second section. The third section introduces the realisation of the distributed bandpass with complete distributed circuit design and full-wave simulated results. The fourth section discusses all the implementation procedures and presents and discusses the measured results. The fifth section focuses on the filter's tuning process, including the biasing circuit of the tuning elements. It also outlines the techniques used to overcome the various difficulties encountered. Additionally, the simulated and measured results are introduced alongside a full description of the findings.

4.2 Design methodology of the Four-Pole Combined MS and SSS Combine filter with two transmission Zeros BP Filter.

A combline filter is a famous topology which is characterized by a simple design, a wide stopband and a small size compared with other types such as an interdigital filter structure [10]. It is typically composed of magnetically coupled resonators. These resonators are grounded at one end and open-circuited at the second far end, while the magnetic coupling is achieved through J-inverters, which are modelled as inductor networks located between the resonators. The equivalent circuit model of the conventional combline filter and J-inverter network are shown in Figures 4.1 (a) and (b) respectively, with the knowledge that the source ports could be coupled directly or magnetically to the circuit.

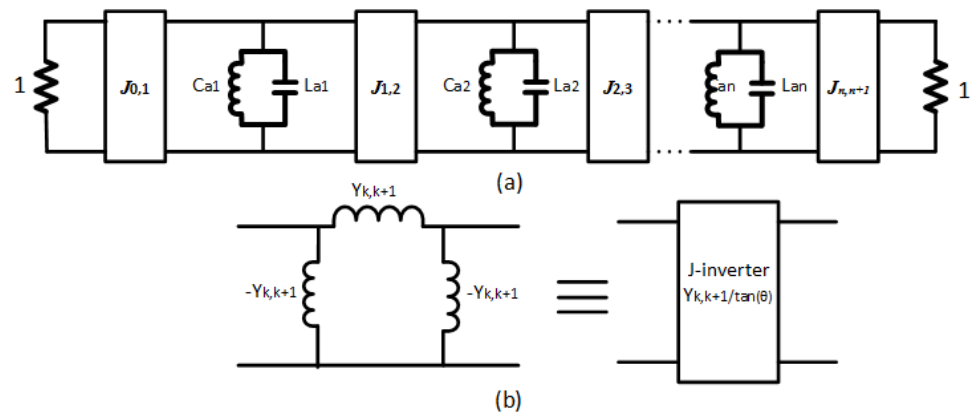


Figure 4.1 Conventional equivalent circuit of (a) Combline filter (b) J-inverter

The centre frequency of the filter is determined by the resonance frequency of the resonators as follows:

$$f_o = \sqrt{C_{an} * L_{an}} \quad 4.1$$

whereas the bandwidth of the filter can be controlled by controlling the coupling inverters $J_{k,k+1}$, where $k = 1, 2, \dots, n - 1$. Moreover, the external coupling which normally affects the quality factor of the filter is controlled by $J_{0,1}$ and $J_{n,n+1}$, where n equals the order of the filter, given that all J-inverters are symbolised as network of inductors in the equivalent circuit of the combline filters as shown above in Figure 4.1 (b). However, the mathematical discussion of the conventional combline filter is offered in [40].

In contrast to the conventional combline filters, the proposed filter uses three coupling reducers placed between the resonators of the filter. Their function is to adjust the mutual coupling between the coupled resonators, and to contribute to minimising the filter circuit's overall size. The coupling reducer is symbolised as an inductance network, as shown in the equivalent circuit model of the designed filter in Figure 4.2 (a). The method for using the coupling reducer is analysed in more detail later on in this chapter. However, it has been proved in [28] that the shorted inductors of the network, which are presented as Y_{c1} , will be absorbed by their adjacent inductance of the resonators. The absorption of these elements will lead the equivalent circuit to be similar to that of the conventional combline filter. Moreover, a frequency deviation might occur due to the change in the resonator inductances. A detailed explanation of the coupling reducers and the technique used to mitigate the expected frequency deviation is presented later in this chapter.

Equally, the proposed filter introduces a new way of generating the transmission zero. This method depends on adding two MS resonators, which are put on either side of the input and output ports, rather than exploiting the cross-coupling which may exist between non-adjacent resonators. The proposed method is aimed at simplifying the controlling the locations of the attenuation poles. The circuit model of the designed filter and the simulated response are introduced in Figures 4.2 (a) and (b) respectively.

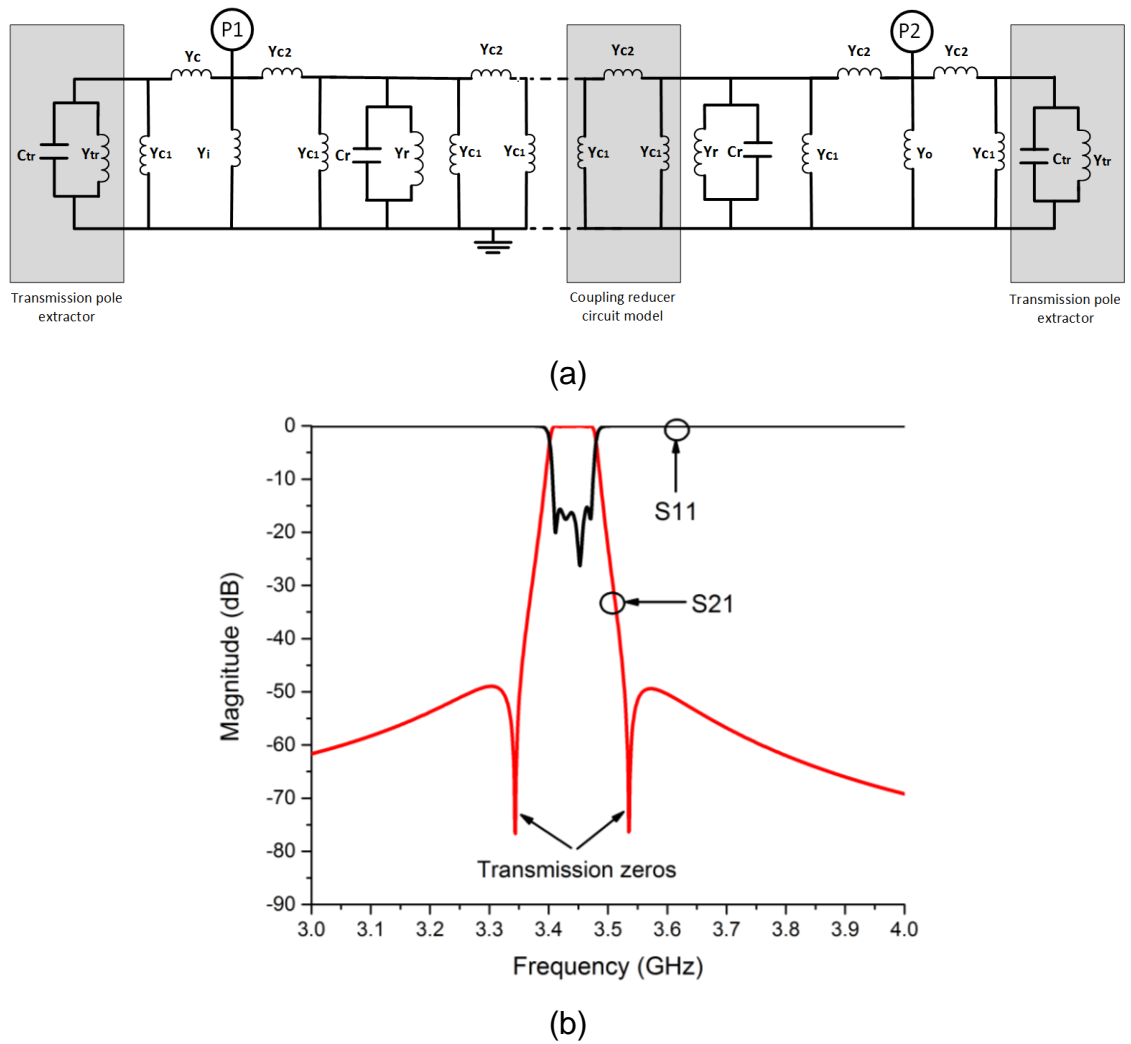


Figure 4.2 The combined MS and SSS BPF (a) Circuit model (b) Simulated response.

4.3 The extraction method for the mutual coupling ($M_{i,i+1}$) and external quality factor (Q_{en}) of the combined MS and SSS BPF

The method presented below may provide a direct and easy method for determining the filter's required dimensions [40]. This method uses another set of parameters to determine the width of the filter elements and the gap between them. These parameters are the mutual coupling between the resonators ($M_{i,i+1}$) and external quality factors (Q_{e1} and Q_{en}) between the first and last resonators and their adjacent input and output ports respectively as shown in figure 4.3. The reason for preferring this method over others is the difficulty of including the exact level of the

parasitic capacitance effect such as open-end fringing, the coupling between non-adjacent resonators, the

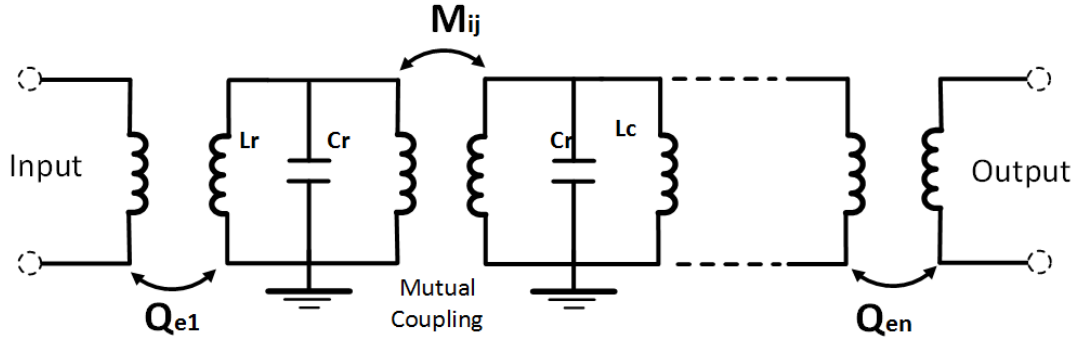


Figure 4.3 Coupling relations between filter's components

effect of the via holes inductance [74] and the effect surrounding box's machining tolerance of the wave travelling channel. These design parameters are given by [40]:

$$M_{i,i+1} = \frac{J_{i,i+1}}{\sqrt{b_i b_{i+1}}} = \frac{FBW}{\sqrt{g_i g_{i+1}}} \quad 4.2$$

$$Q_{e1} = \frac{b_i}{J_{01}^2 / Y_A} = \frac{g_0 g_1}{FBW} \quad 4.3$$

$$Q_{en} = \frac{b_n}{J_{n,n+1}^2 / Y_A} = \frac{g_n g_{n+1}}{FBW} \quad 4.4$$

where, $M_{i,i+1}$ is the mutual coupling coefficient between the neighbouring resonators, $J_{i,i+1}$ is the admittance inverter between the filter's elements, g_i, g_{i+1} are the elements' values of the lowpass prototype filter for $i = 0$ to $n + 1$, Y_A is the terminating line admittance, FBW is the fractional bandwidth of the filter and b_i, b_{i+1} are the susceptance parameters of the resonators for $i = 1$ to n . Whereas, Q_{e1} and Q_{en} are the external coupling coefficients at the input and output. The next phase of this approach is to satisfy the equations (4.2), (4.3) and (4.04) by using full-wave electromagnetic (EM) simulation technique.

In the following sub-sections, the proposed technique discusses the calculated parameters separately.

4.3.1 External coupling extraction

The external coupling coefficients can be extracted using two approaches depending on the obtained reflection response S_{11} . These are the phase response method and the group delay approach of the return loss response S_{11} [40], where the phase response is described as a relation between the phase of the input signal and the output signal passing through a two-port network [75] while group delay is defined in [76] as the time of propagation of the envelope of a wave between two points provided that the envelope is not significantly distorted time. In terms of input admittance of the coupled resonator and the attached conductance (G), the resonator reflection coefficient S_{11} at the excitation port can be expressed as [40].

$$S_{11} = \frac{1 - Y_{in}/G}{1 + Y_{in}/G} \quad 4.5$$

Where

$$Y_{in} = j\omega c \left(\frac{\omega}{\omega_o} - \frac{\omega_o}{\omega} \right) \quad 4.6$$

When, $\omega = \omega_o + \Delta\omega$ and $\omega_o = \sqrt{LC}$, then

$$Y_{in} = j\omega_o c \frac{2\Delta\omega}{\omega_o} \quad 4.7$$

By substituting (4.7) into (4.5), the reflection response at the excitation port can be expressed as [40]

$$S_{11} = \frac{1 - jQ_e(2\Delta\omega/\omega_o)}{1 + jQ_e(2\Delta\omega/\omega_o)} \quad 4.8$$

Where

$$Q_e = \omega_o C / G \quad 4.9$$

It should be noticed that, although $S_{11} = 1$ at resonance, the phase response changes against frequency, as depicted in Figure 4.4 [40]. It is shown that the bandwidth between $\pm 90^\circ$ is equal to:

$$\Delta\omega_{\pm 90} = \Delta\omega_+ - \Delta\omega_- = \frac{\omega_o}{Q_e} \quad 4.10$$

Therefore, the external quality factor by using phase response approach can be introduced as:

$$Q_e = \frac{\omega_o}{\Delta\omega_{\pm 90}} \quad 4.11$$

A phase shift may occur if there is a difference in the reference plane of the design, where the reference plane is an imaginary plane perpendicular to the wave propagation direction at which the circuit is analysed from, so that the shift increases as the difference increases. According to [40], in this case the determination of the $\Delta\omega_{\pm 90}$ should be applied from the frequency at which phase shift ± 90 occurs with respect to the absolute phase at ω_o .

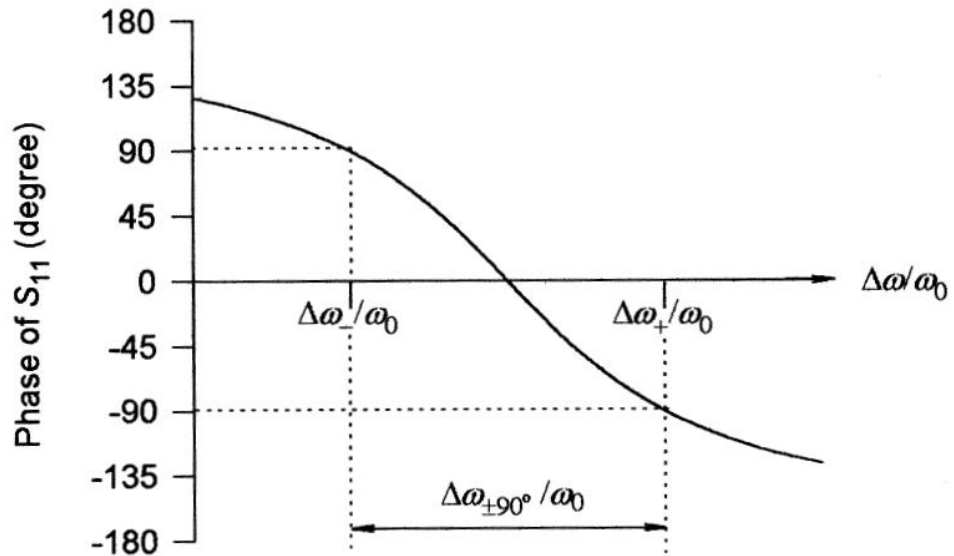


Figure 4.4 phase response of S_{11} [40].

Alternatively, the group delay as shown in Figure 4.5 can be used to extract the Q_e , the group delay could be presented as [40],

$$\tau_{s11}(\omega) = \frac{4Q_e}{\omega_o} \frac{1}{1 + (2Q_e\Delta\omega/\omega_o)^2} \quad 4.12$$

Since $\omega = \omega_o + \Delta\omega$, where $\Delta\omega = 0$ at resonance

$$\tau_{s11}(\omega) = \frac{4Q_e}{\omega_o} \frac{1}{1 + (2Q_e \cdot (\omega_o/\omega_o))^2} \quad 4.13$$

Since $\frac{1}{1+(2Q_e)^2} \ll 1$, then the maximum value of the group delay in equation 4.13 reaches when

$$\tau_{s11}(\omega_o) = \frac{4Q_e}{\omega_o} \quad 4.14$$

Once the group delay is found from the simulated or measured result as shown in figure 4.5, the external quality factor can be calculated by applying equation 4.15.

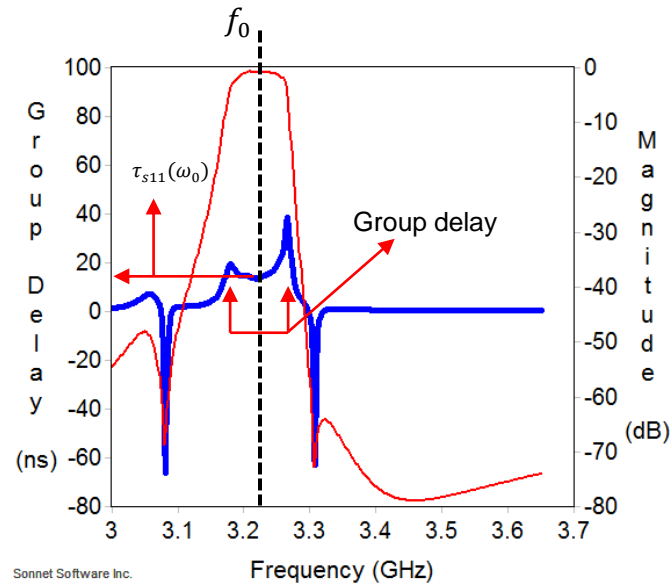


Figure 4.5 Group delay of a bandpass filter

$$Q_e = \frac{\omega_o \cdot \tau_{s11}(\omega_o)}{4} \quad 4.15$$

It is reported in [40] that an extra group delay may be added if two conditions are satisfied. These conditions are when the reference planes of the simulated reflection response S_{11} and that of the singly loaded resonators circuit are not coincided, the second is when the added phase shift is a frequency dependent. Nevertheless, the resonance frequency should be capable of being determined from group delay simulated frequency response. The last phase of this approach is to extract the required gaps between the resonators. This can be achieved by using a design curve for the simulated external couplings against the separation gaps to find the exact value satisfying the external quality factors which are calculated by using equations (4.3) and (4.4).

4.3.2 Mutual coupling extraction

The second phase of this extraction method is to address the internal gaps between the coupled resonators by extracting the mutual coupling coefficients. This method has been described extensively in [40] for electric, magnetic and mixed coupling structures. In the SSS planar filters, the absorption of the electromagnetic fields is smaller than that of other planar filters due to a reduction in the dielectric constant. For the combline filter topology, most of the current exists near the short-circuited end and it reduces slightly along the edges of the transmission lines, leading to a decrease in the magnetic field between the transmission lines, and it becomes larger as it closes the opposite short-circuited end. The electric field remains constant between the transmission lines, and increases at the open-circuited end [74]. In [40], it has been proven that the superposition of both electric and magnetic coupling leads to what is called mixed coupling. Furthermore, it emphasises that both couplings may cancel each other out if the mutual inductance or capacitance has been allowed to change its sign. Nevertheless, it is believed that the predominant coupling in the proposed filter is the magnetic one due to the existence of the coupling reducers between the transmission lines, which mitigate the cross-coupling between non-adjacent lines. The general formula of the coupling coefficient extraction can be expressed as [40]:

$$k = \frac{f_{p2}^2 - f_{p1}^2}{f_{p2}^2 + f_{p1}^2} \quad 4.16$$

where, f_{p1} and f_{p2} are characteristic frequencies corresponding to resonant frequency of the electric or magnetic coupling. The typical response of the coupled resonators is shown in Figure 4.6. The distance between the two resonant peaks depends on the strength of the coupling so that the strongest coupling leads to a wider separation and deeper trough [40].

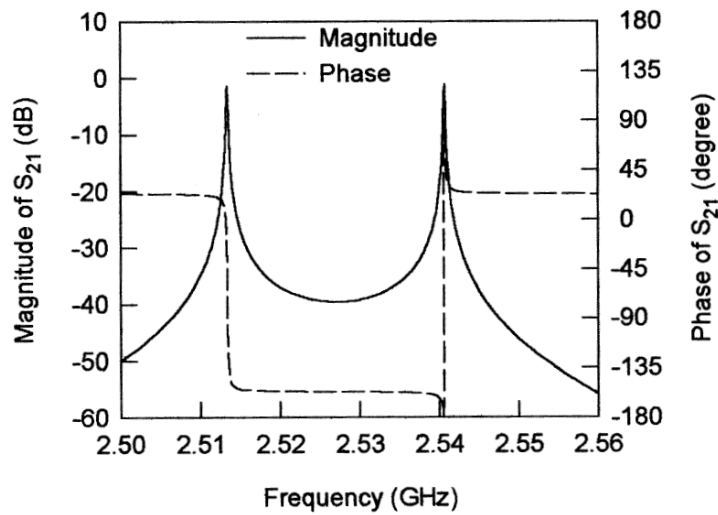


Figure 4.6 typical response of the coupled resonator [40].

4.4 Transmission zeros extraction method.

Transmission zeros are a major issue when working with microwave filters due their importance in the design and implementation of high-selectivity filters.

There are several methods for implementing transmission zeros, however, most of them depend on introducing a cross-coupling between non-adjacent resonators [40]. In the current design, the transmission zeros were extracted by using a couple of pole extractors on either side of the input and output ports. Compared with the cross-coupling method, this way leads to a simpler method for handling the filter's selectivity by controlling the locations of the transmission poles on both sides of the filter's response. The circuit model of the presented extraction method is depicted above in Figure 4.3. The extractors are simply a couple of resonators located at either side of the input and output ports, and they are also magnetically coupled to them. The design of these resonators was started by selecting the resonance frequency of each resonator by using the following equation:

$$f_o = \frac{1}{2\pi\sqrt{L_{Tn}C_{Tn}}} \text{ for } n = 1 \text{ and } 2 \quad 4.17$$

where L_{Tn} and C_{Tn} are the inductance and capacitance of the first and second transmission zero extractors.

The realisation of the resonators began by obtaining the microstrip transmission lines' parameters, namely length and width. These parameters are presented in [40] as follows [40]:

$$\lambda_g = \frac{300}{f_o(\text{GHz})\sqrt{\epsilon_{re}}} \text{ mm} \quad 4.18$$

where c (the speed of light in free space) $\cong 3 \times 10^8 \text{ m/s}$, and ϵ_{re} is the effective dielectric constant calculated with the following equation:

$$\epsilon_{re} = \frac{\epsilon_r + 1}{2} + \frac{\epsilon_r - 1}{2} \left(1 + \frac{10}{u}\right)^{-ab} \quad 4.19$$

where $u = W/h$, and:

$$a = 1 + \frac{1}{49} \ln \left(\frac{u^4 + \left(\frac{u}{52}\right)^2}{u^4 + 0.432} \right) + \frac{1}{18.7} \ln \left[1 + \left(\frac{u}{18.1}\right)^3 \right] \quad 4.20$$

$$b = 0.564 \left(\frac{\epsilon_r - 0.9}{\epsilon_r + 0.3} \right)^{0.053} \quad 4.21$$

The impedance of the transmission line is calculated as follows:

$$Z_c = \frac{\eta}{2\pi\sqrt{\epsilon_{re}}} \ln \left[\frac{F}{u} + \sqrt{1 + \left(\frac{2}{u}\right)^2} \right] \quad 4.22$$

Where, $\eta = 120\pi$, and

$$F = 6 + (2\pi - 6) \exp \left[- \left(\frac{30.666}{u} \right)^{0.7528} \right] \quad 4.23$$

The synthesis of $\frac{W}{h}$ is also discussed in [40]. This ratio has two possibilities, these are whether $\frac{W}{h} \leq 2$ or $\frac{W}{h} \geq 2$. In the case where $\frac{W}{h} \leq 2$, then [40]:

$$\frac{W}{h} = \frac{8 \exp(4)}{\exp(2A) - 2} \quad 4.24$$

Where

$$A = \frac{Z_c}{60} \left(\frac{\epsilon_r + 1}{2} \right)^{0.5} + \frac{\epsilon_r - 1}{\epsilon_r + 1} \left(0.23 + \frac{0.11}{\epsilon_r} \right) \quad 4.25$$

Otherwise

$$\frac{W}{h} = \frac{2}{\pi} \left\{ (B - 1) - \ln(2 * B - 1) + \frac{\epsilon_r - 1}{2 * \epsilon_r} \left[\ln(B - 1) + 0.39 - \frac{0.61}{\epsilon_r} \right] \right\} \quad 4.26$$

$$\text{With } B = \frac{60\pi^2}{z_c \sqrt{\epsilon_r}}$$

Since this proposed design is not a pure microstrip or a suspended substrate stripline and the resonators may suffer from a weak cross-coupling with the first and last SSS resonators, it was essential to perform another step to obtain the accurate parameters satisfying the required filter specifications. The next phase in the design process is the EM full-wave simulation to extract the accurate dimensions of the filter's elements and required distances between them by using simulation graphs. The proposed design method for the transmission zeros extractors is presented extensively in the next section, including the elicitation of the accurate parameters using the design graphs.

4.5 Design Example of the fixed frequency combined MS and SSS combine BPF with two transmission zeros.

Assume that a four-pole Chebyshev lowpass prototype filter with a passband ripple of 0.1dB has been chosen. The parameters of the lowpass prototype filter are [40] $g_0 = 1$, $g_1 = 1.1088$, $g_2 = 1.3062$, $g_3 = 1.7704$, $g_4 = 0.08181$, $g_5 = 1.3554$. The bandpass combline filter is designed to have a fractional bandwidth of 2% at a midland frequency $f_0 = 3.31GHz$. By applying equations (4.02), (4.03) and (4.04) we obtain:

$$M_{12} = 0.01662 \quad M_{23} = 0.01315$$

$$M_{34} = 0.05255 \quad M_{45} = 0.06006$$

$$Q_{e1} = 55.44 \quad Q_{e4} = 5.544$$

The filter is built on a Roger substrate RO3003 with a dielectric constant of 3, a thickness of 0.5mm and a tangent loss of 0.0013, while the design is put in an aluminium box with dimensions of 53mm x 13mm x 29.1mm. This substrate will be settled in an aluminium box which is machined to include both Microstrip and Suspended sections as shown in Figure 4.7.

The width of the coupled resonators can be calculated by using the following equation [55]:

$$W = \frac{b}{4} * \left(\frac{377.6}{Z_0 \sqrt{\epsilon_r}} - 1.84 \right) \quad (4.23)$$

where b is the suspended section height equal to the addition of heights above and underneath the substrates plus the thickness of the substrate in this example it equals 13mm, ϵ_r is the dielectric constant of the substrate. For the SSS situation, it depends on the ratio of the air volume to the thickness of the dielectric substrate. The air volume in this design is very big compared with the thin substrate used, therefore, ϵ_r is assumed to be equal to the dielectric constant of the air, which equals 1. The characteristic impedance (Z_0) of the resonators is assumed to be equal to 120 Ω , this value has been chosen for better manufacturing tolerance and better etching resolution of the distributed transmission line. According to these values, the width was found to be equal to 4mm

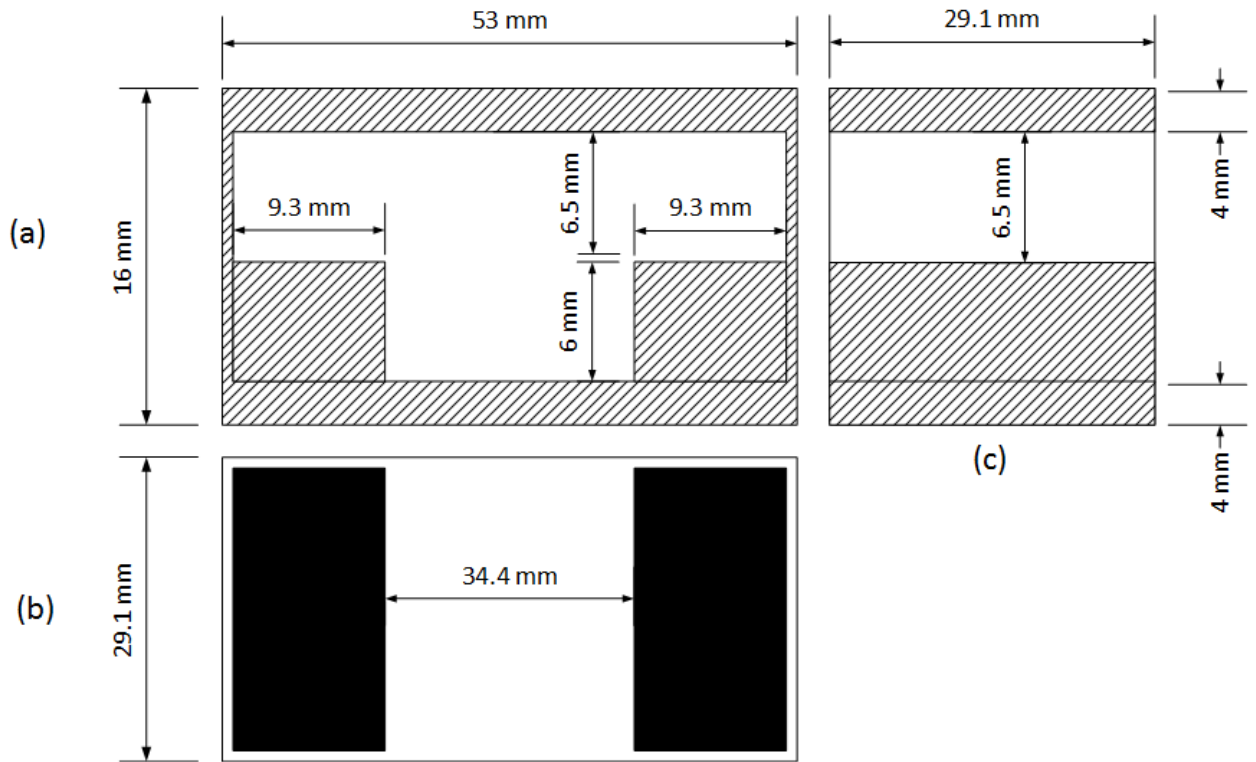


Figure 4.7 Aluminium Enclosure of the filter (a) Front cross section view (b) Top view (c) right cross section view.

Equally, their lengths are assumed to be slightly less than $\lambda/4$ at the filter's resonance frequency f_o , for this design the lengths of the resonators are equal to 17mm. The input and output transmission lines are designed as a microstrip transmission lines, and have a width of 1.1 mm, which is the equivalent of 50Ω terminating impedances[40]. The layout of the distributed circuits used for full-wave electromagnetic (EM) simulation to extract the design parameters $M_{i,i+1}$, Q_{e1} and Q_{en} are shown in Figures 4.8 and 4.8 respectively.

The extraction of the coupling coefficient process is initiated by setting up the full-wave electromagnetic (EM) simulation software, namely sonnet® [36]. The preparation of the software includes the choice of the substrate from the software library and entering the dielectric layers thicknesses of the substrate and the air above and underneath it. In this design, these thicknesses are 0.5mm, 6.5mm and 6mm respectively. Secondly, the resonators, which having the dimensions mentioned earlier and are drawn and separated using a coupling reducer.

After that, the resonators are positioned with their relevant coupling reducer in the middle of the virtual aluminium box, so that the distance between them and the source ports becomes far enough. Next simulation is performed at different gaps (S_1 and S_2) and calculate the coupling coefficient of ($S_1 + S_2$) by applying equation (4.12). The next step is to use the design curve of the coupling coefficient where the y-axis of this graph will host the simulated value of the $M_{i,i+1}$, while the selected distances of the simulation are on the x-axis. After repeating this step for many distances, the required gap can be extracted by locating the calculated value of the $M_{i,i+1}$ on the design curve to find its related distance. Bear in mind that the theoretical coupling coefficient is calculated using the formula (4.2) and placed on the design curve shown in Figure 4.10 (a).

The external coupling extraction used a methodology in which Q_{e1} and Q_{en} were examined separately. This is shown in Figure 4.9, in which the bold wide line represents the Q_{e1} , while the second represents Q_{en} . For instance, in the extraction of the Q_{e1} , the first resonator is set near the input port and quite far from the output to satisfy the condition of the single-loaded resonator method mentioned in Section 4.3.1. The resonator location can be adjusted towards or away from the input source and, after the simulation is run, this distance is symbolised as (S_1), so that at each step the simulated external coupling is located on the design curve of the external coupling shown in Figure 4.9. After several simulations at different spaces, the required gap is obtained by locating the calculated Q_{e1} on the design curve of the external coupling curve, as shown below in Figure 10 (b). Similarly, the external coupling of the last resonator is accomplished by using the dotted resonator and removing the first one as shown in Figure 4.9.

The readings of the simulated coupling coefficients and external coupling are listed in Tables 1 and 2 respectively.

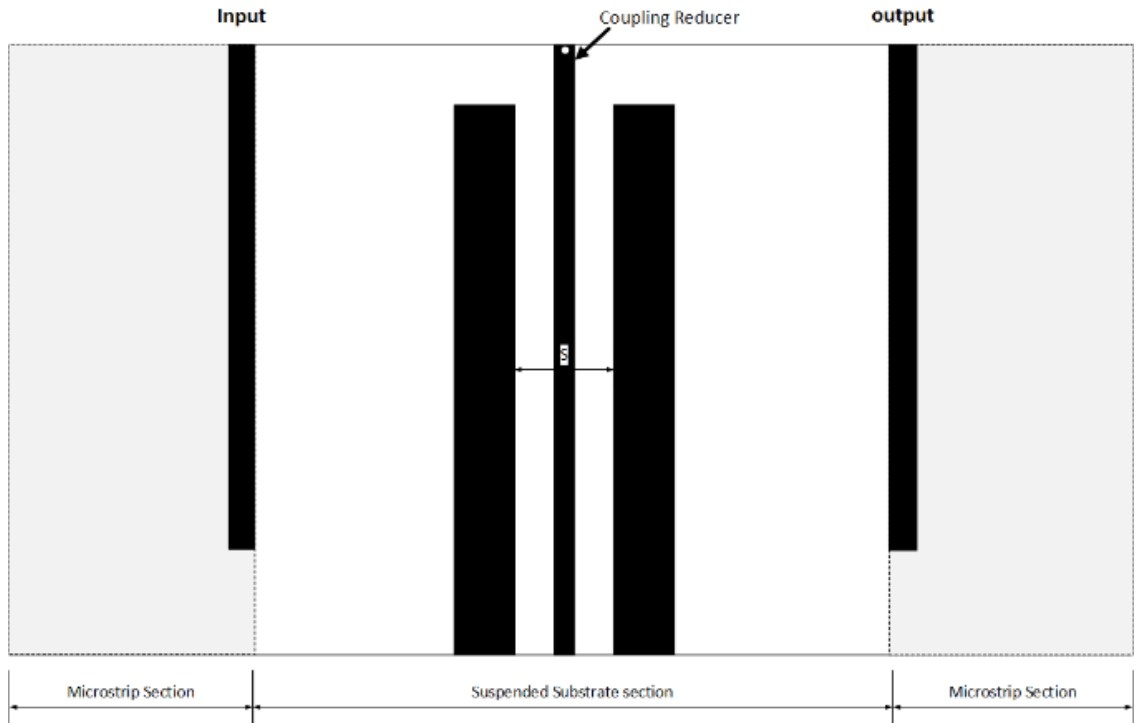


Figure 4.8 Methodology Layout of the Coupling Coefficient Extraction.

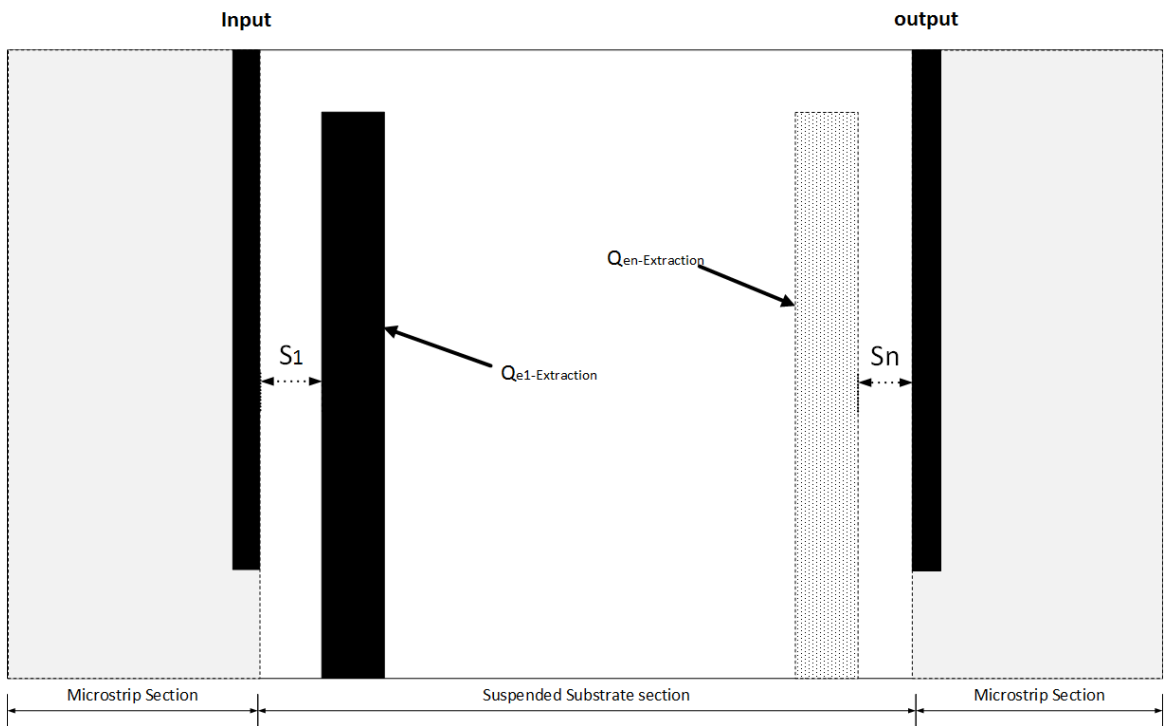


Figure 4.9 External coupling Extraction Methodology Layout.

Table 4.1 Simulated readings of the coupling coefficients

S	M_{12}	M_{23}	M_{34}
0.7	0.02844	0.02594	0.02713
1.4	0.02658	0.02409	0.02589
2.1	0.02534	0.02286	0.02466
2.8	0.02351	0.02104	0.02283
3.5	0.02229	0.02042	0.02163
4.2	0.02108	0.01921	0.02103
4.7	0.02047	0.01799	0.01921
5.4	0.01925	0.01679	0.01801
6.1	0.01805	0.01559	0.01679
6.8	0.01684	0.01498	0.01559
7.5	0.01624	0.01378	0.01498

Table 4.2 Simulated readings of the external couplings

S	Q_{e1}	Q_{e4}
0.1	9.89	5.1
0.3	16.37	8.1
0.5	22.02	11.1
0.7	28.07	14.2
0.9	34.12	17.4
1.1	41.46	20.9
1.3	49.39	24.5
1.5	54.66	28.4
1.7	66.15	31.8
1.9	77.51	36.96
2.1	83.74	40.5

The design curves of the simulated coupling coefficient and external coupling are presented in Figure 4.8.

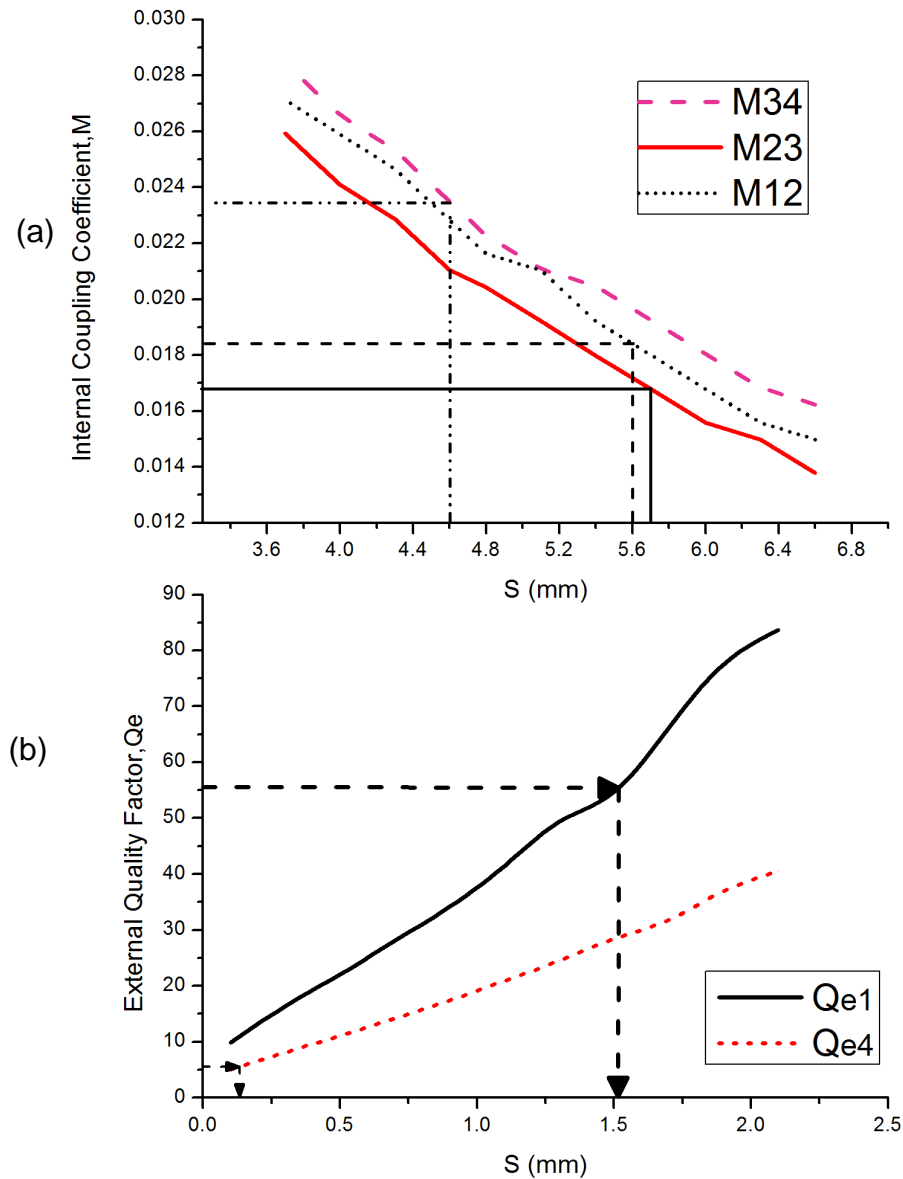


Figure 4.10 Design curves of the filter (a) Internal Coupling Coefficient (b) External Coupling Factor.

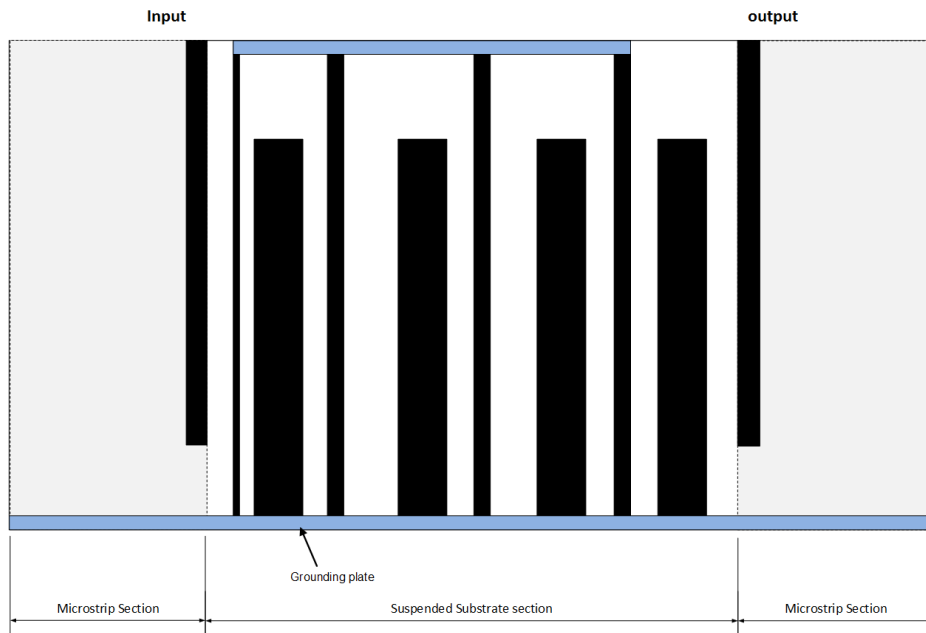
According to the previous readings in Tables 1 and 2, and by using the design curves in Figures 4.8 (a) and (b), the required distances in which the calculated coupling coefficients and external coupling have been satisfied are listed in Table 4.3.

Table 4.3 The extracted distance of the coupling coefficients and external coupling

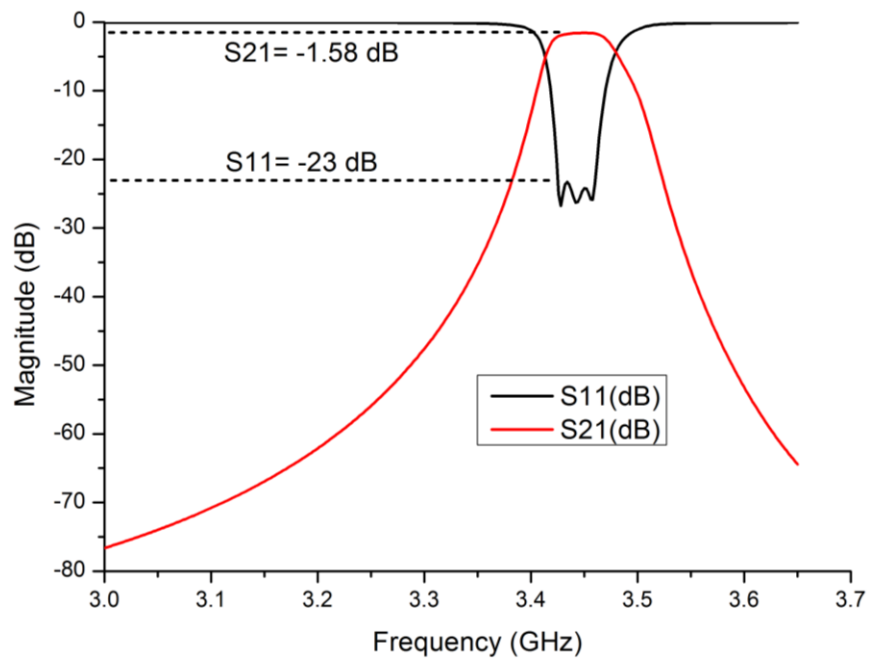
	M_{12}	M_{23}	M_{34}	Q_{e1}	Q_{e4}
S (mm)	5.6	5.7	4.6	1.51	0.13

The next step is to gather the filter's elements together and design them as a distributed element and apply the EM full-wave simulation on the structure to investigate the response and perform the required optimisations if needed. The

complete structure of the (SSS) Chebyshev combline filter, in which the input and output transmission lines are designed as a microstrip structure, and its response, are shown in Figure 4.11 (a) and (b) respectively:



(a)



(b)

Figure 4.11 Combined SSS and MS Chebyshev combline filter (a) Filter circuit (b) Filter response [77]

Figure 4.11 (a) shows that the resonators of the transmission zero have not yet been added, which may explain the flattest of the simulated response.

For the transmission zeros resonators, the required specifications were calculated using Equations 4.17 to 4.25 at $\epsilon_{re}=2.48$, $f_{01}=3.382\text{GHz}$ and $f_{02}=3.61\text{GHz}$, where f_{01} and f_{02} are the attenuation frequencies of the upper and lower attenuation poles. Furthermore, the lengths of the poles extractors are considered as a quarter of the guided wave length. Those lengths are calculated, and are equal to 14.4 for the first attenuator and 13.5 for the second. Both poles' resonators are designed to have the same characteristic impedance as an initial value acceptable for more optimisation, and the transmission line impedance is equal to 50.2Ω .

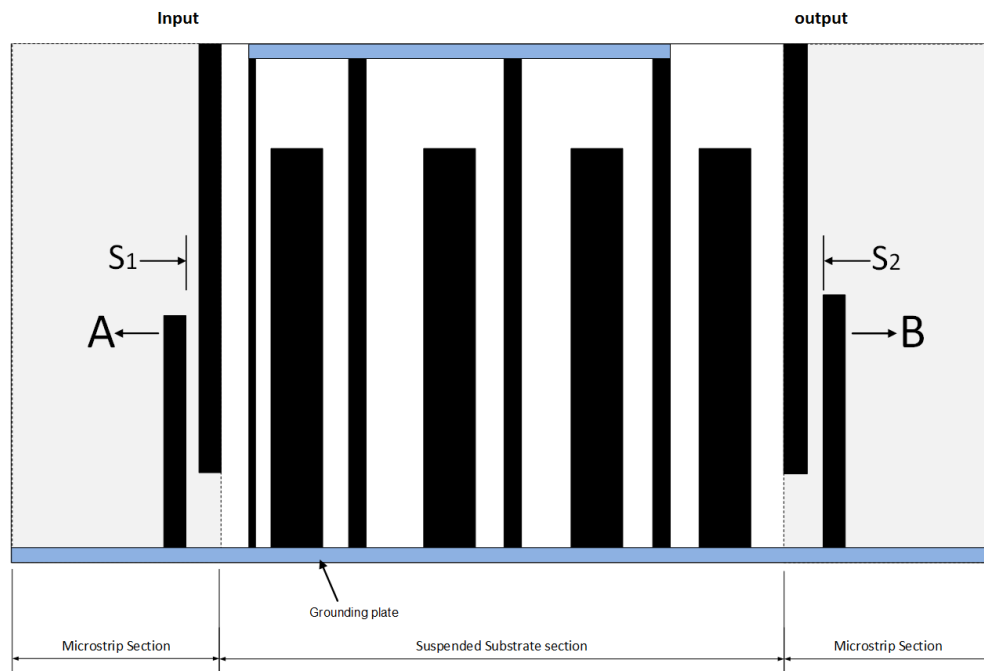


Figure 4.12 Combined SSS and MS Chebyshev including the resonators of the transmission zero [77]

The next step is the addition of the resonators of the transmission zero which are denoted as A and B, as depicted in Figure 4.12.

The resonator A extracts and controls the upper pole, while the resonator B for the lower pole. An EM full-wave simulation is carried out to optimise the width and the length of the poles extractors, whereas the gaps S_1 and S_2 were extracted using a design graph. The extraction method is performed on multi-steps so that at each step the gap and its related frequency were recorded in Origin data analyser software [78]. The processed data of gap A and gap B are shown in tables 4.4 where the lower transmission zero is generated by extractor B and upper transmission zero is extracted by A extractor. The next step is the choosing of the required transmission

location, in this step the appropriate location was selected by simulating the whole filter's structure at different extractors' gaps and choosing the best one.

Table 4.4 The processed data of the upper and lower transmission zeros

Gap	Lower Transmission zero frequencies	Upper Transmission zero frequencies
0.1	3.05	3.48
0.2	3.11	3.55
0.3	3.14	3.59
0.4	3.165	3.615
0.5	3.18	3.635
0.6	3.19	3.645
0.7	3.2	3.655
0.8	3.21	3.665
0.9	3.215	3.67
1	3.215	3.675
1.1	3.22	3.675
1.2	3.225	3.68
1.3	3.23	3.685
1.4	3.23	3.685
1.5	3.23	3.69
1.6	3.235	3.69
1.7	3.235	3.69
1.8	3.24	3.69
1.9	3.24	3.69
2	3.24	3.69

The optimised length and width of the first transmission pole extractor is equal to 1.1mm and 12.9mm respectively, while the second extractor dimensions equal 1.6mm and 13.5mm. The design graphs used to extract S1 and S2 are presented in Figure 4.13.

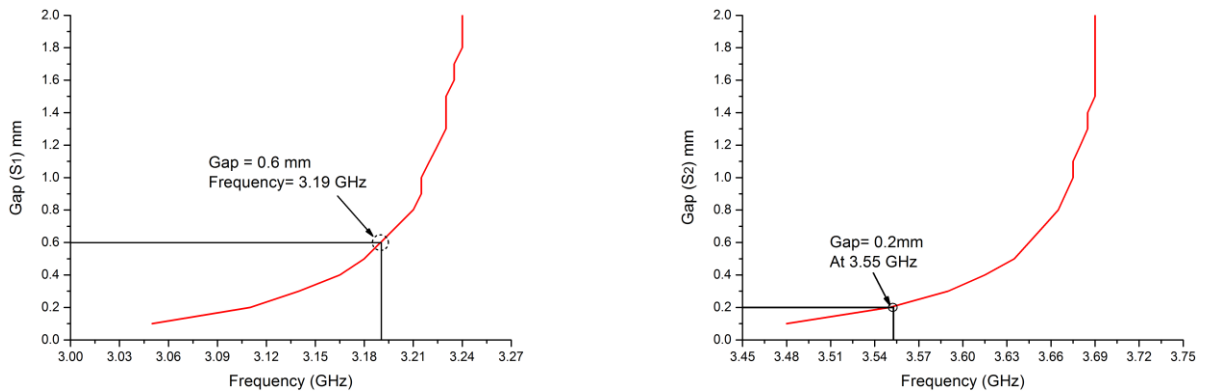


Figure 4.13 The processed design graphs of transmission Zero extractors (a) Lower transmission zero Gap (S1) (b) Upper transmission zero Gap (S2)

The final full-wave (EM) simulation response of the designed combined Microstrip and Suspended substrate stripline filter with two transmission zeros is shown in Figure 4.14. However, the explained processes of the Combined bandpass filter should fulfil the conditions of good selectivity, manufacturing simplicity and high resonator accuracy.

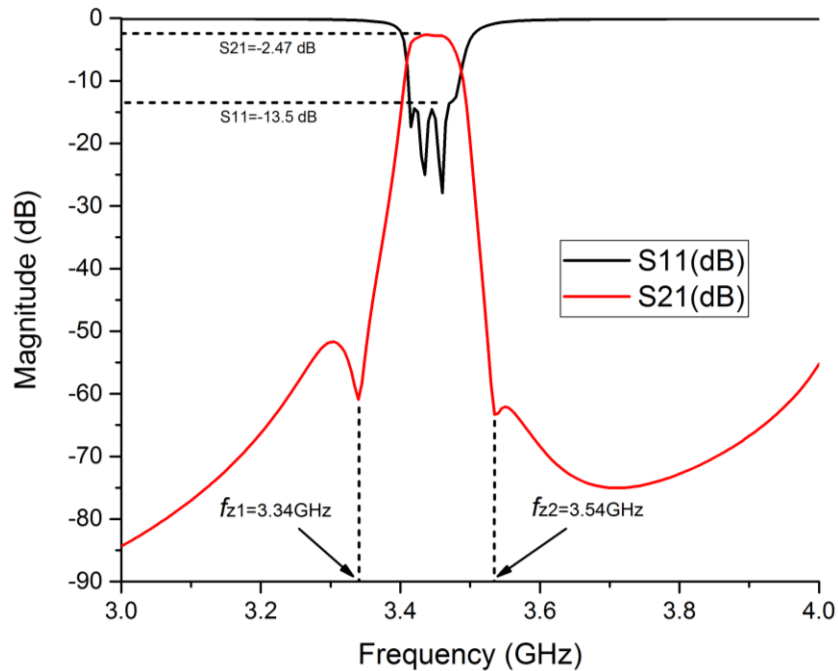


Figure 4.14 Simulated Combined SSS and MS Chebyshev Bandpass filter with two transmission zeros.

4.6 Results and discussion of the Simulated and measured responses of the fixed frequency combined MS and SSS bandpass filter

The combined MS and SSS bandpass filter with two transmission zeros has been fabricated and measured using HP 8510C Microwave Network Analyser. The measured and simulated results of the filter have been combined and are presented below in Figure 4.15. They show a good agreement between them in terms of the fractional bandwidth (FBW), and remarkable selectivity.

Nevertheless, a marked difference between the measured and simulated losses can be seen. The measured insertion and return losses were -4.23 dB and -14.32 dB respectively, whereas the simulated losses were -2.47 dB 13.5 dB for the insertion and return losses respectively. There are thought to be two reasons behind this variance. The first is the manufacturing tolerance of the aluminium box surrounding

the filter and the weak grounding of the filter's resonators, given that the tolerance is about $\pm 10\%$. Manufacturing tolerance is critical, especially at the edges of the Microstrip sections, and it may affect the impedance of the input and output transmission lines significantly. This effect may cause a mismatch increasing the

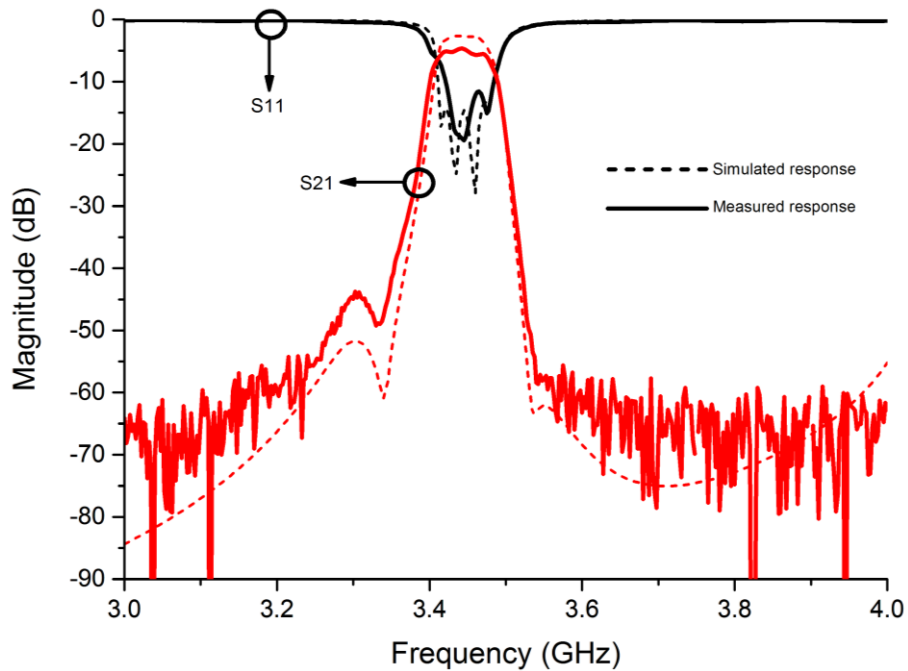


Figure 4.15 Simulated and measured responses of the Combined SSS and MS Chebyshev Bandpass filter with two transmission zeros [77]

reflected power from the source ports. The second expected reason for the lack of the grounding is the substrate and the grounding mechanism used. The used substrate is very soft, while the mechanism of the grounding relies on the upper half of the aluminium box overlapping the transmission line, as shown in Figure 4.16. Consequently, the screws connecting the box's two halves were tightened, leading to the compression of the dielectric substrate between them. This in turn led to a weak contact between the grounding plate and the bottom ends of the resonators.

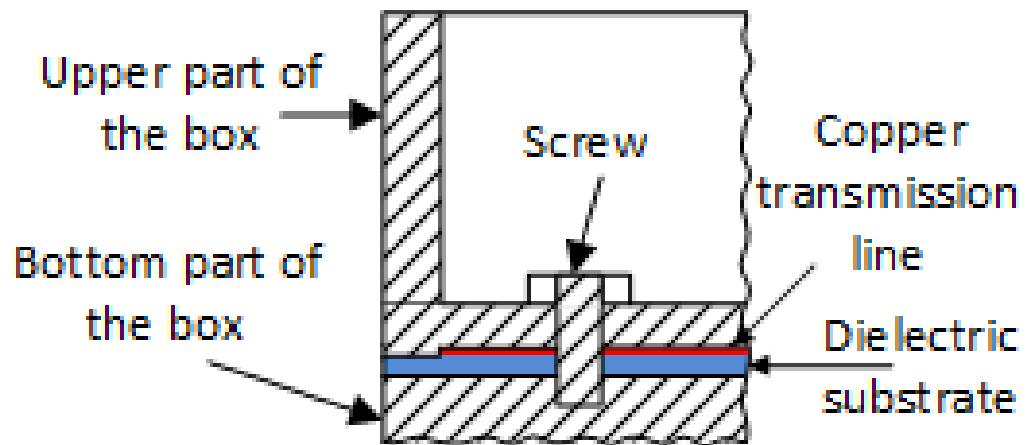


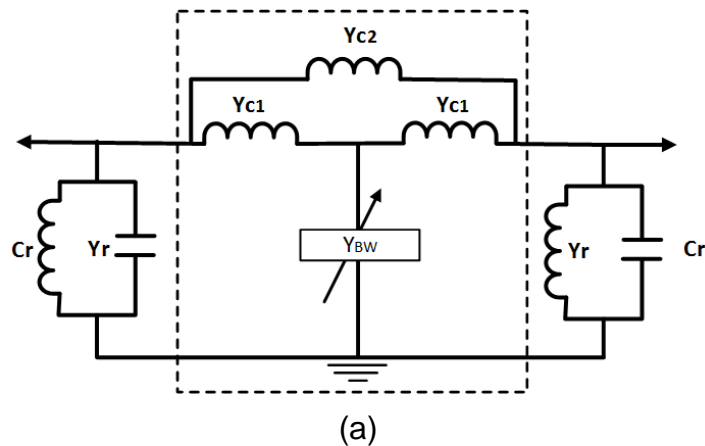
Figure 4.16 Used grounding structure

4.7 Tunable combined MS and SSS filter

In this section, the continuous tuning of the narrow bandwidth combined MS and SSS BPF filter and its relevant transmission zeros are discussed and supported by a numerical example, given that varactors are used in the tuning function.

4.7.1 Methodology of the bandwidth tuning

The proposed method for tuning the bandwidth of the combline filters is presented in [28]. This method proved that the bandwidth could be tuned by using a variable coupling subnetwork reducer between the coupled resonators. The authors clarified that the bandwidth tuning subnetwork could take two different structures according to the value of the variable admittance (Y_{BW}), as depicted in Figures 4.17 (a), (b) and (c) for $Y_{BW} \rightarrow \infty$ and $Y_{BW} \rightarrow 0$, respectively.



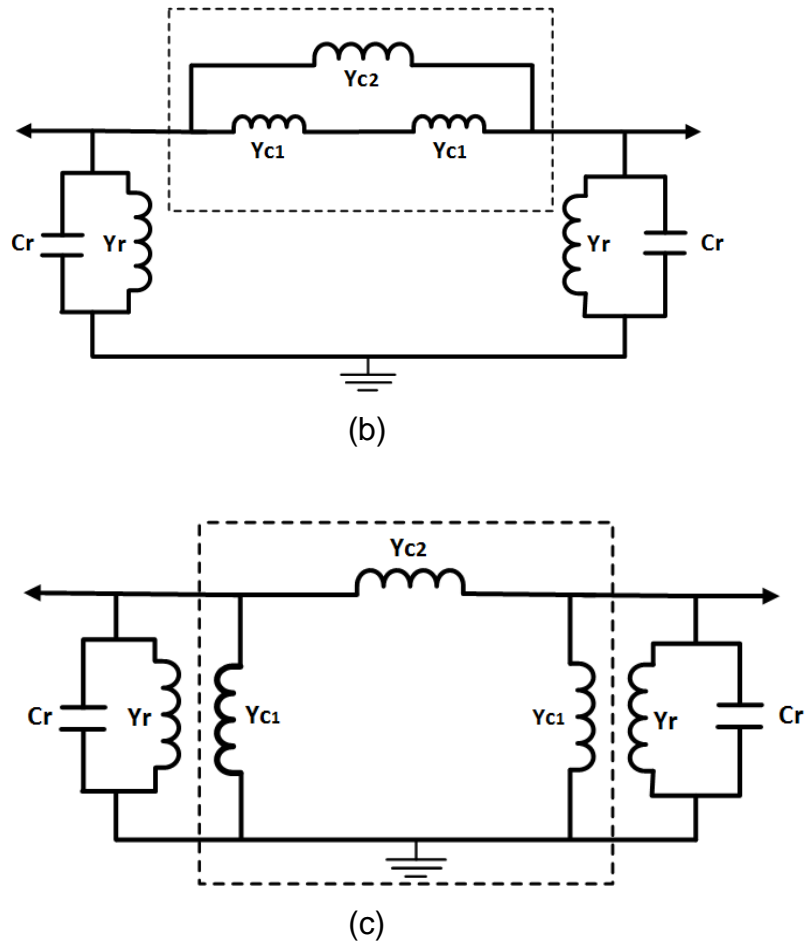


Figure 4.17 The coupling reducer subnetwork at (a) Bandwidth control subnetwork (b) $Y_{BW} \rightarrow 0$ (c) $Y_{BW} \rightarrow \infty$ [79]

By using the same principles of [28], the case where $Y_{BW} \rightarrow 0$, the equivalent admittance of the bandwidth control circuit of the proposed filter could be expressed as:

$$Y_C^{(0)} = \frac{Y_{c1}}{2} + Y_{c2} \quad 4.27$$

while the resonance frequency is the same as the LC resonator, that is:

$$f_0^0 = \frac{1}{2\pi\sqrt{C_r L_r}} \quad 4.28$$

where L_r and C_r are the inductance and capacitance of the LC resonators.

On the other hand, in the case where the admittance approaches infinity ($Y_{BW} \rightarrow \infty$), the circuit model of the coupled resonator is turned in to that of Figure 4.16 (C). As can be seen, the admittance Y_{c1} would be absorbed by their adjacent resonators,

which in turn leads to the circuit model being modified to be similar to the circuit model of the conventional combline filter as shown in Figure 4.18.

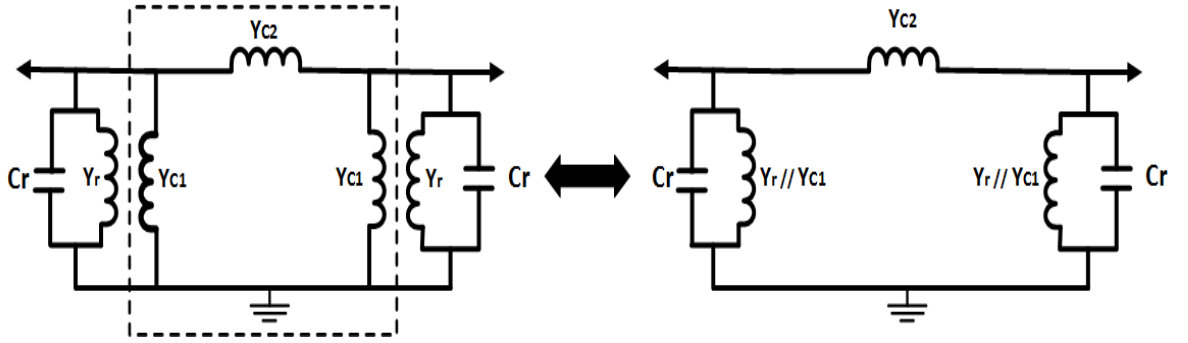


Figure 4.18 Circuit model of the combline filter with coupling reducer

Thus, the equivalent admittance of the circuit can be expressed as [28]:

$$Y_{Ceq} = Y_{c2} \quad 4.29$$

As is evident from Equations 4.26 and 4.28, $Y_c^{(\infty)} < Y_c^0$, so it can be deduced that the filter's bandwidth has reduced during the transition from $0 \rightarrow \infty$ states of the variable admittance of the coupling subnetwork shown in Figure 4.16 (a). Simultaneously, the resonance frequency of the filter could deviated slightly due to the alteration of the resonator inductance, this deviation is expressed in [28]:

$$\Delta f = \frac{\alpha - f_0^{(0)} \tan \theta_0^{(0)}}{\theta_0^{(0)} + \left(1 + \frac{\alpha \theta_0^{(0)}}{f_0^{(0)}}\right) \tan \theta_0^{(0)}} \quad 4.30$$

Where

$$\theta_0^{(0)} = \tan^{-1} \left(\frac{Y_r + Y_{c1} + Y_{c1}}{2\pi C_r f_0^0} \right) \quad 4.31$$

And

$$\alpha = \frac{Y_r + Y_{c1} + Y_{c2}}{2\pi C_r} \quad 4.32$$

Furthermore, due to the lack of grounding through the use of the overlap technique that was seen in previous work, the authors decided to use a different grounding method. This method uses the grounding VIAS connecting the bottom end of the

resonators to the ground through the metallic box. Since these VIAS function as an inductance connected in series to the resonators' admittances, they may add a slight frequency deviation to the resonance frequencies of those resonators. Therefore, their diameter should be chosen carefully to decrease the expected deviation as much as possible. However, the authors suggested the addition of a tuning elements to the resonators to overcome the issue of frequency deviation. This proposal has been applied by adding fine tuning screws above the resonators as shown in figure 4.19. The working principle of these screws is the same as the capacitor design, which is based on two opposite plates separated by an insulator. By changing the separating distance, the value of the capacitor changes according to this formula:

$$C = \frac{\epsilon_0 \epsilon_r A}{d} \text{ Farad} \quad 4.33$$

where ϵ_0 is the free-space electric constant that equals 8.854×10^{12} F/m, and ϵ_r is the dielectric constant of the insulator. In this design, it equals 1, for air, A is the area of the overlapped plates in square metres and d is the separating distance between the plates in meters.

This method has been chosen to reduce deviation because of the limited space. It also avoids the grounding complexity of the varactors' biasing circuits, and minimises the losses that occur due to use of the electronic components, given that these screws have been manually rotated because of the prohibitive cost of the servomotors which could be used to perform this function.

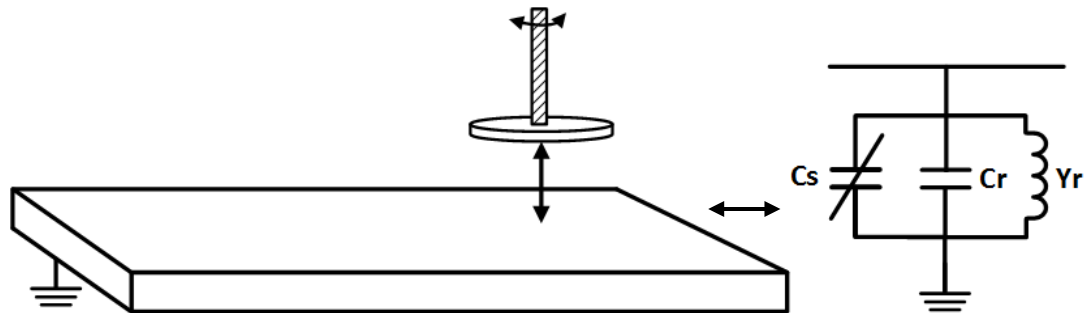


Figure 4.19 Fine tuning screws [80]

4.7.2 Design Example of the narrow bandwidth tunable combined MS and SSS combine BPF with two transmission zeros.

A narrow bandwidth tunable combined microstrip and suspended substrate stripline filter with two transmission zeros was designed and fabricated [80]. Firstly, the filter was designed and tuned as a lumped element circuit using a commercial design software that is Microsoft office (AWR) [81]. The circuit diagram and simulation result of the designed circuit is shown in Figures 4.20 (a) and (b):

The next step in the design is to transform the circuit from the lumped element to the distributed element form. The circuit was designed on a Roger substrate of 0.5mm thickness, a loss tangent of 0.0013 and a dielectric constant equal to 3, as depicted in Figure 4.21.

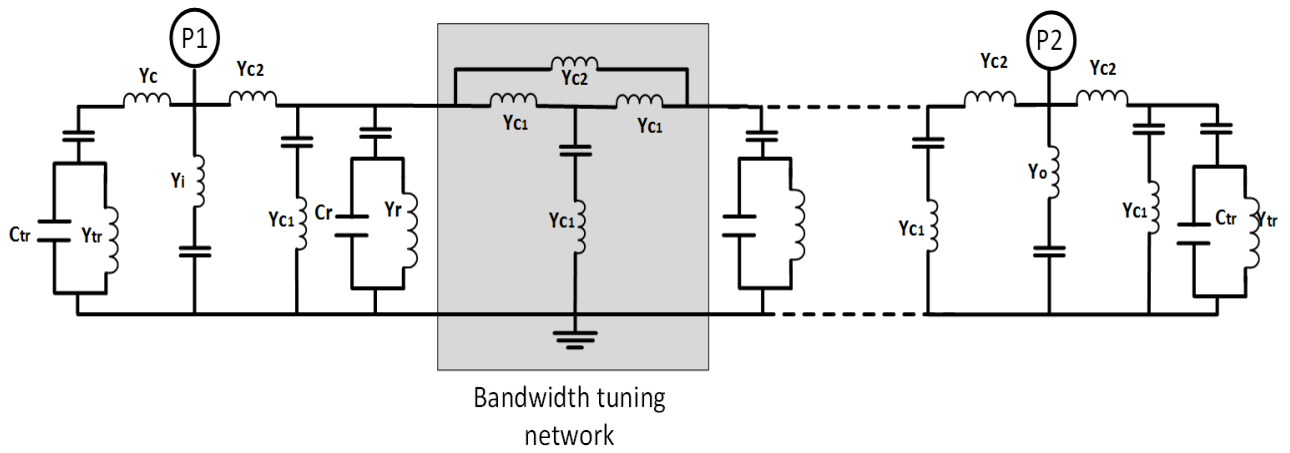
As clearly shown in Figure 4.21 (a), grounding was achieved using VIAS that connecting the far end of the resonators to the bottom grounded layer [80]. It was thought this method could provide the required level of grounding. The dimensions of the designed filter and the coupling distances between them are listed in Tables 4.5 and 4.6, respectively:

Table 4.5 Filter distributed elements' dimensions in (mm) [80]

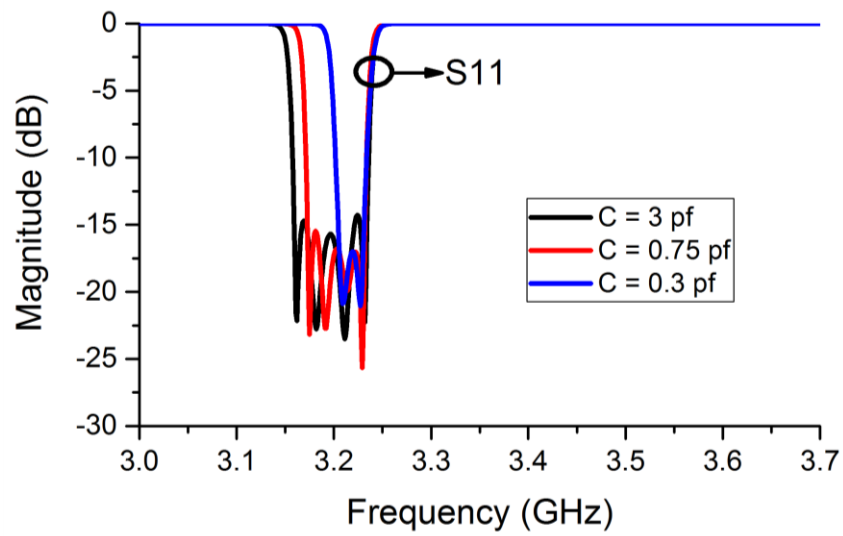
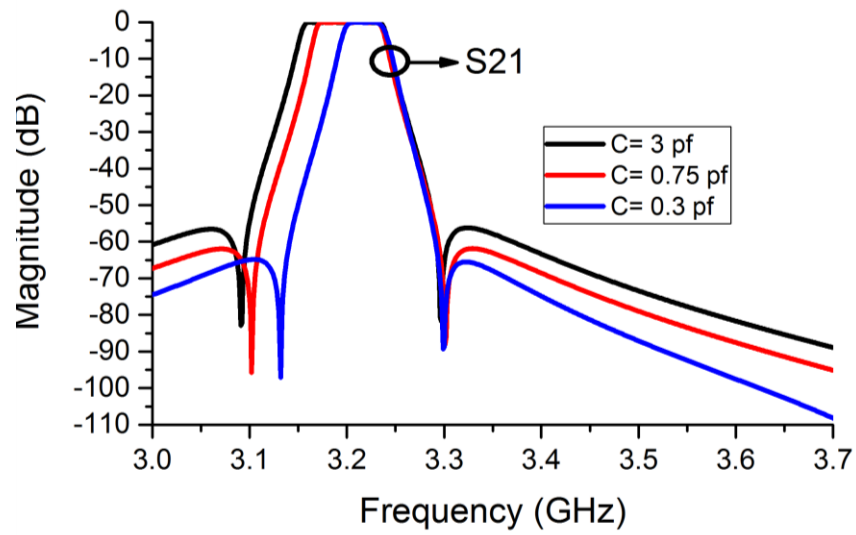
	Transmission zero extrac1	Transmission zero extrac2	Rsn1	Rsn2	Rsn3	Rsn4	CR1	CR2	CR3	CR4
Length	14.3	14.5	17.9	17.7	17.7	17.7	24.5	24.5	24.5	24.5
Width	1.3	1.6	4	4	4	4	0.4	1.4	1.6	1.4

Table 4.6 Filter elements coupling distances in (mm) [80]

Coupled Elements	Distance in (mm)
Transmission zero extractor 1 and Input port	0.3
Input port and Coupling reducer 1 (CR1)	0.4
CR1 and Resonator 1	1
Resonator 1 and CR2	1.8
CR 2 and Resonator 2	3
Resonator 2 and CR 3	0.7
CR 3 and Resonator 3	3.4
Resonator 3 and CR 4	0.7
CR 4 and Resonator 4	1.8
Resonator 4 and Output port	0.8
Output port and Transmission zero extractor 2	0.6



(a)



(b)

Figure 4.20 The tunable designed filter (a) Circuit model (b) Simulated response

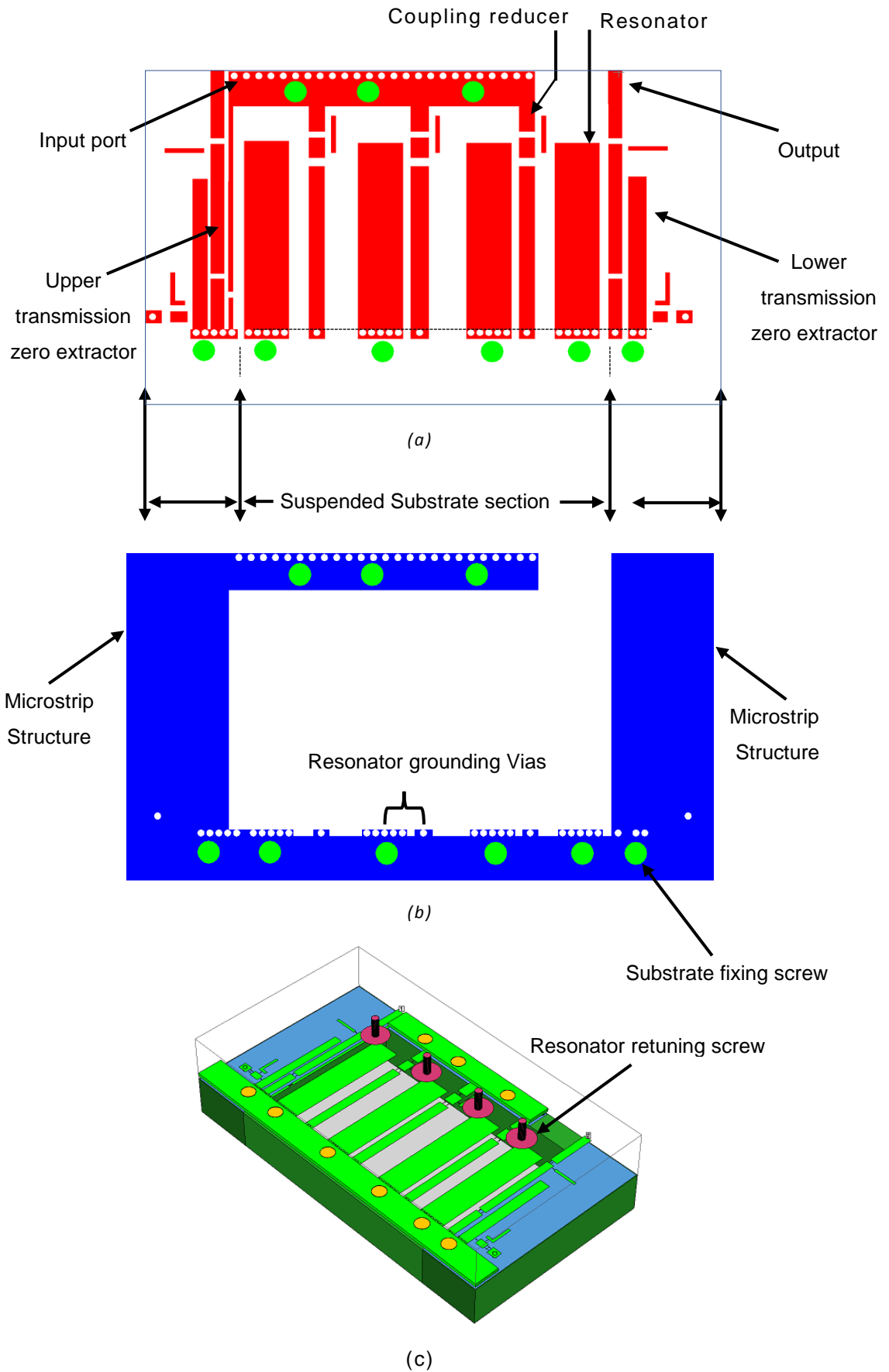


Figure 4.21 The layouts of the tunable combined Microstrip and SSL filter (a) Top layer (b) Bottom layer (c) 3D View including tuning screws. [80]

The filter has been tuned electrically and fine-tuned mechanically using tuning screws as shown in Figure 4.21 (c). The tuning elements are listed below in Table 4.7, while the EM full-wave simulation result is shown in Figure 4.22.

Table 4.7 A list of the used tuning varactor diodes [80]

Tuning Components	V1 (pf)	V2 (pf)	V3 (pf)
V _{c1}	0.7	0.56	0.56
V _{c2}	0.32	0.35	0.34
V _{c3}	3.2	0.57	0.35
V _{c4}	3.2	0.57	0.35
V _{c5}	3.2	0.57	0.35
V _{c6}	0.36	0.48	0.46
V _{c7}	1.31	1.35	0.97

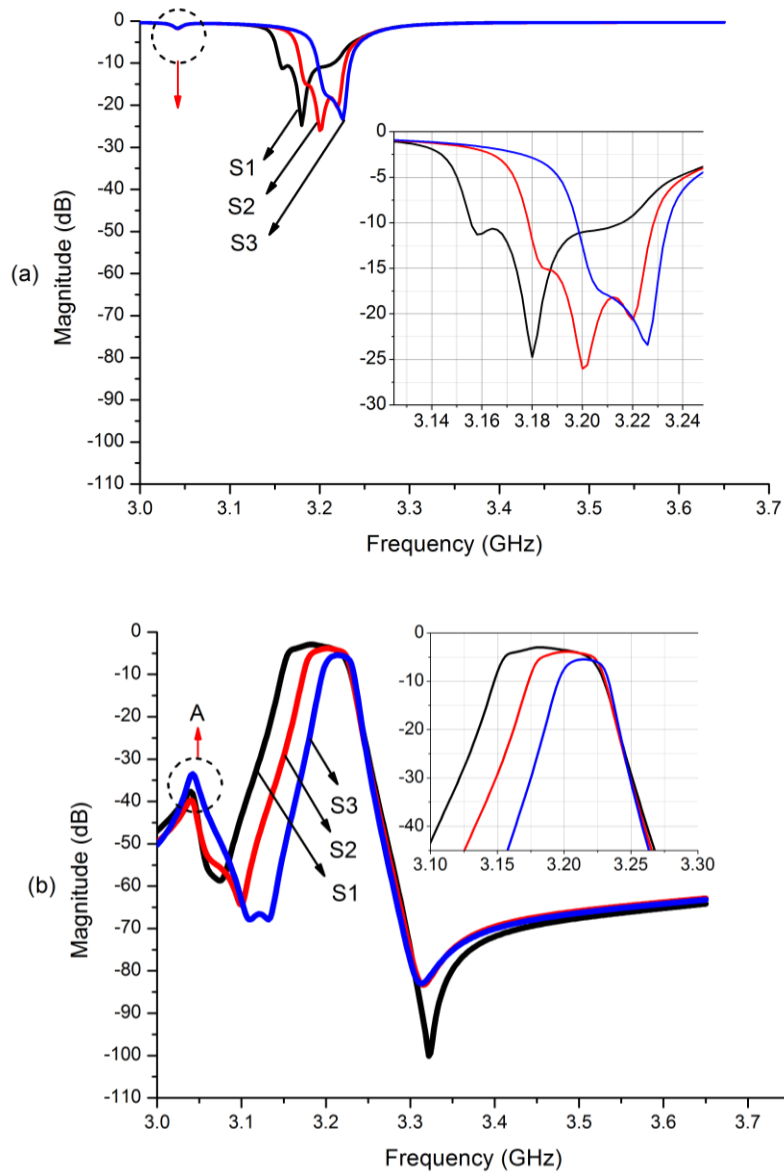


Figure 4.22 Simulation result of the proposed filter at different varactor values (a) insertion loss (S21) in dB (b) return loss S11 in dB [80]

The simulated performance of the filter against different tuning values of the varactors is presented in Table 4.8:

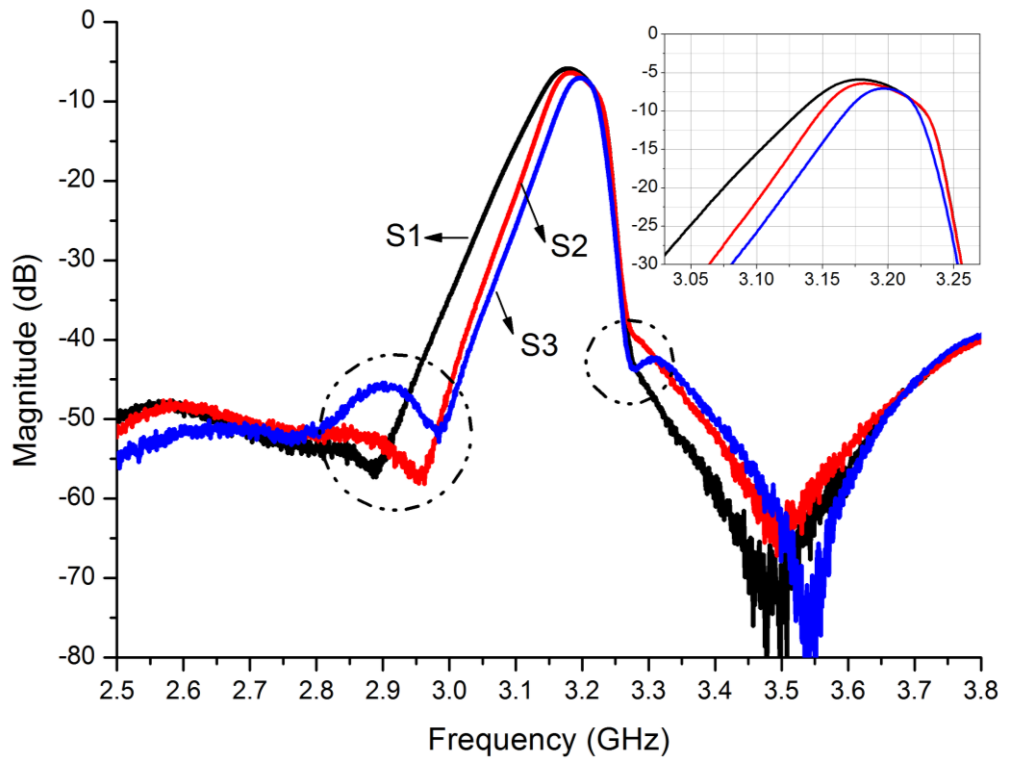
Table 4.8 The tunability of the proposed filter versus tuning elements [80]

	State 1	State 2	State 3
F_0 (GHz)	3.189	3.2	3.22
BW (MHz)	74	52	37
FBW (%)	2.32	1.62	1.15
Insertion Loss (dB)	-3.1	-3.81	-5.37
Return Loss (dB)	-12.2	-14.99	-17.34

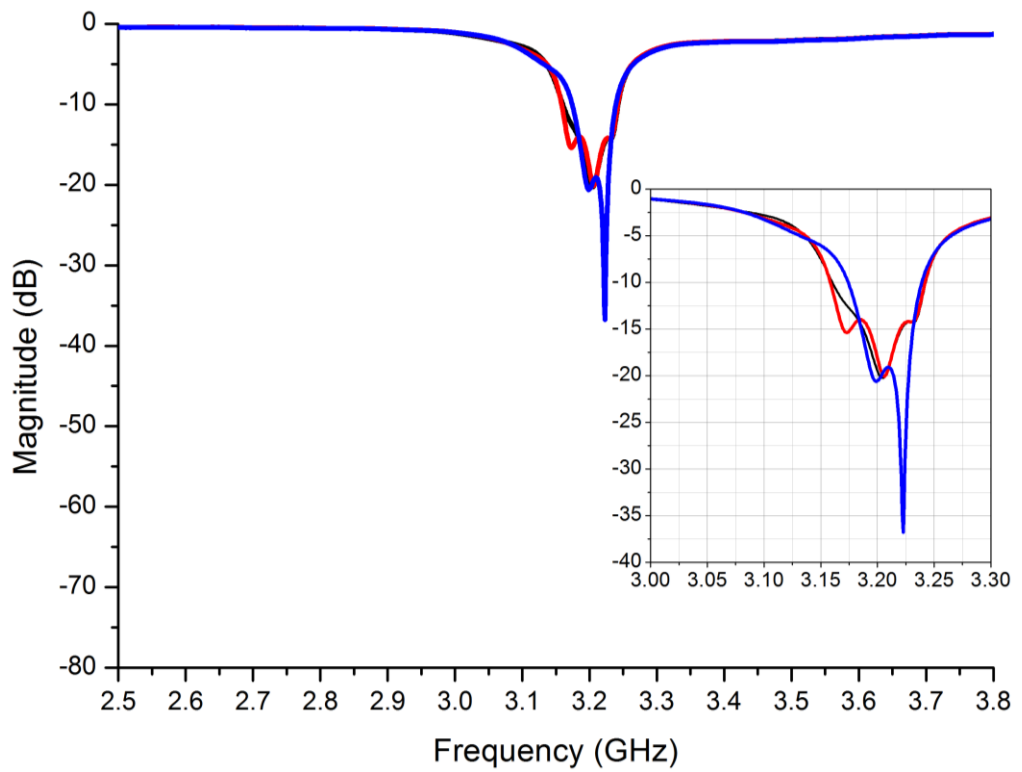
4.7.3 Measured results and discussion of the fabricated filter

The same substrate of the fixed frequency combined filter was used for fabricating the tunable one. Two types of Skyworks Hyperabrupt Junction tuning varactors were used to tune the filter's bandwidth, the first one was the SMV2019-079LF, which was used to adjust the external coupling to mitigate the mismatch during the tuning process, whereas, the second type was the SMV2020-079LF, used to tune internal coupling between the resonators and to tune the resonators of the transmission zeros [80][82]. As presented in [80], the coupling coefficient between the resonators is controlled by changing the admittances of the coupling subnetwork that is formed after inserting the coupling reducers between the filter's resonators. This aim was satisfied by developing the coupling reducers so that the tuning varactors could be inserted to variate their admittances, leading to the variation in the filter's bandwidth. Moreover, the selectivity of the filter is managed by changing the electrical length of the transmission zeros. This objective was accomplished by attaching the tuning varactors to the pole extractors so that the electrical length of the extractors varied by changing the capacitance of the varactors, which relocated the transmission poles.

Furthermore, tuning screws are cooperated with filters resonators to avoid the all-stop network cases which may occur when both the resonators and the couplings resonate at a quarter wavelength ($\lambda/4$) [55]. The performance measurements of the fabricated filter are shown in Figures 4.23 (a) and (b) while the manufactured filter is shown in figure 4.24.



(a)



(b)

Figure 4.23 Measured result of the proposed filter at different varactor values: (a) insertion loss (S21) in dB (b) return loss S11 in dB [80]

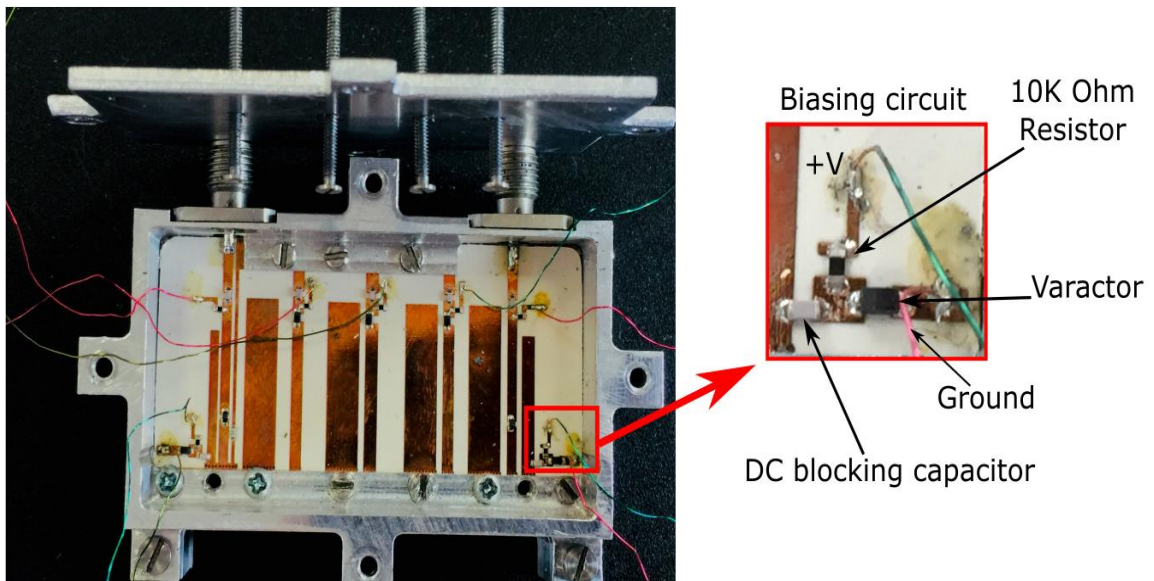


Figure 4.24 Fabricated prototype of the filter and biasing circuit.

The values of the tuning varactors and the recorded tunability are listed in tables 13 and 14, respectively.

Table 4.9 A list of the used tuning varactor diodes.

Tuning Components	V1 (pf)	V2 (pf)	V4 (pf)
V_{cm1}	0.32	0.3542	0.3426
V_{cm2}	0.557	0.557	0.557
V_{cm3}	3.2	0.5721	0.35
V_{cm4}	3.2	0.5721	0.35
V_{cm5}	3.2	0.5721	0.35
V_{cm6}	0.362	0.48	0.464
V_{cm7}	1.309	1.35	0.97

Table 4.10 The measured tunability of the filter

	State 1	State 2	State 3
F_0 (GHz)	3.194	3.196	3.2
BW (MHz)	88	82	59
FBW (%)	2.76	2.57	1.94
Insertion Loss (IL) dB	-5.86	-6.46	-7
Return Loss (RL) dB	-11.2	-14.2	-19

Table 4.9 shows that the measured bandwidth of the manufactured narrow tunable bandpass combined filter is from 59-88 MHz with a 3dB fractional of 1.94-2.7 and an insertion and return loss between 5.86-7dB and 11.2-19 dB respectively. The asymmetrical response of the transmission zeros might be due to the filter's circuit

asymmetrical structure and the existence of another transmission pole on the upper stopband. This pole is believed due to weak cross-coupling between non-adjacent resonators, which may lead to making the tuning process of the upper transmission zero more difficult, in contrast with the lower transmission zero.

On the other hand, a remarkable difference could be seen between the measured and simulated results as presented in tables 4.8 and 4.10. Many factors are presented in [15] which are believed to cause this variance. The first one is the effect of the grounding via, these vias act as a shunt inductor, and their effect becomes more marked as their number increases, as explained previously. This effect is added to effect of the mismatch which increased during the tuning process.

According to [28], the effect of mismatch could be decreased by adding two tunable coupling reducers at the input and output to rematch the filter. However, this suggestion may increase the circuit dimensions and complicated the tuning process of the filter [28]. Manufacturing tolerance is another crucial reason. This may affect both the electrical circuit during the etching process and the aluminium box during the mechanical turning of the metal, each of which is about 10%, which has a meaningful impact on the filter's performance. As an example, an electrical circuit etching error could lead to a different resonator length or width, meaning a different resonance frequency and different coupling coefficient.

Moreover, the change of the coupling reducers widths may lead to narrowing the bandwidth. despite of the fine tuning which was applied by using asynchronous tuning of the tuning's screws to reduce the frequency shift, as shown in Figure 4.20 (c). However, an easier and more accurate fine tuning could be achieved electrically by adding tuning elements to the open end of the resonators for better response on the expense of the on increased tuning complexity.

The bad tolerance in the box manufacturing may result in displacement of the microstrip and suspended elements, or a different height of the grounding planes, meaning different admittances mismatched circuit elements. However, these factors are unavoidable, and it is strongly believed that they cause this difference. Furthermore, the softness of the substrate may add another reasonable reason that cause this difference between the measured and simulated responses. It believed the substrate has bent slightly because of the screws fighting, this may lead to a different

impedance values of the suspended elements which in turn leads to the mismatch between them.

Another reason for the disparity measured is the low-quality factor of the electronic tuning elements, which increases the insertion loss during the tuning process, however, this factor is a trade-off of the varactor tuning.

4.7.4 Conclusion

A narrowband combined microstrip and suspended substrate stripline with two transmission zeros was designed and fabricated as a fixed and tunable bandwidth filter. Both filters use two different structures, are combined in one circuit and introduce a new method of presenting transmission zeros on either side of the filter response, rather than the conventional cross-coupling method. The method introduced depends on two different Microstrip transmission zero extractors being placed on either side of the circuit and resonated at certain frequencies.

The bandwidth tuning approach uses three coupling reducers, located between the coupled resonators. The transmission zeros are tuned effectively and easily compared with traditional methods of tuning the transmission poles. Furthermore, the tuning process was performed with tuning varactors, and asynchronous mechanical fine-tuning was used to mitigate the effect of the frequency shift of the low manufacturing tolerance, and to avoid the all stop-network at the quarter wave length ($\lambda/4$) of the resonators.

However, a good agreement between the simulated and measured results was obtained from the newly presented structure.

Study of Tunable Cascaded Suspended Stripline Bandpass Filter

5.1 Introduction

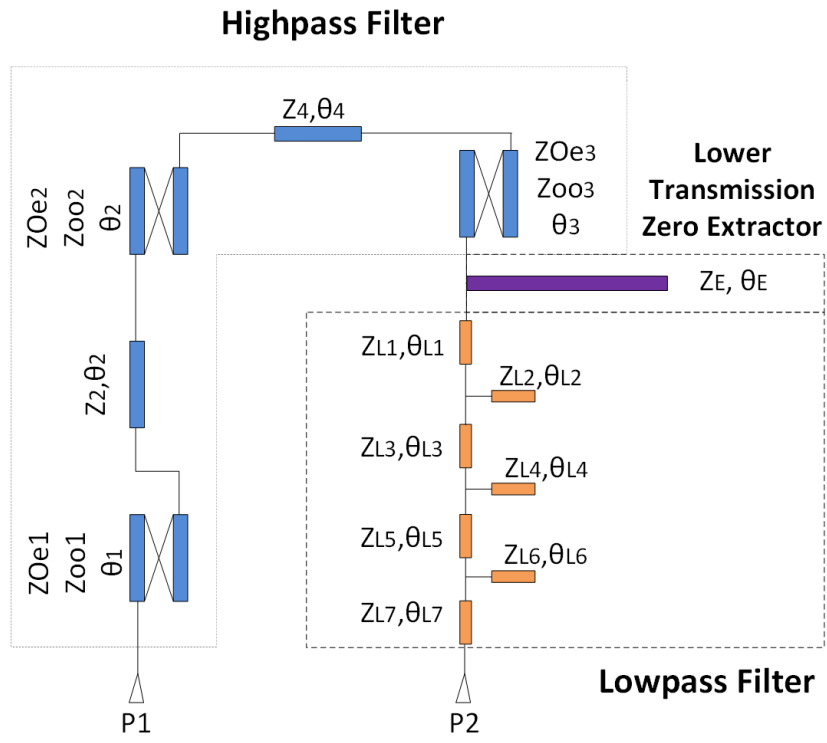
Wise use of the frequency spectrum and effective management of this non-renewable medium are the main challenges in working with recent and future wireless systems. This can be achieved by using reconfigurable/tunable filters, which have an adjustable front-end for selecting the required signals and isolating unwanted interferences on the crowded radio frequency spectrum. Bandpass filters (BPF) are potentially one of the good solutions to accomplish the mission of saving such that exhaustible and costly source. Therefore, several design methods and techniques for fabricating and tuning bandpass filters have been studied and extensively discussed. The cascading method, in which filters with distinct functions are integrated to perform a specific task, is one of the promising new BPF design methods. It offers the advantage of combining the diverse properties of two or more filters and structures to acquire the features of the various integrated filters. Several structures have been put forward for designing and implementing tunable cascaded BPFs so that each one has its own, predetermined job and specifications. In [83] and [84], two different topologies were used to design two microstrip wide band bandpass filters. In this work, cascaded high and lowpass filters were combined to design a wide passband filter. However, the filter's response showed very narrow stopband, which may increase the probability of interference with neighbouring frequency bands. However, the second author used a broadband bandpass filter cascaded with a bandstop filter. This design aimed to obtain an ultra-wideband bandpass filter and increase the isolation band of the designed bandpass filter. In [85], a cascaded inductive and capacitive irises to design a waveguide BPF. However, the use of the bulky waveguide filters is limited to the high frequency applications to miniaturise the size of the fabricated filter, although their extraordinary performance. Another method of designing and implementing cascaded BPFs is presented in [17]. This method used the Substrate Integrated

Waveguide (SIW) bandpass and bandstop filters on a single layer to implement a mechanically tuned BPF with a wide stopband. Despite its remarkable performance, the low tolerance regarding the required tighter spaces between VIAs may complicate the manufacturing process. As well as that, the introduction of frequency-dependent dielectric loss into the guide makes the choice of the millimetre-wave application's operating frequency a crucial matter. In [86], the authors introduced a cascaded highpass and lowpass Suspended SSS. However, they did not represent the isolation band of the filter, which is very important to avoid any expected interference in the high-power frequency bands.

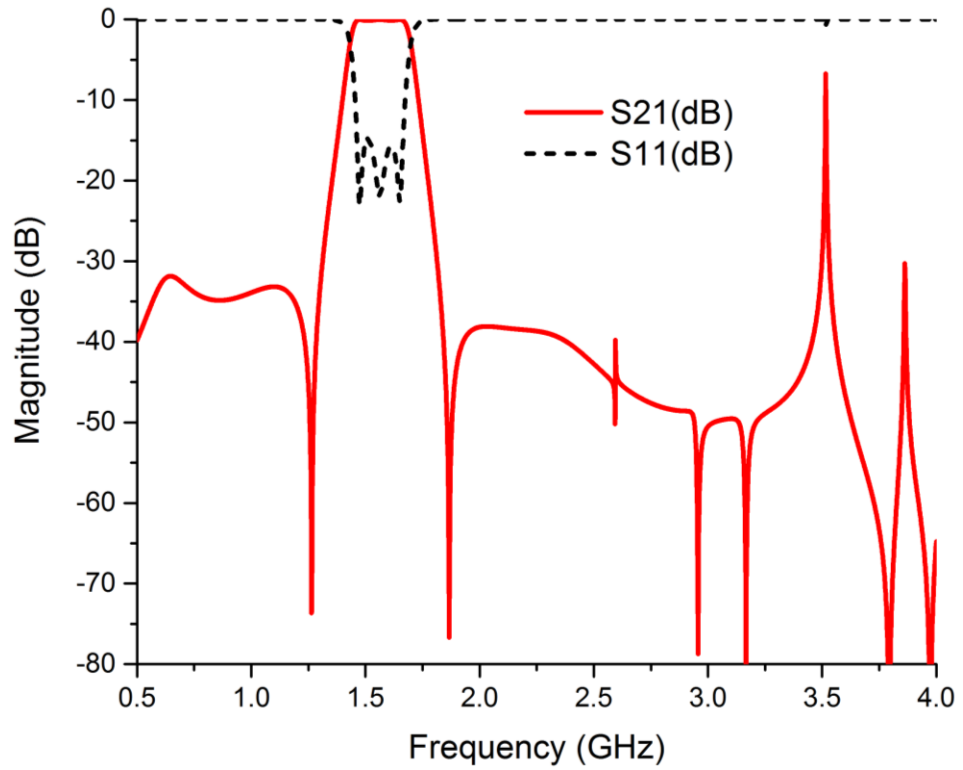
This chapter offers a new cascaded bandpass filter. It comprises of step impedance resonator (SIR) highpass filter and generalized Chebyshev lowpass filter. It includes two main subjects. The first of which revolves around the design methodology of a fixed frequency cascaded bandpass. It starts with a general view on the circuit model of the purposed cascaded filter, this is followed by a detailed explanation of the design of the highpass and generalized lowpass Chebyshev filters, finally the cascading of these filters including the simulated and measured responses of the cascaded bandpass filter will be presented. The second subject discusses the designed filter's tuning procedure. Furthermore, the design simulations and measurements at different tuning varactors values are offered alongside a detailed discussion. Finally, Section 3 presents the chapter's conclusion.

5.2 Designing and implementing of a fixed-frequency cascaded BPF

The concept of the cascaded filter was started by designing its general structure to verify its validity and feasibility. The filter comprised two integrated highpass and lowpass filters, as shown in Figure 5.1. The initial parameters of the highpass and lowpass filters were calculated by applying the method of the step impedance resonator (SIR) [74] and the generalised Chebyshev lowpass filter [69] respectively, as presented later in this section. Moreover, the coupled lines were calculated using the parallel coupled line equation which can be found in [40]. The optimisation process was applied using AWR simulation software [81] to obtain the required response. The design parameters of both filters are listed in Table 5.1 for the highpass filter and Table 5.2 for the lowpass filter.



(a)



(b)

Figure 5.1 The designed cascaded bandpass filter: (a) AWR filter layout (b) AWR simulation of the filter [87]

Table 5.1 The design parameters of the proposed cascaded bandpass filter

Evaluated at $f_{Hc} = 1.68$ GHz			
Highpass filter	Impedance		Electrical length
	Z_{oe1}	200	68.7°
	Z_{oo1}	100.8	
	Z_{oe2}	100.1	83.4°
	Z_{oo2}	60.54	
	Z_{oe3}	200	90°
	Z_{oo3}	10	
	Z_2	19.2	
	θ_2		75°
	Z_4	172.2	
	θ_4		61.2°

Table 5.2 The design parameters of the proposed cascaded bandpass filter

Evaluated at $f_{Lc} = 1.478$ GHz			
Lowpass filter	Impedance		Electrical length (θ)
	Z_E	117.8	θ_E 89.5°
	Z_1	117.8	θ_1 8°
	Z_2	199.95	θ_2 30°
	Z_3	61	θ_3 1°
	Z_4	102.1	θ_4 81.1°
	Z_5	192.4	θ_5 14.9°
	Z_6	119.98	θ_6 56.9°
	Z_7	10.99	θ_7 10.7°

5.2.1 Lowpass filter design

As with all designs, the design process of the lowpass filter was initiated by choosing the right method to meet the final filter's general requirements. The filter's circuit model is shown in Figure 5.2. A generalised Chebyshev lowpass prototype filter of order 7 was chosen to obtain good selectivity and fast roll-off at the band edge of the proposed lowpass filter using fewest elements [87].

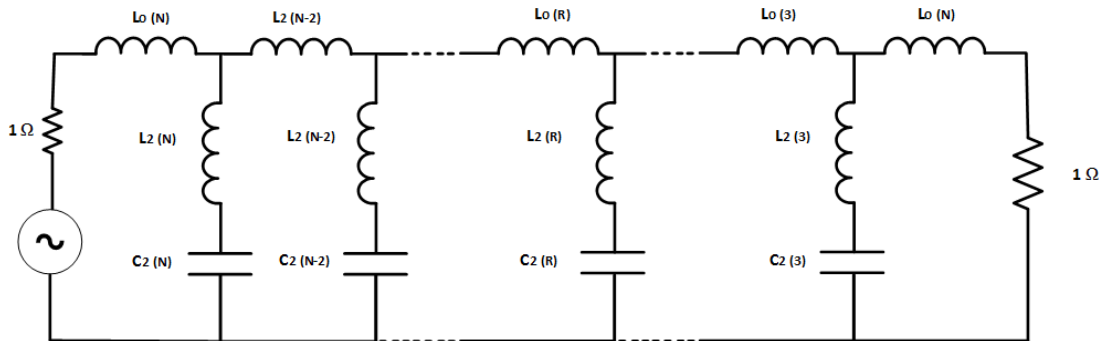


Figure 5.2 Circuit model of the proposed generalised lowpass Chebyshev filter [87]

The parameters of this order are listed in [88], where the proposed insertion loss of the stopband and the return loss of the passband were selected to be ≥ 40 and ≤ 20 respectively. Accordingly, the prototype filter's elements' values are listed in Table 5.3, accompanied by their transformation at cut-off frequency of 1.478GHz. The transformation process is accomplished using the following expressions [40]

$$L = \left(\frac{\Omega_c}{\omega_c}\right) Z_o L_r \quad (1)$$

$$C = \left(\frac{\Omega_c}{\omega_c}\right) \frac{C_r}{Z_o} \quad (2)$$

Table 5.3 Prototype filter element values and their transformed values [87]

R	Element	Prototype value	Transformed value	Unit
7	L ₀ (7)	0.59781	2.687695	nH
	L ₂ (7)	0.572575	2.574241	nH
	C ₂ (7)	0.871735	1.567694	pf
5	L ₀ (5)	1.36486	6.136277	nH
	L ₂ (5)	0.440692	1.981308	nH
	C ₂ (5)	1.13261	2.036842	pf
3	L ₀ (3)	1.36486	6.136277	nH
	L ₂ (3)	0.572575	2.574241	nH
	C ₂ (3)	0.871735	1.567694	pf
1	L ₀ (1)	0.59781	2.687695	nH

These values have been simulated using Microwave Office AWR software [81]. The simulated result is shown in Figure 5.3.

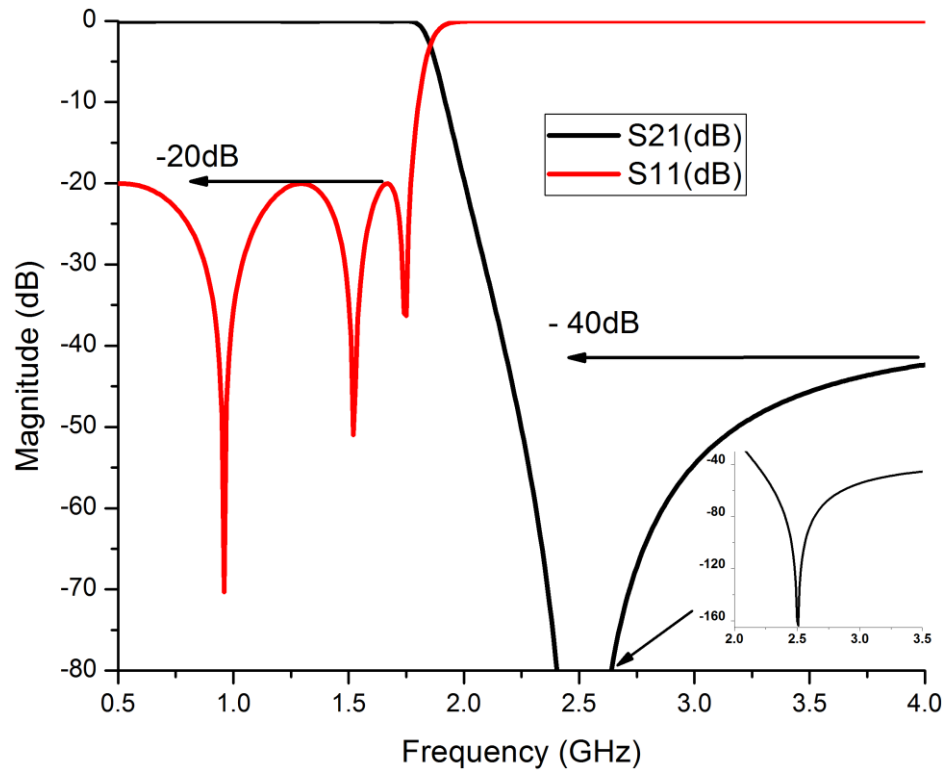


Figure 5.3 Lowpass filter circuit model response [87]

Next the lowpass prototype filter was realised to its equivalent distributed lowpass prototype filter by applying Richard's transformation [55] and [56] :

$$p \rightarrow \omega_o * \tanh(a_L p) \quad 5.1$$

where a_L is a constant, p is a complex frequency variable [69] and ω_o is the resonators' angular frequency in the lumped lowpass prototype filter.

This transforms the series elements into short stubs of impedance $Z = \alpha L$, while the shunt LC series combination is converted to an open-circuited stub of admittance $Y = \alpha C$ [70], as shown in Figure 5.4.

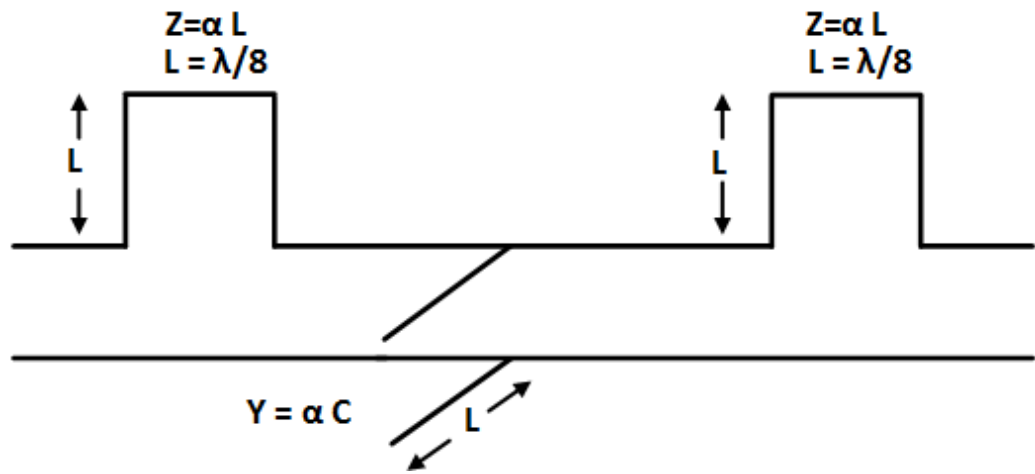


Figure 5.4 Richard's transformation of the proposed generalised lowpass Chebyshev filter

The next phase of the generalised Chebyshev lowpass filter design process is the realisation of the equivalent full-wave structure, done using the transformed values presented in Table 1 and by applying the equations of the SSS [69]. The circuit was designed on Roger's substrate of dielectric constant $\epsilon_r=3$, thickness (h) = 0.5mm and loss tangent = 0.013. This substrate was placed inside a metal box made of aluminium with a width (a) = 50mm, length (L) = 70mm and height (b) = 12.5mm, so that the distances above and below the substrate were equal to 6mm, as shown in Figure 5.5. The calculated dimensions of the designed low pass filter are listed in Table 5.4. The circuit was simulated using full-wave electromagnetic (EM) simulation software SONNET [36]. The filter's periodic structure and response are shown below in Figure 5.6 (a) and (b) respectively.

Table 5.4 Lowpass filter elements' dimensions (mm)

	1	2	3	4	5	6	7
W_{L2}	0.9	8.1	0.3	9.5	0.3	8.1	2.1
L_{L2}	4	31.7	2.8	32.6	2.4	31.7	3.4

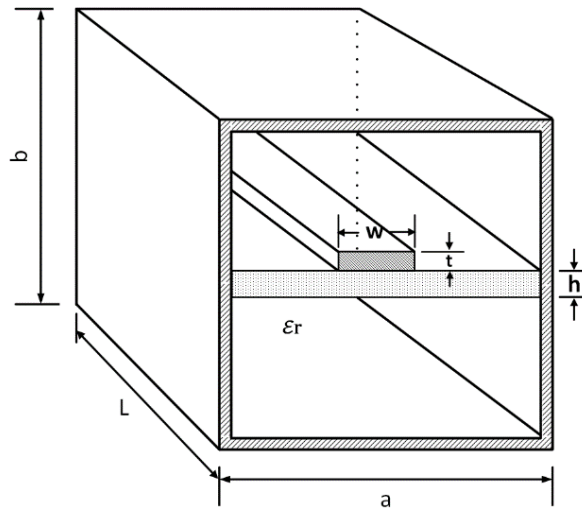


Figure 5.5 The filter's proposed mechanical structure

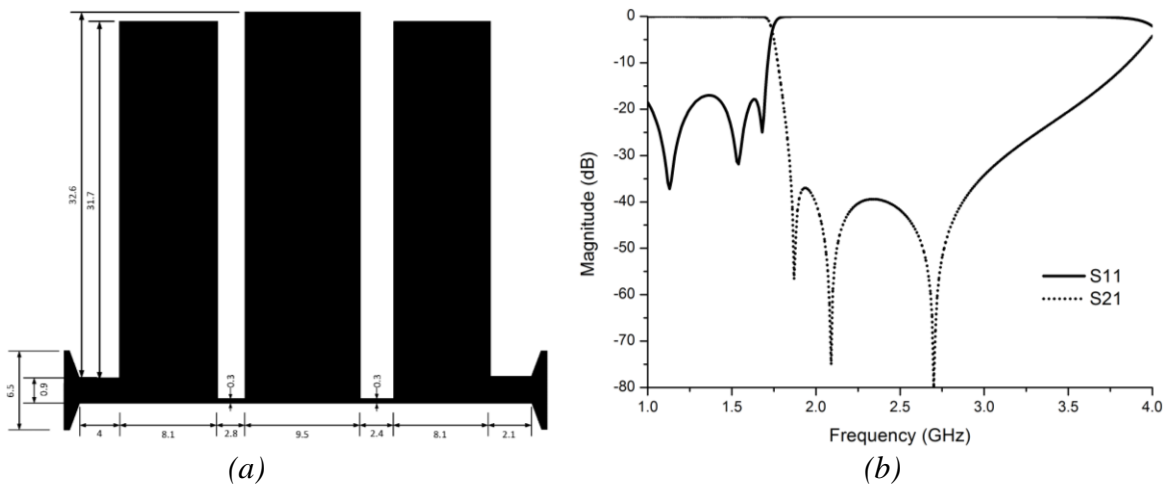


Figure 5.6 Generalised lowpass filter (a) distributed circuit (b) EM full-wave simulation of the filter [87]

5.2.2 The design method for the proposed highpass filter

A highpass filter (HPF) It can be designed by applying different techniques such as a quasi-lumped lumped or optimum distributed element [40]. However, the design process starts by constructing the equivalent circuit model of the filter to verify the proposed design method and to specify the required specifications.

The proposed HPF is designed using two cascaded folded Step Impedance Resonators (SIRs) as well as a single pole extractor to generate a transmission zero prior to the cut-off frequency of the filter, as shown in Figure 5.7.

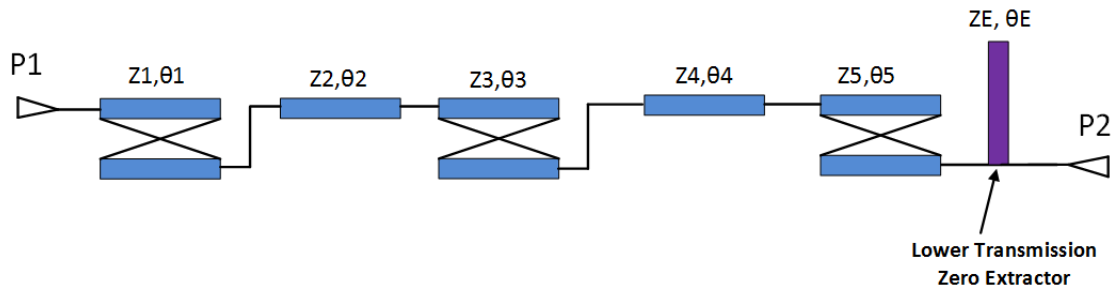


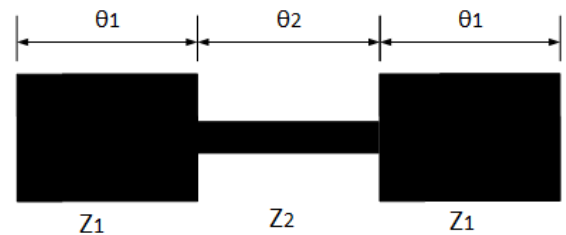
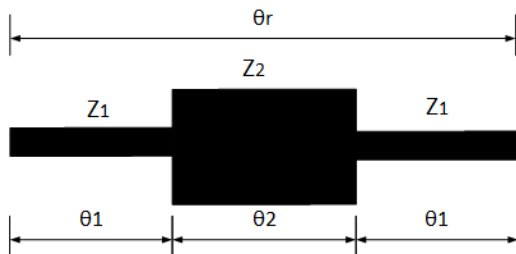
Figure 5.7 The equivalent circuit model of the proposed filter

The aim of using SIR is to achieve the required passband with the least number of elements, while the aim of the transmission zero is to enhance the selectivity of the filter easily and effectively.

5.2.2.1 The fundamentals of the SIR

A step impedance resonator (SIR) is a transmission line which is used as a resonator to analyse the discontinuity in a transmission line having a step impedance [89]. There are many features for SIR such as the flexibility of tuning its transmission zeros by changing the transmission line parameters for instance the impedance ratio [89]. SIR has also the advantage of minimizing the circuit size by using less number of elements. Moreover, the characteristic impedance of SIR can be controlled independently during the design process, more details about SIR are offered in appendix C. The effect of Step Impedance Resonators is discussed in [74], where it is explained that it comprises two transmission lines with different impedances, Z_1 and Z_2 . The layout of the SIR distributed transmission line and its equivalent lumped element circuit are shown below in Figure 5.8 (a) for $K = \frac{Z_1}{Z_2} > 1$ and Figure 5.8 (b) for $K = \frac{Z_1}{Z_2} < 1$. The electrical length of the SIR was calculated using two assumptions according to the required design. The first one can be expressed as

$$\theta_t = \theta_2 + 2\theta_1 \tag{5.2}$$



(a)

(b)

Figure 5.8 The distributed and lumped element circuit of the SIR (a) for $k > 1$ (b) for $k < 1$

The impedance ratio (k) is another important design factor used to obtain the condition of the fundamental resonance, where $k = Z_1/Z_2$ [74]. The input impedance of the SIR can be written as:

$$Z_i = jZ_1 \cdot \frac{(1 + k^2) \cdot (\tan \theta_2 + \tan \theta_1) - K(1 - \tan^2 \theta_1)}{2k \tan \theta_1 + \tan \theta_2 (k^2 - \tan^2 \theta_1)} \quad 5.3$$

At the resonance $Z_i \rightarrow 0$, this leads to:

$$\frac{\tan \theta_2 \cdot \tan \theta_1}{1 - \tan^2 \theta_1} = \frac{k}{1 + k^2} \quad 5.4$$

For the case when $\theta_t = \theta_2 + 2\theta_1$, and since

$$1 - \tan^2 \theta_1 = \frac{2 \cdot \tan \theta_1}{\tan 2\theta} \quad 5.5$$

Also, Assume that, $\frac{k}{1+k^2} = A$

Then

$$\frac{\tan 2\theta_1 \cdot [\tan \theta_2 \cdot \tan \theta_1]}{2 \tan \theta_1} = A \quad 5.6$$

$$\tan 2\theta_1 \cdot \tan \theta_2 = 2A$$

Using equation 5.2, leads to

$$\tan \theta_2 = \frac{2A \cdot [1 + \tan \theta_r \cdot \tan \theta_2]}{\tan \theta_r - \tan \theta_2} \quad 5.7$$

By applying cross multiplication and direct processing on the equation, then

$$\tan^2 \theta_2 + 2A = (1 - 2A) \cdot \tan \theta_r \cdot \tan \theta_2 \quad 5.8$$

Therefore,

$$\tan \theta_r = \frac{2D + \tan^2 \theta_2}{\tan \theta_2 (1 - 2D)} \quad 5.9$$

Where $D = \frac{k}{1+k^2}$ and $k \neq 1$ and using Equation 5.2

According to [74], the minimum length with varying K occurs when:

$$\theta_2 = \tan^{-1} \sqrt{2D} \quad 5.10$$

The second case is for $\theta_1 = \theta_2 = \theta_0$, and then the input impedance can be expressed as:

$$Z_i = jZ_1 \cdot \frac{(1+k+k^2)\tan^2\theta_0 - k}{\tan\theta_0(2k+k^2 - \tan^2\theta_0)} \quad 5.11$$

As with 5.3, the resonance condition can be obtained from 5.7, so that $Z_i \rightarrow 0$, and then:

$$(1+k+k^2)\tan^2\theta_0 - k=0 \quad 5.12$$

$$\theta_0 = \tan^{-1} \sqrt{\frac{k}{1+k+k^2}} \quad 5.13$$

Since the spurious frequencies at $Z_i \rightarrow 0$ and the transmission poles at $Z_i = \infty$ are important to figure out the bandwidth of the proposed cascaded bandpass filter, it's reported [74] that the electrical lengths θ_{sn} ($n = 1,2,3, \dots$) of the spurious frequencies f_{sn1} and f_{sn2} can be derived from (5.7), resulting in [74]:

$$\theta_{s1} = \frac{\pi}{2} \quad 5.14$$

$$\theta_{s2} = \pi - \tan^{-1} \sqrt{\frac{k}{1+k+k^2}} \quad 5.15$$

Therefore,

$$\frac{f_{s1}}{f_0} = \frac{\theta_{s1}}{\theta_0} = \frac{\pi}{2 \tan^{-1} \sqrt{\frac{k}{1+k+k^2}}} \quad 5.16$$

$$\frac{f_{s2}}{f_0} = \frac{\theta_{s2}}{\theta_0} = \frac{\pi}{\tan^{-1} \sqrt{\frac{k}{1+k+k^2}}} - 1 \quad 5.17$$

These equations could also be used to plot the relation between spurious frequency and the impedance ratio as shown in Figure 5.9.

For the transmission poles, the numerator of (5.7) is assumed to be equal to 0, so the electrical length θ_{pn} ($n = 1,2,3, \dots$) for the transmission zeros f_{pn1} and f_{pn2} can be formulated as follows [74]:

$$\theta_{p1} = \tan^{-1} \sqrt{2k+k^2} \quad 5.18$$

$$\theta_{p2} = \pi - \theta_{p1} \quad 5.19$$

$$\frac{f_{p1}}{f_0} = \frac{\theta_{p1}}{\theta_0} = \frac{\tan^{-1} \sqrt{2k + k^2}}{\tan^{-1} \sqrt{\frac{k}{1+k+k^2}}} \quad 5.20$$

$$\frac{f_{p2}}{f_0} = \frac{\theta_{p2}}{\theta_0} = \frac{\pi - \theta_{p1}}{\theta_0} \quad 5.21$$

The relation between the spurious frequencies, transmission poles and the impedance relation (K) can be seen in Figure 5.10.

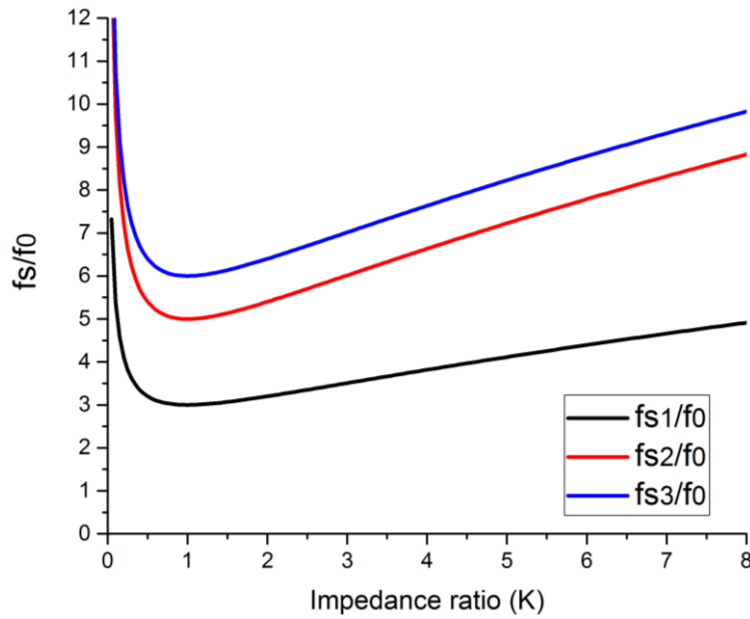


Figure 5.9 The resonance condition of the SIRs

Moreover, it can be seen below in Figure 10 that the bandwidth of the SIR is inversely proportional to the impedance ratio, so that the passband becomes narrower as the impedance ratio increases [7]. At the same time, the second spurious frequency moves away the first one. These facts are very important in choosing the right ratio of the SIR impedances in which the required fractional bandwidth and stopband are satisfied.

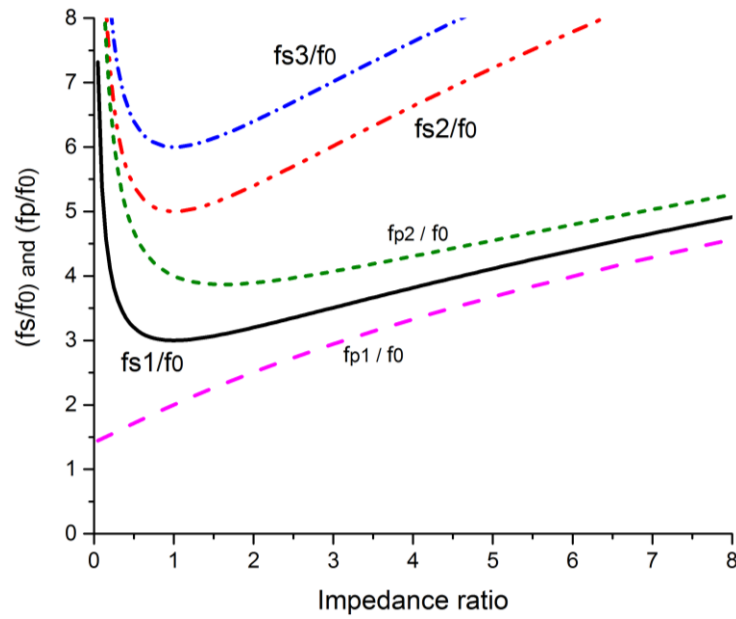


Figure 5.10 SIR spurious frequencies and transmission poles against the impedance ratio (K)

5.2.2.2 SIR parallel coupling methodology

Referring to the proposed HPF equivalent circuit model which is shown above in Figure 6, it can be seen that the proposed HPF comprises two coupled SIRs. The parallel coupling approach has been chosen to ease the manufacturing process by avoiding the problems which may occur to the response during the alignment of the broadside coupling. The parallel coupling approach and its equivalent circuit are depicted in Figure 5.11, where Z_{oe} , Z_{oo} and θ are the odd and even impedances of the coupled lines and their associated electrical length, while the equivalent circuit is offered as two transmission lines of characteristic impedance Z_0 , with an electrical length of θ and separated by a J-inverter.

According to [90], the general form of the odd and even impedances of the coupled lines of an arbitrary lengths can be expressed as:

$$\frac{Z_{oe}}{Z_0} = \frac{1 + (J/Y_0)\operatorname{cosec}\theta + (J/Y_0)^2}{1 - (J/Y_0)^2 \cot^2\theta} \quad 5.22$$

$$\frac{Z_{oo}}{Z_0} = \frac{1 - (J/Y_0)\operatorname{cosec}\theta + (J/Y_0)^2}{1 - (J/Y_0)^2 \cot^2\theta} \quad 5.23$$

where J/Y_0 parameter is a ratio of the J -inverter characteristic admittance to the characteristic admittance of the terminating line. This ratio can be expressed as [40]:

$$\frac{J_{01}}{Y_0} = \sqrt{\frac{\pi FBW}{2 g_0 g_1}} \quad 5.24$$

$$\frac{J_{j,j+1}}{Y_0} = \frac{\pi FBW}{2} \frac{1}{\sqrt{g_j g_{j+1}}} \quad 5.25$$

$$\frac{J_{n,n+1}}{Y_0} = \sqrt{\frac{\pi FBW}{2 g_n g_{n+1}}} \quad 5.26$$

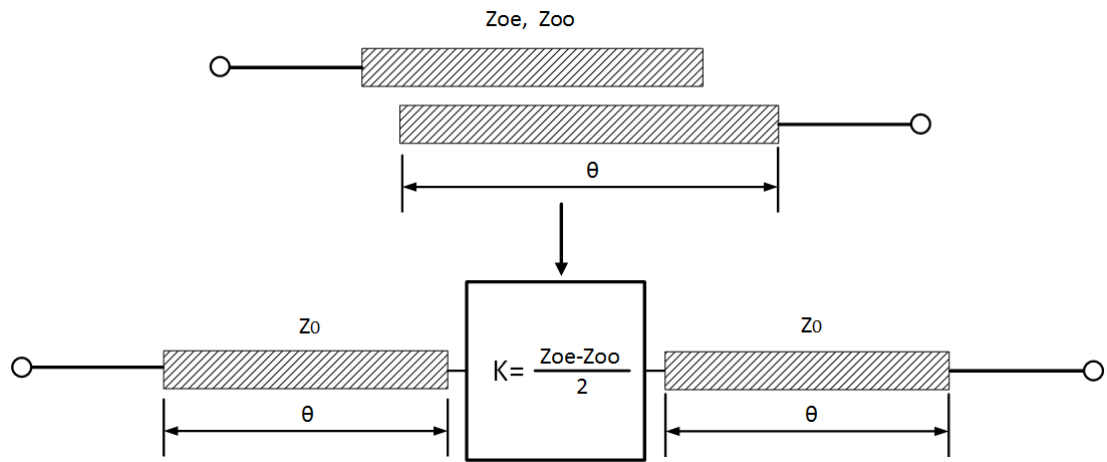


Figure 5.11 Parallel coupled line and its equivalent circuit [2]

where g values are those of the lumped element lowpass prototype filter and the FBW is the fractional bandwidth of the proposed filter.

5.2.3 HPF design example

Since the lengths of the coupled SIR had already been obtained as listed in Table 5.5, the second step was to get their widths, and this aim could be done by using the characteristic impedances of the SIR elements and applying the following equation [55]:

$$W = \frac{b}{4} \left(\frac{377}{Z_o} - 1.84 \right) \quad 5.27$$

Where b is the distance between the two ground planes of the enclosure and Z_o is impedance of the transmission line. Equally, the physical lengths of the SIR elements were calculated as follows [40]:

$$l = \frac{\theta^o}{\beta} \quad 5.28$$

where θ^o is the electrical length of the SIR elements and β is the propagation velocity which equals $2\pi/\lambda_g$, also λ_g is the guided wavelength which is equal to $\frac{c}{f_o*\sqrt{\epsilon_{re}}}$, where c is the speed of light in free-space, which is equal to 3×10^8 m/s, f_o is the resonance frequency and ϵ_{re} is the effective dielectric constant of the SSS.

Table 5.5 The calculated characteristics and dimensions of the SIR

Impedance ratio	K=1.5
Z_1, w_1	174 Ω , 4.5mm
Z_2, w_2	114 Ω , 1.3mm
SIR elements' lengths (θ_1) and (θ_2)	50.8 o
l_1, l_2 and l_3	23.7 mm

The third phase is to obtain the odd and even impedances, and these were calculated by applying the parallel coupled resonators method [40], where the electrical length is assumed to be $\lambda/8$. These values are listed in Table 5.6, and have been used to construct the circuit model of the filter using an AWR simulator [81]. The required response was achieved with a slight tuning of those parameters, as shown in Figure 5.12, the tuned values of the odd and even impedance mode were as listed in Table 5.6.

Table 5.6 The obtained parameters of the parallel coupled resonators method

SIR parameters	Calculated	Tuned
Z_{oe1}	251.279	236.502
Z_{oo1}	127.139	105.646
Z_{oe2}	197.42	261.96
Z_{oo2}	143.377	79.46
Z_{oe3}	251.282	277.902
Z_{oo3}	127.138	70.237
Z_1	166	257.8
Z_2	114	130.6

Z_3	114	71.63
Z_4	166	151.6

After this phase, it was necessary to choose a proper substrate, which in this project was a Roger substrate of dielectric constant ϵ_r , thickness (h) and loss tangent equal to 3, 0.5 and 0.013 respectively. This substrate was suspended inside a metal box made of aluminium of width (a), length (L) and height (b), equal to 50mm, 70mm and 12mm respectively, where the distances above and below the substrate were equal to 6mm, as shown in Figure 5.13.

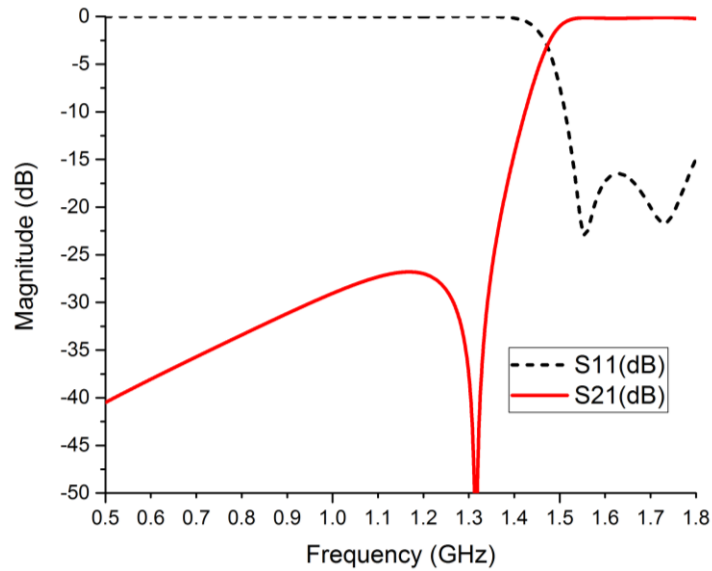


Figure 5.12 HPF circuit model response

The next step was to apply the extraction method at different distances between the coupled lines using the EM full-wave software SONNET® [11]. This approach aimed to obtain the required gaps in which the value of the calculated odd and even impedances were equal to the extracted values at the filter's specified resonance frequency.

The results of the coupling impedance and the relevant gaps which satisfy the required response of the HPF are shown in Figure 5.14.

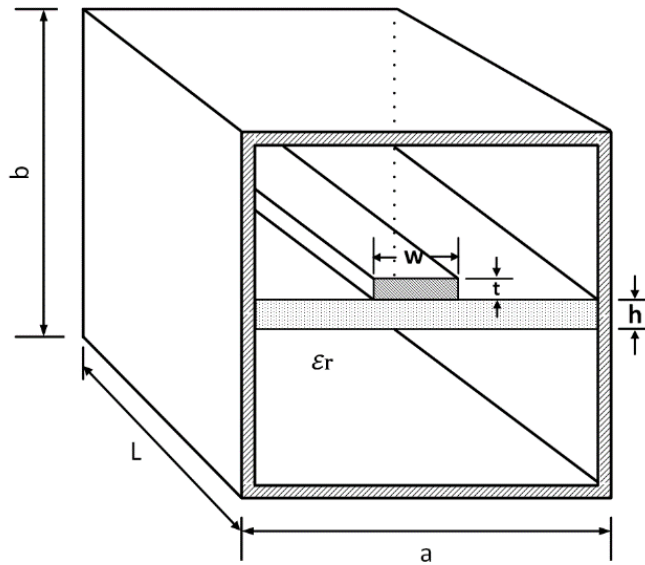


Figure 5.13 The proposed mechanical structure of the filter

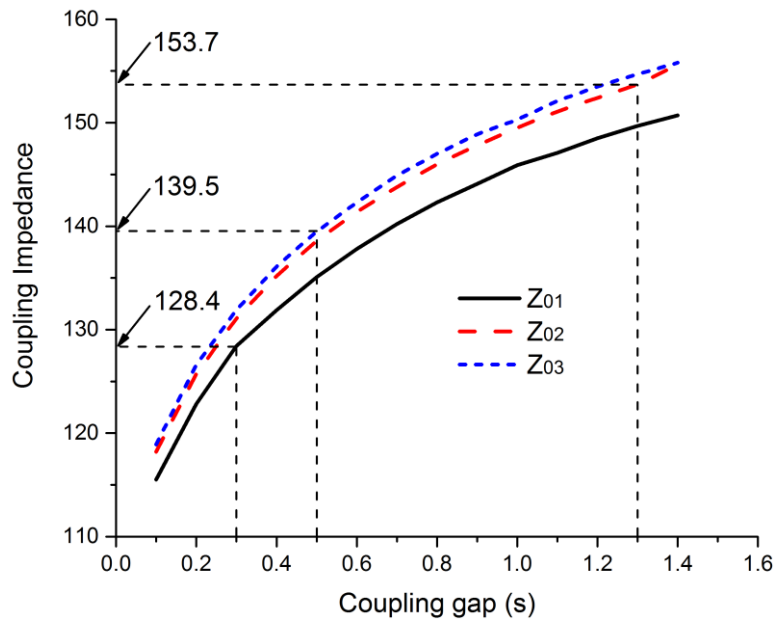


Figure 5.14 The coupling Impedances design graph

The last phase of the HPF design process is the transmission zero resonator design. The proposed resonator was designed using Equations 5.20 and 5.21 at a frequency of 1.26. The distributed circuit of the proposed highpass filter has been constructed and simulated using full-wave simulation software Sonnet® [36]. The layout of the designed highpass filter is shown in Figure 5.15 (a), while the full-wave simulated response is shown in Figure 5.15 (b):

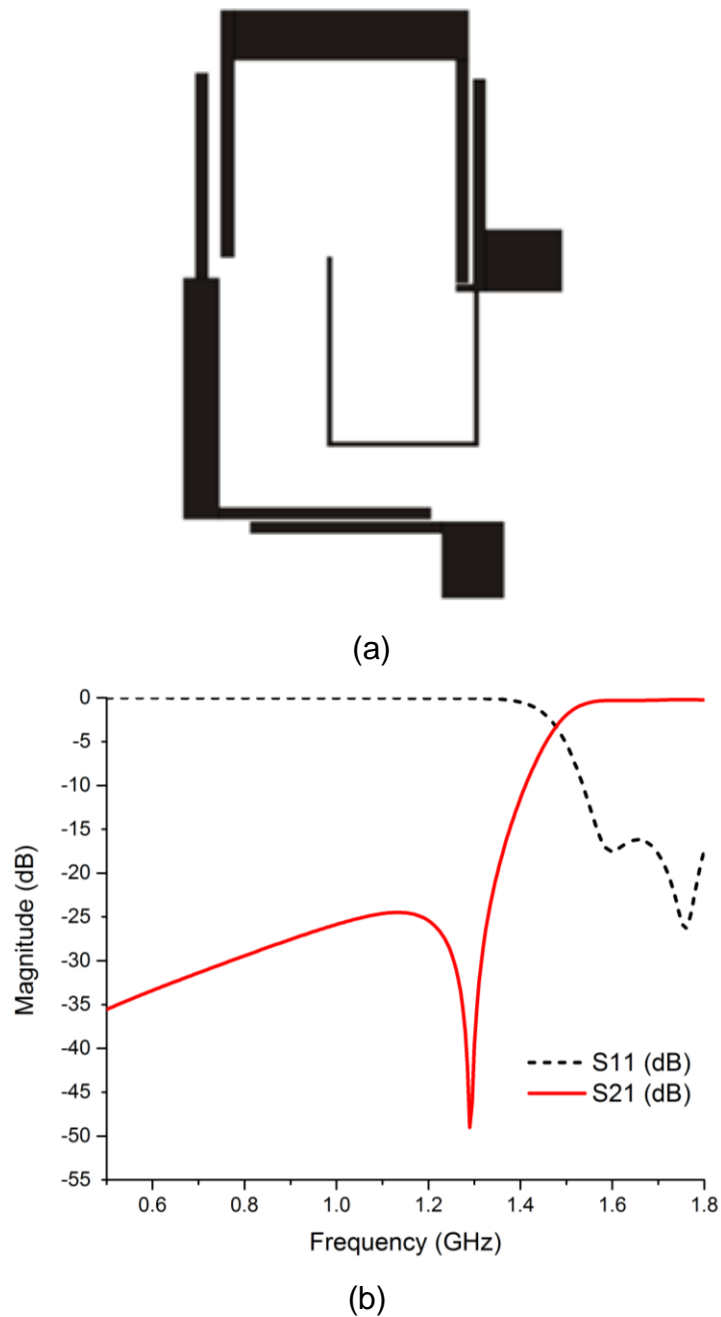


Figure 5.15 The designed highpass filter (a) The distributed circuit (b) The full-wave EM simulated response [87]

Since the highpass and lowpass filters were designed separately, it was necessary to connect them to form the cascaded filter as shown in Figure 5.16. Another optimisation and slight modification was applied to achieve the required matching impedance between the integrated filters. For example, a slight change can be seen in that the width of last coupled line is minimised from 1.2mm to 0.4 mm. Another change is the addition a small fan stub to the line of the transmission pole

extractor, to suppress the stop-band harmonics of the upper stopband of the cascaded filter. A comparison of the EM simulation with the AWR simulation is shown in Figure 5.17, the results for the cascaded filters show a narrow bandpass filter of very good selectivity, and a fractional bandwidth equalling 30% that ranges from 1.401GHz to 1.74GHz.



Figure 5.16 The final circuit layout of the cascaded SSS BPF filter [87]

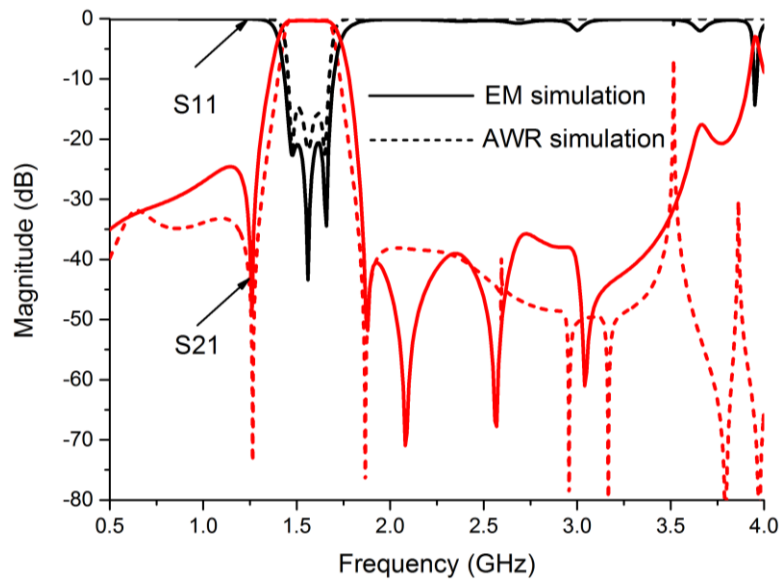


Figure 5.17 The designed cascaded SSS BPF filter (a) The distributed circuit (b) The full-wave EM simulation [87]

The filter designed was fabricated using the same substrate of the previous designs, while the metallic box was modified to fit the size of the cascaded filter as

shown in Figure 5.19. The dimensions of the aluminium box were 85mm x 70mm x 12.5mm. The measured response of the fabricated filter is shown in Figure 18.

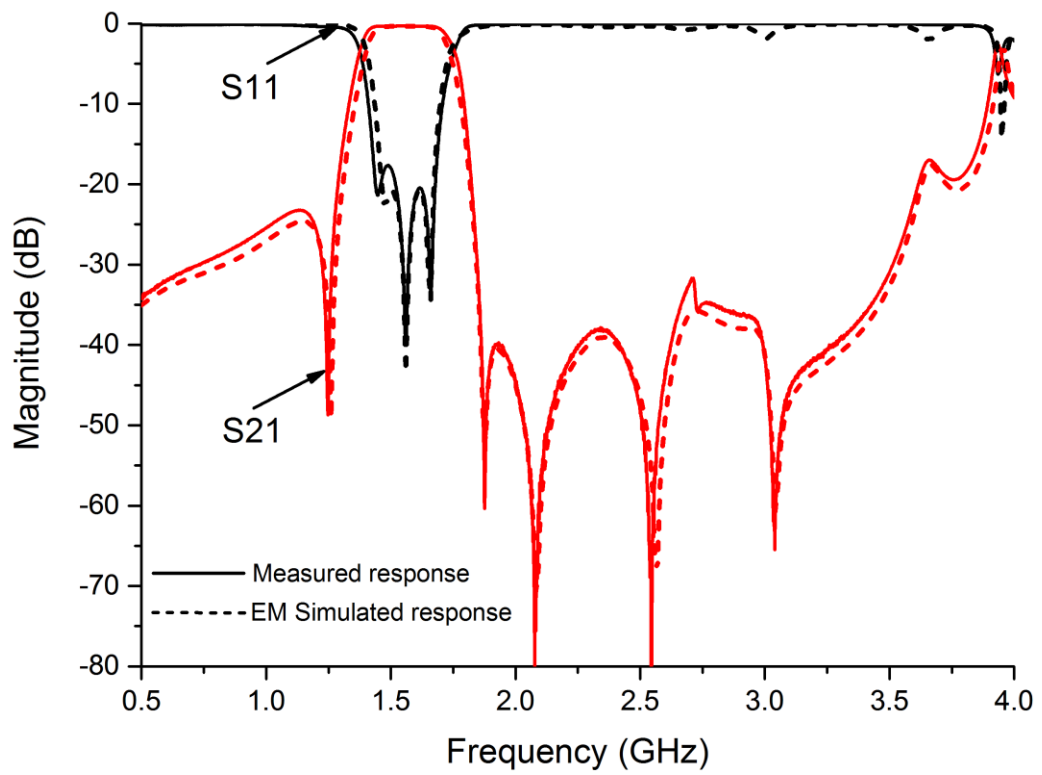


Figure 5.18 The measurement of the fabricated cascaded bandpass filter and its EM simulated response [87]

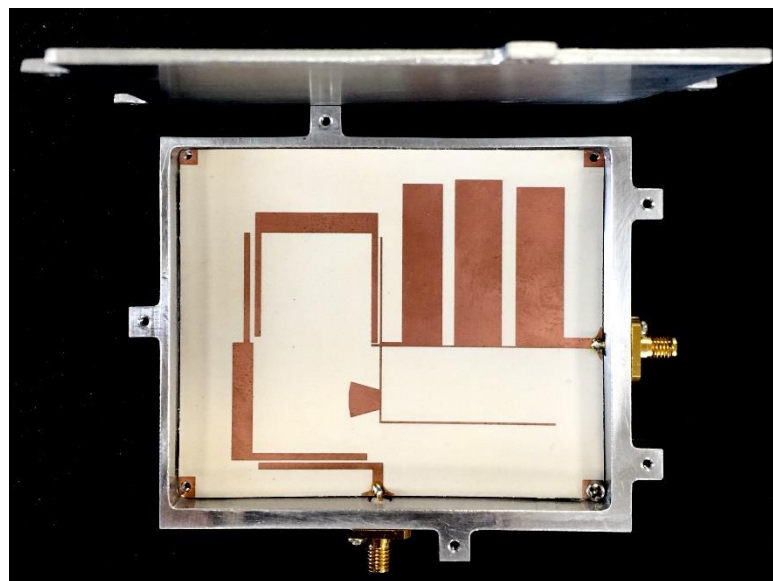


Figure 5.19 The manufactured cascaded SSS bandpass filter

5.2.3.1 Conclusion

The new cascaded bandpass filter design was designed, simulated, fabricated and measured as presented previously. It was realised on a Roger substrate RO3003 with a thickness, dielectric constant and dielectric loss tangent equal to 0.5, 3 and 0.0013 respectively. The filter was then fixed in an aluminium box of dimensions equalling 50 x 70 x 12mm. The measured filter's response showed very good agreement with simulated response, as shown in Figure 5.17. The responses were found to be almost identical, with a fractional bandwidth of 30%, plus insertion and return losses equal to 0.3dB and 18 dB respectively. However, the slight difference between the measured and simulated responses might be due to the manufacturing tolerance during the etching process.

5.3 Feasibility of tuning the cascaded SSS BPF

In this section, the continuous bandwidth tuning of the designed cascaded SSS BPF is discussed, given that this was done with electronic tuning. Figure 5.20 shows that two modifications were made to the cascaded filter's previous design. Firstly, the input edge coupling was replaced with a broadside coupling, to provide enough space for the additional lowpass filter, and avoid the delay which could have resulted from making another metal box to fit the filter's circuit, while keeping the size as small as possible. Secondly, an extra lowpass filter was added to the circuit to suppress the spurious frequencies were seen in the filter's response after adding the tuning elements to the filter's circuit, and which became unacceptable during the tuning process. However, these modifications did not change the general specifications of the designed filter.

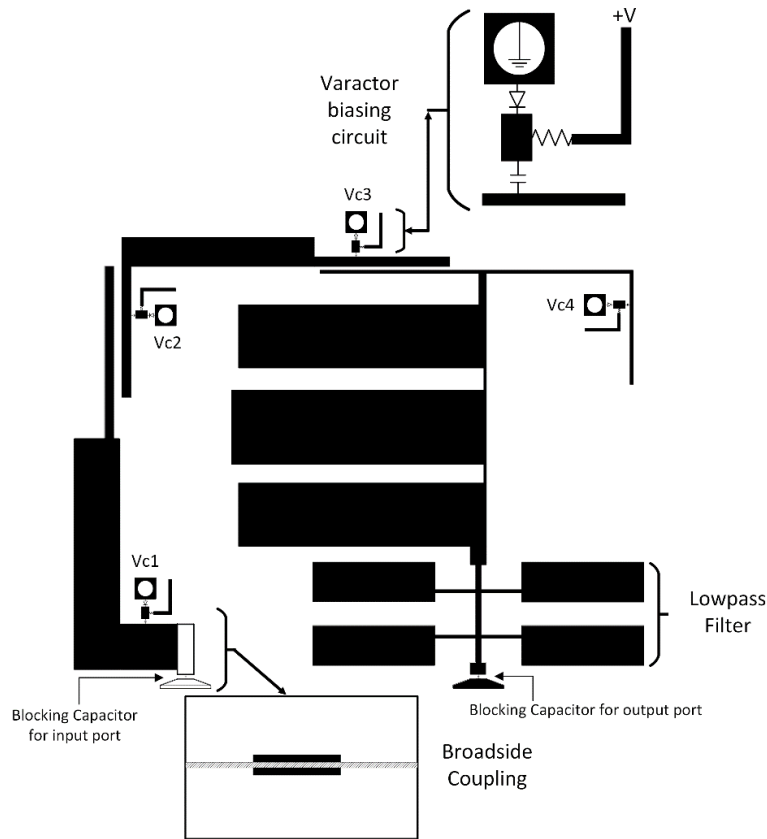


Figure 5.20 The full-wave circuit layout of the tunable cascaded SSS bandpass filter

The added lowpass filter was designed using AWR simulation software [81] at a cut-off frequency of 2.045GHz. As shown in Figure 5.21, the filter circuit comprises two identical Step Impedance Resonators (SIRs) which were connected in parallel on either side of the feeding line. The simulated response of the circuit model is shown in Figure 5.22.

These SIRs are realized using the methodology described in subsection (5.2.1.1), in which the impedance ratio (K) was chosen to be 0.58, the high and low impedances are 169Ω and 98Ω respectively, while the feeding line impedance is 192Ω . By using equations 5.1, 5.3, 5.4 and 5.5, the total length of the SIR was found to be equal to 50.44° , so that the lengths of the low and high impedance sections (θ_1, θ_2) were equal to 23.46° and 26.98° respectively. The widths of the SIR elements were obtained using Equation (5.20). The full-wave circuit of the proposed stopband lowpass filter is shown in Figure 5.23. It was designed, simulated and optimised using EM full-wave simulation software SONNET [36]. The filter's physical dimensions are listed in Table 5.7, and the simulation result is shown in Figure 5.24.

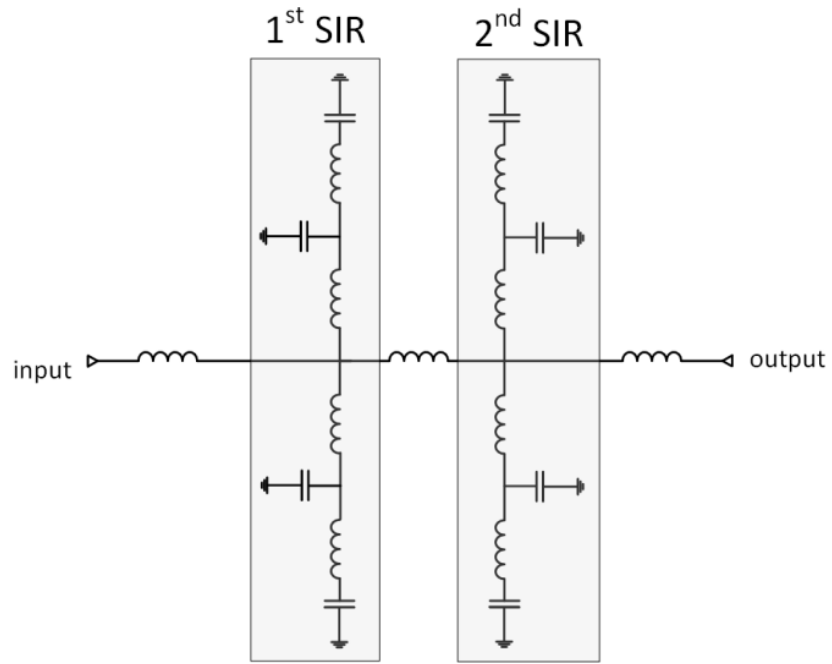


Figure 5.21 The circuit model of the proposed stopband lowpass filter

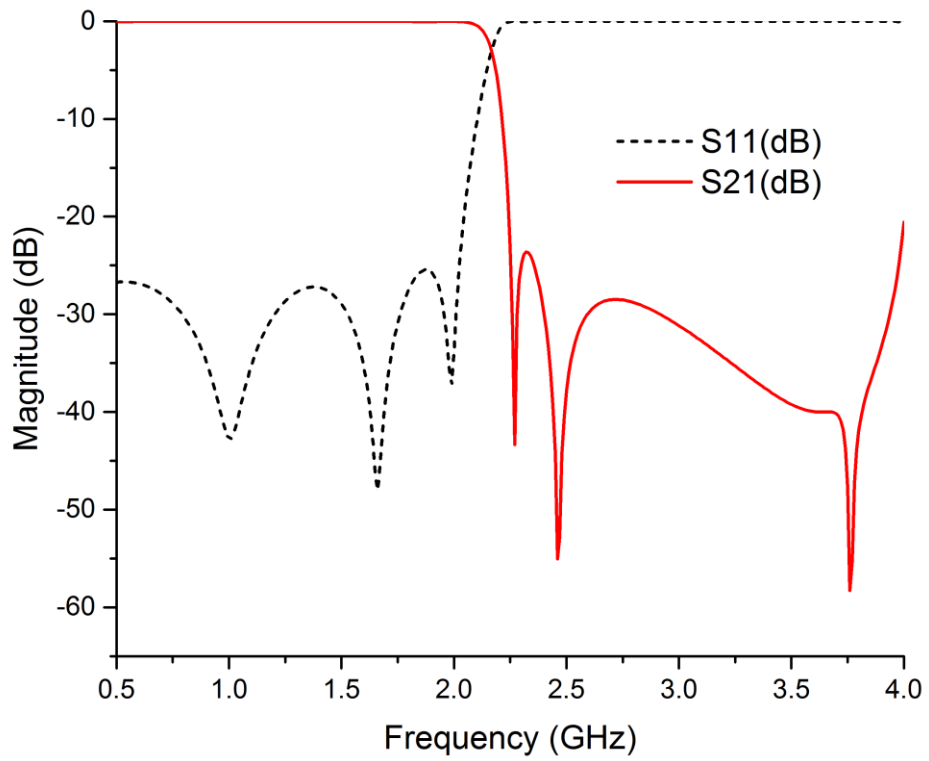


Figure 5.22 The circuit model of the proposed stopband lowpass filter

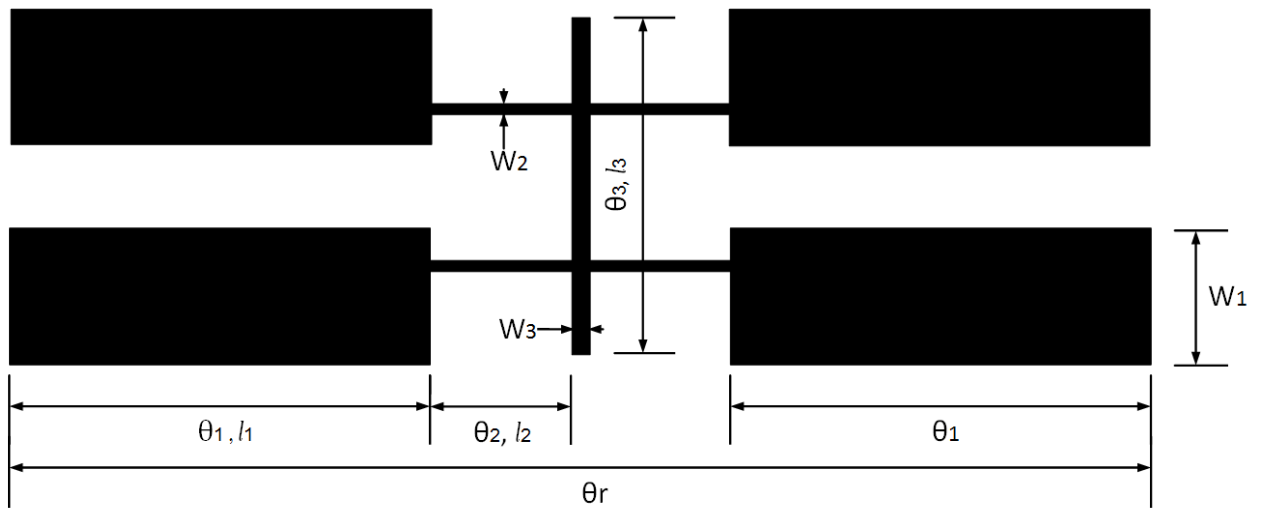


Figure 5.23 Stopband lowpass filter based on SIR

Table 5.7: The optimised physical dimensions of the proposed stopband lowpass filter in mm

W_1	l_1	W_2	l_2	W_3	l_3
5.1	11.6	0.4	11.1	0.7	12.5

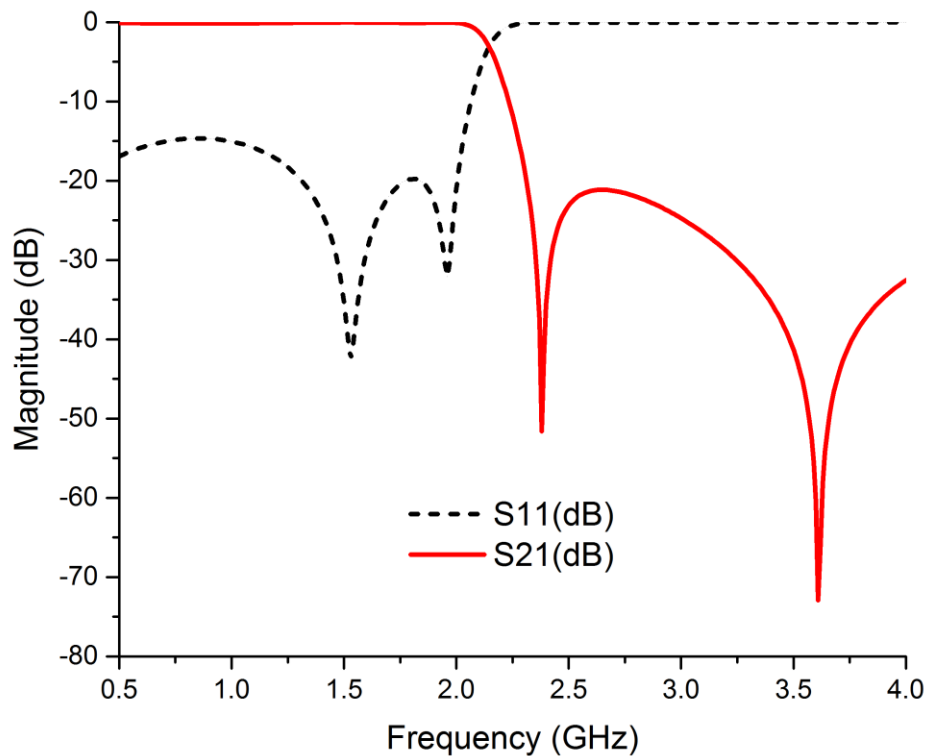


Figure 5.24 EM full-wave simulation of the stopband lowpass filter based on SIR

The tuning method for this filter was based on two methods. The first was mechanical tuning, done using tuning screws as explained in Chapter 3. This was done on the low pass filter section to tune the upper side of the filter's response as shown in Figure

5.25. The resonance frequency of the lowpass filter f_{OL} moved downwards along the frequency axis as the tuning screws moved down towards the resonators of the lowpass filter. The relationship between the resonance frequency and the height of the tuning screws can be expressed as follows:

$$f_{OL} = \frac{1}{2\pi\sqrt{C_r + \left(\frac{\epsilon_r * A}{d}\right)}} \quad 5.29$$

where C_r is the resonator capacitance found in Table 5.3, d is the distance between the screws plate and the resonators in mm, ϵ_r is the dielectric constant of the air in this design, which separates the two conductors in this design, and A is area of the screws which can be calculated as the area of the circle, given that the diameter of each screw equals 8mm.

The second method depends on the tuning varactors, whose capacitances change by changing the biasing voltage. These varactors were connected to one of the coupled stubs, as shown above in Figure 5.20, bearing in mind that the lengths of the loaded stubs were lessened before connecting the varactors. Accordingly, the electrical lengths of the loaded stubs change by changing the biasing voltage of the tuning devices, leading to change in strength of the magnetic coupling between the parallel coupled resonators, which in turns changes the filter's bandwidth. In conjunction with this process, the location of the lower transmission zero is changed electronically to enhance the filter's selectivity. The values of the tuning elements for different states are listed in Table 5.8 while the tuning full-wave simulated response is shown in Figure 5.26

Table 5.8 A list of the used tuning varactor diodes [80]

Tuning state	Tuning components	V1 (pf)	V2 (pf)	V3 (pf)	V4 (pf)
S1	V _{c1}	0.95	0.34	0.39	0.3
S2	V _{c2}	0.3	0.31	0.31	0.3
S3	V _{c3}	0.35	0.35	0.38	0.45

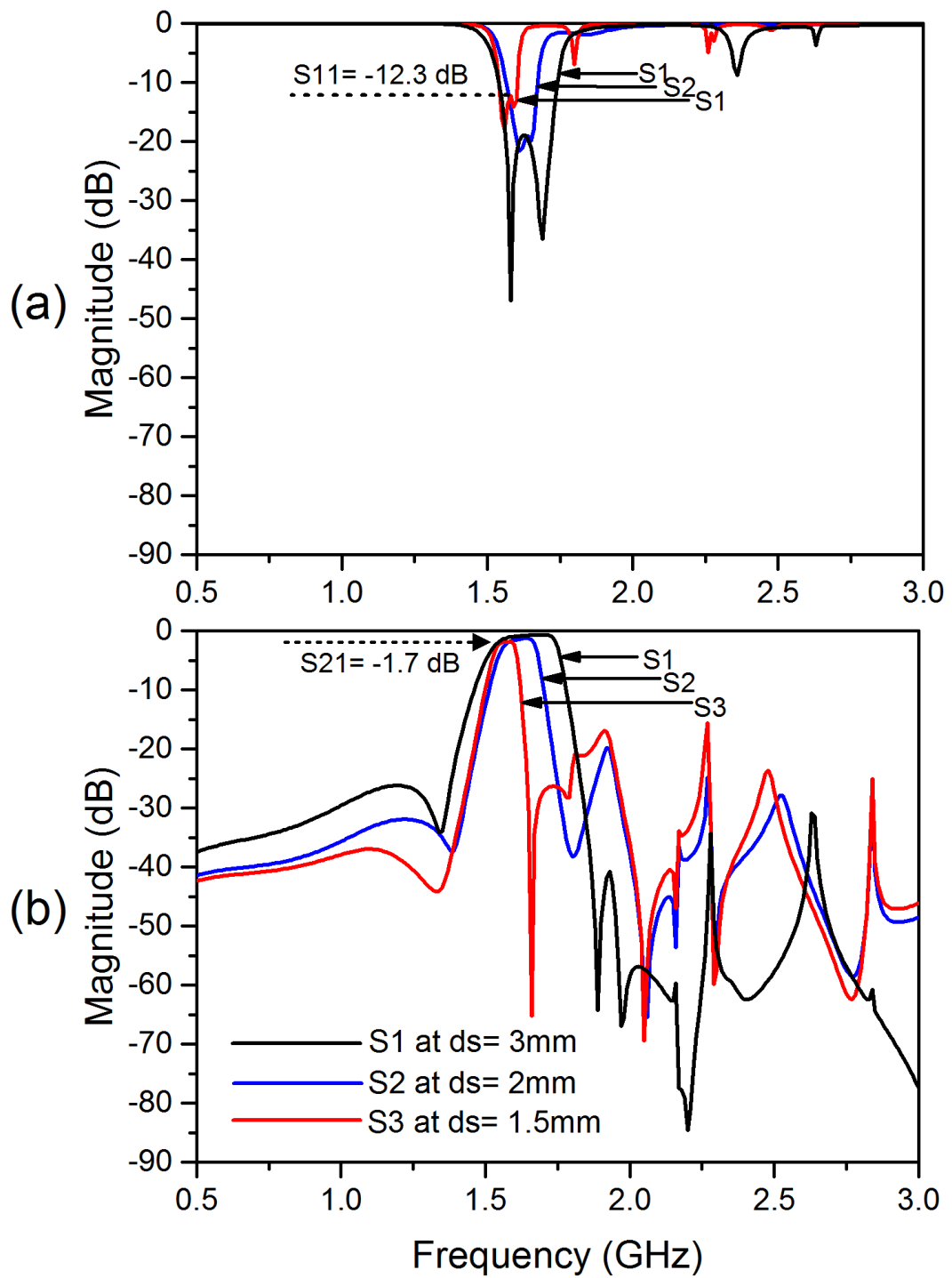


Figure 5.25 EM full-wave simulation of the integrated lowpass filter's mechanical tuning (a) Return loss (b) Insertion loss

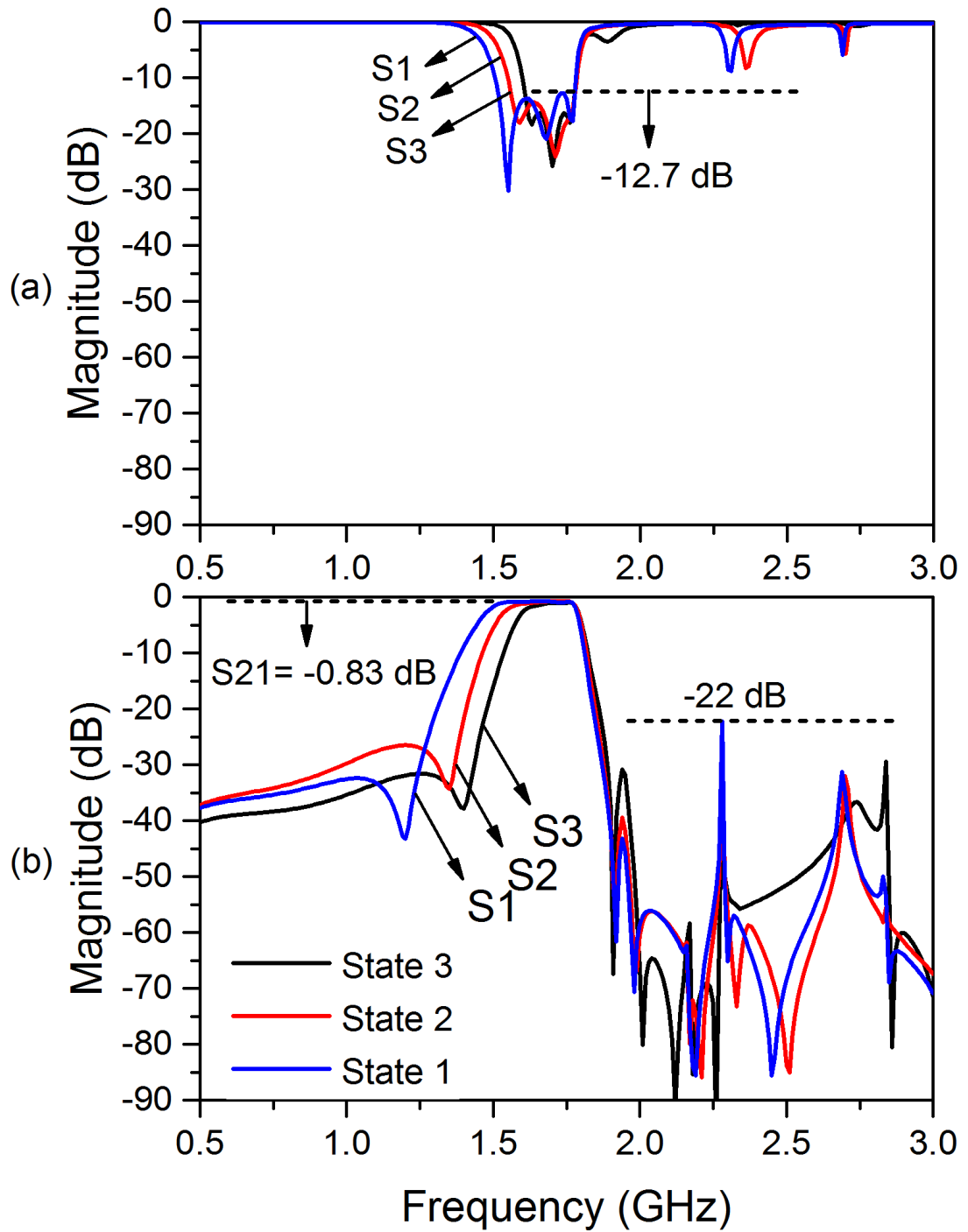


Figure 5.26 EM full-wave simulation of the integrated highpass filter's electronic tuning (a) Return loss (b) Insertion loss.

5.4 Conclusion

A cascaded bandpass filter has been designed, it is composed of a generalized lowpass filter integrated with step impedance highpass filter. The project is divided into three main sections, the first one is the circuit model design and simulation result presentation. The second one is customised to present the design methodology of the fixed frequency cascaded bandpass filter starting by presenting the design process of its lowpass and highpass. The third section is for the tunable bandpass filter, so that the tuning approach has been explained and justified using an EM full-wave simulator. Two tuning methods have used in this project, the first one is electrical tuning which is used to tune the upper lower side of the passband where the tuning was used to tune the upper side of the passband. The principle of the used tuning techniques based on the tuning of the resonance frequency of both highpass and lowpass filters individually. The measurements of the filter were not included due to insufficient time. It will be completed once its circuit is fabricated and the electronic elements are soldered.

6.1 Conclusion

Suspended Substrate Stripline filters (SSS) are a type of filter combining the benefits of Microstrip filters in terms of planar structure and of waveguide filters in terms of high unloaded quality factor [31]. They also have a number of advantages, such as low dispersion and reduced dependency on temperature variation. Nevertheless, there are also many disadvantages to this structure, including the relatively large size of the circuit element and surrounding metal box, particularly in low-frequency applications. This may be a major reason to limit the use of this type of filter in small mobile communications systems such as mobile phones, but only on fixed systems such as mobile phone base stations (BS). Secondly, there is the difficulty of obtaining good grounding levels for the suspended elements, which might be the cause of the wide gap in the terms of tunable SSS filters. A third problem is integration which forms a major concern and a problem for researchers because of the difficulty of exploiting the designs in various communications systems. For these reasons, this research focused on studying SSS filters in an attempt to present the advantages of this design and solve some of its disadvantages to expand its use across all areas of civil and military communications.

A mechanically tuned generalised lowpass filter was introduced [91]. This project was started by introducing the design method and providing complete mathematical analysis of a fixed frequency filter. Following an EM full-wave simulation, the filter was fabricated and measured. It showed strong agreement between the simulation and measurement, with insertion and return losses of -0.2 dB and -13.03 dB respectively [91]. Next, a new structure for tuning screws was designed and used to tune the filter's resonance frequency. A synchronous tuning method was applied manually. However, if an electronic tuning system such as servo-motors is available, it can be connected to the designed filter and used to tune it. The tuned filter was simulated and measured, and the tuning range was 109MHz from 1.675 to 1.784MHz with a passband's return

and insertion losses from -7 dB to -13.03 dB and from -2.5 dB to -0.2 dB respectively [91]. The importance of obtaining a good grounding for the tuning elements was clarified from the resulting measured stopband's spurious frequencies during the tuning process.

The second project introduced in this thesis was a combined Microstrip and SSS combine bandpass filter with two transmission zeros [77]. This project investigated two major problems related to SSS structures, namely the possible and appropriate grounding techniques which can be used with the suspended transmission lines and finding a suitable method to integrate the SSS with other parts of the system. This design also aimed to introduce a new method for transmission zero extraction rather than the conventional cross-coupling method. This was done by constructing the filter's circuit model and exploring the effect of different elements on the filter's response using an AWR simulator [81]. Additionally, the method for extracting the transmission zeros involved adding two resonators on either side of the input and output ports, followed by simulation and an investigation into the effect of the lossy elements on the filter's passband losses. Next, the external coupling and coupling coefficient extraction methods [40] were reviewed, and the metallic box for the proposed filter has been designed. Afterwards, the transformation from lumped element full-wave structure was started. During this phase, the length of the resonators was initially assumed to be equal to $\lambda/4$ at the resonance frequency, which was 3.31GHz, while their width was calculated by applying the equation of the SSS transmission lines, which is introduced in [55] and [40], for the lines placed in the Microstrip section. The grounding of the resonator was realised at this stage by overlapping the enclosure internal edges and the transmission lines, while the tuning screws were placed above the resonators for fine-tuning to overcome the expected frequency shift which could be caused by the phase velocity discontinuity related to the use of different structures. The filter was simulated using EM full-wave simulator SONNET® [36], then fabricated and measured. The return and insertion losses of the measured filter were 4.23 dB and -14.23 dB respectively. An investigation into the results found that the insertion loss had increased due to the lack of the resonators' grounding. To start the second phase of this project, VIAs were added to the filter's

circuit to ground the filter's elements instead of using the overlapping method. As well as that, screws were used to fix the substrate to the box. Afterwards, the tuning elements were added to the circuit to tune the filter's bandwidth. This was done by controlling a variable coupling subnetwork reducer electrically using varactors [82]. These were placed on the coupling reducers so that, by tuning their values, the coupling coefficients changed and, as a result, the bandwidth was tuned. In conjunction with that, there were two extra tuning tasks. The first one was to tune the external coupling to maintain the required coupling strength during the tuning of the coupling coefficients. The second was to tune the transmission zeros by changing the electrical lengths of their extractors using varactors. The filter was simulated, fabricated and measured, and then tuned from 59MHz to 88MHz with a fractional bandwidth of 1.94-2.7 and insertion and return losses between 5.86-7dB and 11.2-19 dB respectively. The measurements were investigated and it is thought that varactors played a key role in the losses' increase, as did the displacement of the filter's elements, which affected their characteristic impedances. This displacement could have occurred due to the manufacturing tolerance of the enclosure, which is equal to 10%.

The third project was to design a cascade SSS tunable bandpass filter. A low filter was integrated to a highpass one to form the complete circuit of the cascaded filter. In the first phase of this project, the fixed frequency cascaded filter was designed comprising a generalised lowpass filter of order 7 cascaded with a Step Impedance Resonator (SIR) highpass filter. The filter was simulated, fabricated and measured, and there was a great match between the simulated and measured responses with a Fractional Bandwidth (FBW) of 21.4% and return and insertion losses of 18 dB and 0.3 dB respectively. Next, the tuning phase was completed. In this phase, some small modifications were made to the original circuit. The first one was the addition of a lowpass filter to maintain the upper stopband of the filter. In the second modification, the input port was changed from edge coupling to broadside coupling in order to create enough space for the added lowpass filter. The tuning of this filter is based on two methods. The first one is to electrical change the coupling coefficients between the coupled SIR lines, which in turn tuned the passband's lower side. The second tuning

method involved placing three tuning screws above the lowpass filter resonators, which tuned the passband's upper side.

6.2 Future work

Although the proposed works were investigated extensively, however, due to time restrictions, several aspects which emerged have not yet been explored. These need to be further investigated, and some promising outcomes are expected. These are listed below:

- 1- completing the measurements and investigating the results of the tunable cascaded SSS bandpass filter.
- 2- Investigating the capability of using 3D- printing technology to fabricate substrate-less planar SSS microwave filters.
- 3- Investigating the use of different tuning devices rather than lossy and bulky tuning elements.
- 4- The possibility of miniaturizing the SSS-sized design for low-frequency applications using different design techniques such as a stripline structure. It is expected that using such techniques with high dielectric constant substrates will reduce the size of the transmission lines significantly.

RO3000® Series Circuit Materials



RO3000® Series Circuit Materials RO3003™, RO3006™, RO3010™ and RO3035™ High Frequency Laminates

RO3000® high frequency circuit materials are ceramic-filled PTFE composites intended for use in commercial microwave and RF applications. This family of products was designed to offer exceptional electrical and mechanical stability at competitive prices.

RO3000 series laminates are ceramic-filled PTFE based circuit materials with mechanical properties that are consistent regardless of the dielectric constant selected. This allows the designer to develop multi-layer board designs that use different dielectric constant materials for individual layers, without encountering warpage or reliability problems.

RO3000 materials exhibit a coefficient of thermal expansion (CTE) in the X and Y axis of 17 ppm/°C. This expansion coefficient is matched to that of copper, which allows the material to exhibit excellent dimensional stability, with typical etch shrinkage (after etch and bake) of less than 0.5 mils per inch. The Z-axis CTE is 24 ppm/°C, which provides exceptional plated through-hole reliability, even in severe thermal environments. The dielectric constant versus temperature for RO3003™ and RO3035™ materials is very stable (Chart 1).

RO3000 series laminates can be fabricated into printed circuit boards using standard PTFE circuit board processing techniques, with minor modifications as described in the application note "Fabrication Guidelines for RO3000 Series High Frequency Circuit Materials."

RO3000 laminates are manufactured under an ISO 9001 certified system.



Advanced Connectivity Solutions
100 S. Roosevelt Avenue, Chandler, AZ 85226
Tel: 480-961-1382 Fax: 480-961-4533 www.rogerscorp.com

Data Sheet



Features and Benefits:

Low dielectric loss (RO3003™ laminates)

- Laminates can be used in applications up to 77 GHz.
- Excellent mechanical properties versus temperature
- Reliable stripline and multi-layer board constructions.

Uniform mechanical properties for a range of dielectric constants

- Ideal for multi-layer board designs with a range of dielectric constants
- Suitable for use with epoxy glass multi-layer board hybrid designs

Stable dielectric constant versus temperature and frequency (RO3003 laminates)

- Ideal for band pass filters, microstrip patch antennas, and voltage controlled oscillators.

Low in-plane expansion coefficient (match to copper)

- Allows for more reliable surface mounted assemblies
- Ideal for applications sensitive to temperature change
- Excellent dimensional stability

Volume manufacturing process

- Economical laminate pricing

Some Typical Applications:

- Automotive radar applications
- Global positioning satellite antennas
- Cellular telecommunications systems - power amplifiers and antennas
- Patch antenna for wireless communications
- Direct broadcast satellites
- Datalink on cable systems
- Remote meter readers
- Power backplanes

Chart 1: RO3003 and RO3035 Laminate Dielectric Constant vs. Temperature

The data in Chart 1 demonstrates the excellent stability of dielectric constant over temperature for RO3003 & RO3035 laminates, including the elimination of the step change in dielectric constant, which occurs near room temperature with PTFE glass materials.

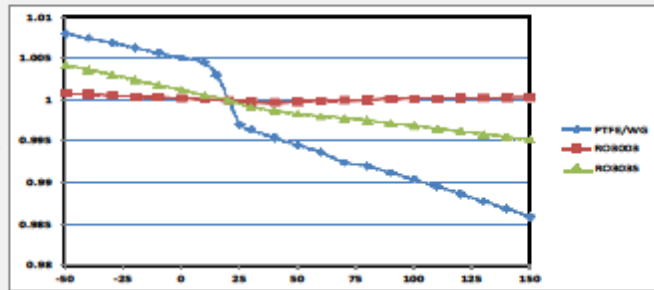


Chart 2: RO3003 and RO3035 Dissipation Factor

The data in Chart 2 shows the distribution of dissipation factor for RO3003 and RO3035 materials.

Test Method: IPC-TM-650 2.5.5.5
Condition: 10 GHz 23° C

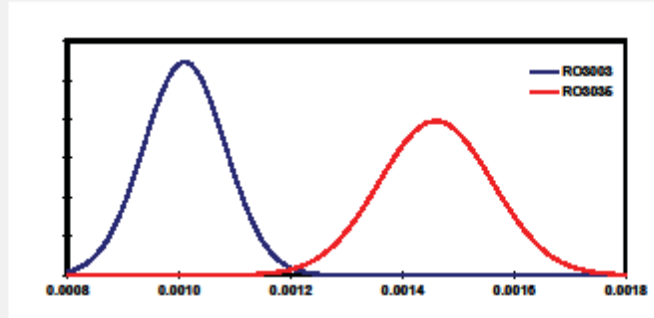
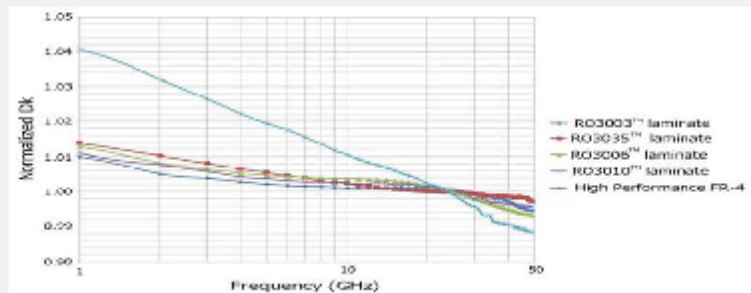


Chart 3: Normalized Dk vs. Frequency using microstrip differential phase length method 50 ohm microstrip circuits based on ~20mil thick laminates

Chart 3 demonstrates the stability of dielectric constant for RO3000 series products over frequency. This stability simplifies the design of broadband components as well as allowing the materials to be used in a wide range of applications over a very broad range of frequencies.



Advanced Connectivity Solutions
100 S. Roosevelt Avenue, Chandler, AZ 85226
Tel: 480-961-1382 Fax: 480-961-4533 www.rogerscorp.com

Property	Typical Value ⁽¹⁾				Direction	Unit	Condition	Test Method
	RO3003	RO3035	RO3006	RO3010				
Dielectric Constant, ϵ , Process	3.00 ± 0.04	3.50 ± 0.05	6.15 ± 0.15	10.2 ± 0.30	Z	-	10 GHz 23°C	IPC-TM-650 2.5.5.5 Clamped Stripline
⁽²⁾ Dielectric Constant, ϵ , Design	3.00	3.60	6.50	11.20	Z	-	8 GHz - 40 GHz	Differential Phase Length Method
Dissipation Factor, tan δ	0.0010	0.0015	0.0020	0.0022	Z	-	10 GHz 23°C	IPC-TM-650 2.5.5.5
Thermal Coefficient of ϵ	-3	-45	-262	-395	Z	ppm/°C	10 GHz -50 to 150°C	IPC-TM-650 2.5.5.5
Dimensional Stability	-0.06 0.07	-0.11 0.11	-0.27 -0.15	-0.35 -0.31	X Y	mm/m	COND A	IPC-TM-650 2.2.4
Volume Resistivity	10 ⁹	10 ⁹	10 ⁹	10 ⁹		M Ω -cm	COND A	IPC 2.5.17.1
Surface Resistivity	10 ⁹	10 ⁹	10 ⁹	10 ⁹		M Ω	COND A	IPC 2.5.17.1
Tensile Modulus	930 823	1025 1006	1498 1293	1902 1934	X Y	MPa	23°C	ASTM D638
Moisture Absorption	0.04	0.04	0.02	0.05	-	%	D48/50	IPC-TM-650 2.6.2.1
Specific Heat	0.9		0.86	0.8		J/g/K		Calculated
Thermal Conductivity	0.50	0.50	0.79	0.95	-	W/m/K	50°C	ASTM D5470
Coefficient of Thermal Expansion	17 16 25	17 17 24	17 17 24	13 11 16	X Y Z	ppm/°C	-55 to 288°C	ASTM D3386-94
Td	500	500	500	500		°C TGA		ASTM D3850
Density	2.1	2.1	2.6	2.8		gm/cm ³	23°C	ASTM D792
Copper Peel Strength	12.7	10.2	7.1	9.4		lb/in	1 oz. EDC After Solder Float	IPC-TM-2.4.8
Flammability	V-0	V-0	V-0	V-0				UL 94
Lead Free Process Compatible	YES	YES	YES	YES				



NOTES:

- (1) Typical values are a representation of an average value for the population of the property. For specification values contact Rogers Corporation.
- (2) The design Dk is an average number from several different tested lots of material and on the most common thickness/s. If more detailed information is required, please contact Rogers Corporation or refer to Rogers' technical papers in the Roger Technology Support Hub available at <http://www.rogerscorp.com/acm/technology>.

Appendix B

Richard's Transformation

Richard's transformation is an approximate equivalence between the lumped and distributed elements [40]. According to Richards, the distributed networks made up of transmission lines having equal electrical lengths and lumped resistors [40].

Richard's transformation of the lumped elements can be applied as follows:

$$p \rightarrow \alpha \tanh(a_L p) \quad \text{B.1}$$

Where $p = \sigma + j\omega$ is the complex frequency variable.

By applying (B.1) to a capacitor then [55]

$$Y_{(p)} = C_p \rightarrow \alpha C \tanh(a p) \quad \text{B.2}$$

Therefore

$$Y_{(p)} \rightarrow Y_0 \cdot \tanh(a p) \quad \text{B.3}$$

and

$$Y_{(j\omega)} \rightarrow jY_0 \cdot \tan(a \omega) \quad \text{B.4}$$

where

$$Y_0 = \alpha C \quad \text{B.5}$$

From (B.4) it can see that a capacitor has been transformed to in an open circuited stub by using Richard's transformation. On the other, an inductor is converted to a short-circuited stub as follows

$$Z_{(p)} = L_p \rightarrow \alpha L \tanh(a p) \quad \text{B.6}$$

Therefore

$$Z_{(p)} \rightarrow Z_0 \cdot \tanh(a p) \quad \text{B.7}$$

and

$$Z_{(j\omega)} \rightarrow jZ_0 \cdot \tan(a \omega) \quad \text{B.8}$$

where

$$Z_0 = \alpha L \quad \text{B.9}$$

The transformation process (B.1) to (B.9), are shown in Figure B.1

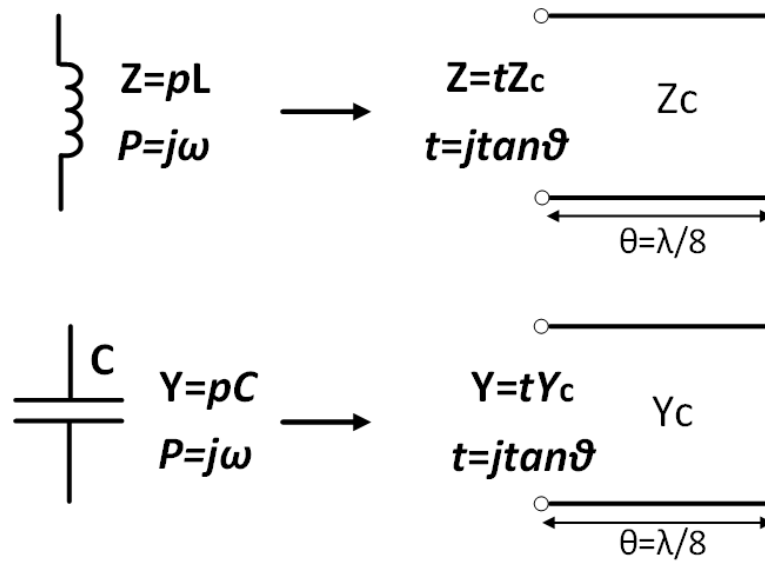


Figure B.1 Lumped elements' Richard's Transformation

Appendix C

Step Impedance Fundamentals

Step impedance resonators have several types according to their electrical lengths as shown in Figure C 1.

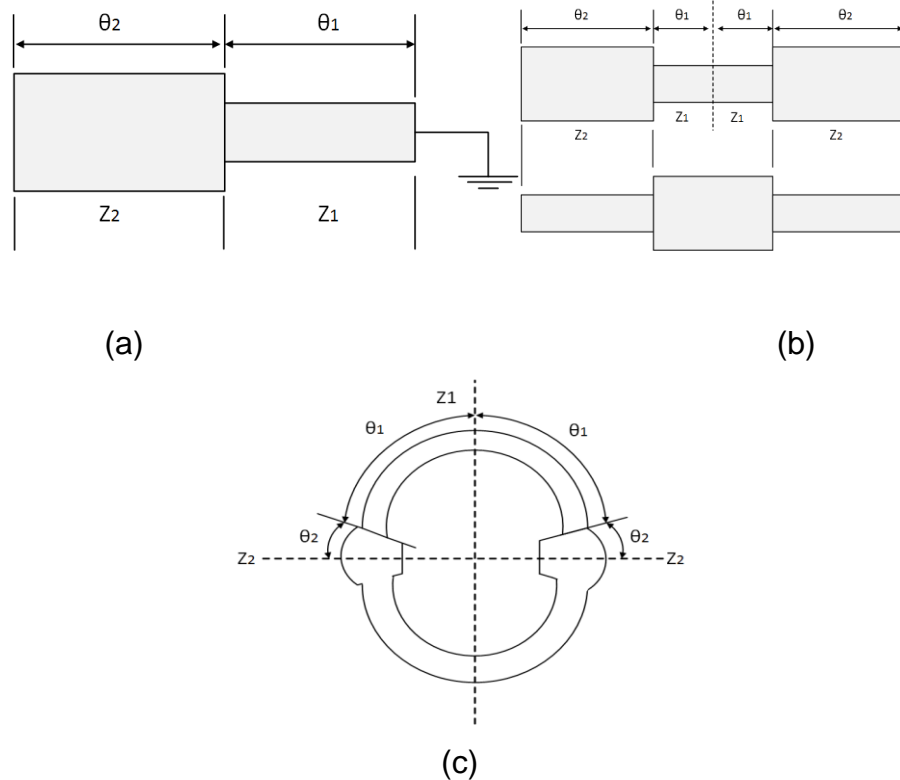


Figure C1 The SIR basic structures (a) $\lambda_g/4$ (b) $\lambda_g/2$ (c) λ_g [92].

As can be seen from Figure C1, that the basic structures compose of different fundamental elements as follows one for $\lambda_g/4$, two for $\lambda_g/2$ and four for λ_g [92]. The mathematical analysis of the resonance conditions, spurious frequencies and poles frequencies has been offered in section 5.2.2.1.

It is also mentioned in [92] that the $\lambda_g/4$ SIR types are popular used with high dielectric constants due to small size. On the other hand, it is clarified that the $\lambda_g/2$ can be an open ended or short ended SIR [92], where the open ended is more suitable for the stripline structures. There are several structures in which $\lambda_g/2$ could

be used, for instance the hairpin SIR structure can be utilized for structure miniaturizing [93], moreover, a multistep and tapered structures shown in figure C2 are considered as

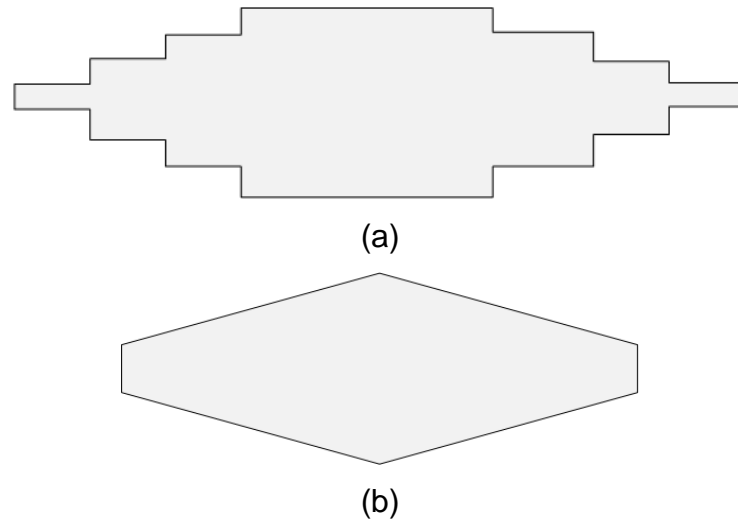


Figure C2 advanced structures of SIR resonators (a) Multisteped (b) Tapered [92]

an advanced structure of the $\lambda_g/2$ SIR resonators. Nevertheless, the multisteped is useless since its features are not important as that the step SIR's and tapered resonators, it is very useful for analysing the line tapered resonators [92].

the Furthermore, the λ_g is useless as a single mode resonator due to it large-size, However, it is very useful in the applications of two orthogonal modes within a ring resonator of one wavelength [92].

References

- [1] K. Konanur, "CMOS RF transceiver chip tackles multiband 3.5 G radio system," *RF Des.*, vol. 29, no. April, p. 4, 2006.
- [2] J. Ni, "Development of turnable and miniature microwave filters for modern wireless communication," PhD dissertation, Institute of Sensors, Signals and Systems, Heriot-Watt University, Edinburgh, 2014.
- [3] S. R. Chandler, I. C. Hunter, and J. G. Gardiner, "Active varactor tunable microwave filters," in *1993 23rd European Microwave Conference*, 1993, pp. 244–245.
- [4] J. Zhou, "Microwave Filters," in *Microwave and Millimeter Wave Technologies from Photonic Bandgap Devices to Antenna and Applications*, I. Minin, Ed. Rijeka: InTech, 2010, p. Ch. 6.
- [5] I. Electromagnetic and C. Society, "IEEE Standard for Methods of Measurement of Radio-Frequency Power-Line Interference Filter in the Range of 100 Hz to 10 GHz," *IEEE Std 1560-2005*, no. February. pp. 1–92, 2006.
- [6] S. Committee, "IEEE Recommended Practice for Radio-Frequency (RF) Absorber Evaluation in the Range of 30 MHz to 5 GHz," *IEEE Std 1128-1998*, vol. 1998. pp. 1–68, 2012.
- [7] T. Shen, K. A. Zaki, and C. Wang, "Tunable dielectric resonators with dielectric tuning disks," *IEEE Trans. Microw. Theory Tech.*, vol. 48, no. 12, pp. 2439–2445, 2000.
- [8] M. Naser-Moghadasi and R. Sadeghzadeh-Sheikhan, "Ferrite Tuned Dual-Mode Dielectric Resonator Filters," in *Information and Communication Technologies, 2006. ICTTA'06. 2nd*, 1992, vol. 2, pp. 2182–2186.
- [9] T. Agarwal, "PIN Diode Basics, Working and Applications," 2017. [Online]. Available: <https://www.elprocus.com/pin-diode-basics-working-applications/>.
- [10] C. Lugo and J. Papapolymerou, "Dual-mode reconfigurable filter with asymmetrical transmission zeros and center frequency control," *IEEE Microw. Wirel. Components Lett.*, vol. 16, no. 9, pp. 499–501, 2006.
- [11] A. Miller, "Electronically reconfigurable wideband microwave filters." Citeseer, 2012.

- [12] G. M. Rebeiz, K. Entesari, I. C. Reines, S.-J. Park, M. A. El-Tanani, A. Grichener, and A. R. Brown, "Tuning in to RF MEMS," *IEEE Microw. Mag.*, vol. 10, no. 6, 2009.
- [13] J. Meyer, R. Bischoff, and G. Feltrin, "Microelectromechanical systems (MEMS)," *Encycl. Struct. Heal. Monit.*, 2009.
- [14] M. Golio, *The RF and microwave handbook*. CRC press, 2000.
- [15] M. A. El-Tanani and G. M. Rebeiz, "High-performance 1.5–2.5-GHz RF-MEMS tunable filters for wireless applications," *IEEE Trans. Microw. Theory Tech.*, vol. 58, no. 6, pp. 1629–1637, 2010.
- [16] Z. Brito-Brito, J. C. B. Reyes, and I. Llamas-Garro, "Recent advances in reconfigurable microwave filters," in *Microwave & Optoelectronics Conference (IMOC), 2011 SBMO/IEEE MTT-S International*, 2011, pp. 338–346.
- [17] S. Saeedi, J. Lee, and H. H. Sigmarsson, "Tunable, High-Q, Substrate-Integrated, Evanescent-Mode Cavity Bandpass-Bandstop Filter Cascade," *IEEE Microw. Wirel. Components Lett.*, vol. 26, no. 4, pp. 240–242, 2016.
- [18] F. Mira, J. Mateu, and C. Collado, "Mechanical tuning of substrate integrated waveguide resonators," *IEEE Microw. Wirel. components Lett.*, vol. 22, no. 9, pp. 447–449, 2012.
- [19] S. Kurudere and V. B. Erturk, "Novel microstrip fed mechanically tunable combline cavity filter," *IEEE Microw. Wirel. Components Lett.*, vol. 23, no. 11, pp. 578–580, 2013.
- [20] F. Mira, J. Mateu, and C. Collado, "Mechanical tuning of substrate integrated waveguide filters," *IEEE Trans. Microw. Theory Tech.*, vol. 63, no. 12, pp. 3939–3946, 2015.
- [21] A. Collado, F. Mira, and A. Georgiadis, "Mechanically tunable substrate integrated waveguide (SIW) cavity based oscillator," *IEEE Microw. Wirel. components Lett.*, vol. 23, no. 9, pp. 489–491, 2013.
- [22] M. Cariou, S. Cadiou, B. Potelon, C. Quendo, R. Ségalen, and F. Mahé, "New tunable substrate integrated waveguide bandstop resonator," in *Microwave Conference (LAMC), IEEE MTT-S Latin America*, 2016, pp. 1–3.
- [23] A. Anand, Y. Liu, and X. Liu, "Substrate-integrated octave-tunable combline bandstop filter with surface mount varactors," in *Wireless Symposium (IWS)*,

- 2014 *IEEE International*, 2014, pp. 1–4.
- [24] A. Anand and X. Liu, “Substrate-integrated coaxial-cavity filter with tunable center frequency and reconfigurable bandwidth,” in *Wireless and Microwave Technology Conference (WAMICON), 2014 IEEE 15th Annual*, 2014, pp. 1–4.
- [25] J. R. Chen, M. D. Benge, A. Anand, H. H. Sigmarsson, and X. Liu, “An evanescent-mode tunable dual-band filter with independently-controlled center frequencies,” in *Microwave Symposium (IMS), 2016 IEEE MTT-S International*, 2016, pp. 1–4.
- [26] T. Yang and G. M. Rebeiz, “Tunable 1.25–2.1-GHz 4-pole bandpass filter with intrinsic transmission zero tuning,” *IEEE Trans. Microw. Theory Tech.*, vol. 63, no. 5, pp. 1569–1578, 2015.
- [27] S. Kumar, “Electronically tunable ring resonator microstrip and suspended-substrate filters,” *Electron. Lett.*, vol. 27, no. 6, pp. 521–523, 1991.
- [28] M. Sánchez-Renedo, R. Gómez-García, J. I. Alonso, and C. Briso-Rodríguez, “Tunable combline filter with continuous control of center frequency and bandwidth,” *IEEE Trans. Microw. Theory Tech.*, vol. 53, no. 1, pp. 191–199, 2005.
- [29] N. Zahirovic, S. Fouladi, R. R. Mansour, and M. Yu, “Tunable suspended substrate stripline filters with constant bandwidth,” in *Microwave Symposium Digest (MTT), 2011 IEEE MTT-S International*, 2011, pp. 1–4.
- [30] M. Armendariz, V. Sekar, and K. Entesari, “Tunable SIW bandpass filters with PIN diodes,” in *Microwave Conference (EuMC), 2010 European*, 2010, pp. 830–833.
- [31] C.-C. Cheng and G. M. Rebeiz, “High-Q 4–6-GHz suspended stripline RF MEMS tunable filter with bandwidth control,” *IEEE Trans. Microw. Theory Tech.*, vol. 59, no. 10, pp. 2469–2476, 2011.
- [32] I. Reines, A. Brown, M. El-Tanani, A. Grichener, and G. Rebeiz, “1.6-2.4 GHz RF MEMS tunable 3-pole suspended combline filter,” in *Microwave Symposium Digest, 2008 IEEE MTT-S International*, 2008, pp. 133–136.
- [33] B. Schulte, V. Ziegler, B. Schoenlinner, U. Prechtel, and H. Schumacher, “RF-MEMS tunable evanescent mode cavity filter in LTCC technology at Ku-band,” in *Microwave Conference (EuMC), 2011 41st European*, 2011, pp. 1075–1078.

- [34] S. Sirci, J. D. Martínez, and V. E. Boria, “Low-loss 3-bit tunable SIW filter with PIN diodes and integrated bias network,” in *Microwave Conference (EuMC), 2013 European*, 2013, pp. 1211–1214.
- [35] F. He, X.-P. Chen, K. Wu, and W. Hong, “Electrically tunable substrate integrated waveguide reflective cavity resonator,” *2009 Asia Pacific Microw. Conf.*, no. 2, pp. 119–122, 2009.
- [36] S. S. Inc., “SONNET® USER’S GUIDE.” Sonnet Software Inc., 100 Elwood Davis Road North Syracuse, NY 13212, 2011.
- [37] J.-S. Hong, “Reconfigurable planar filters,” *Microw. Mag. IEEE*, vol. 10, no. 6, pp. 73–83, Oct. 2009.
- [38] S. A. Maas, *The RF and microwave circuit design cookbook*. Artech House, 1998.
- [39] J.-S. Hong, *Microstrip Filters for RF/Microwave Applications*. Hoboken, NJ, USA: John Wiley & Sons, Inc., 2011.
- [40] J. Hong, *Microstrip Filters for RF/Microwave Applications*, vol. 7. Hoboken, NJ, USA: John Wiley & Sons, Inc., 2011.
- [41] J.-S. Kim, N.-S. Kim, W.-G. Moon, S.-G. Byeon, and H. Shin, “A novel broadband suspended substrate stripline filter using resonators with T-shaped open-circuited stubs,” in *Microwave Symposium, 2007. IEEE/MTT-S International*, 2007, pp. 917–920.
- [42] H.-H. Chen, R.-C. Hsieh, Y.-T. Shih, Y.-H. Chou, and M.-H. Chen, “Coaxial combline filters using the stepped-impedance resonators,” in *Microwave Conference Proceedings (APMC), 2010 Asia-Pacific*, 2010, pp. 1724–1727.
- [43] S. W. Wong, K. Wang, Z.-N. Chen, and Q.-X. Chu, “Design of millimeter-wave bandpass filter using electric coupling of substrate integrated waveguide (SIW),” *IEEE Microw. Wirel. Components Lett.*, vol. 24, no. 1, pp. 26–28, 2014.
- [44] R. Lay, “Phase and group delay of S-band megawatt Cassegrain diplexer and S-band megawatt transmit filter,” *Novemb. andembi 1976*, p. 198, 1977.
- [45] J. Golio and M. Golio, *RF and microwave applications and systems*. CRC Press, 2007.
- [46] Y. Shu, X. Qi, and Y. Wang, “Analysis equations for shielded suspended substrate microstrip line and broadside-coupled stripline,” in *Microwave*

- Symposium Digest, 1987 IEEE MTT-S International*, 1975, vol. 2, pp. 693–696.
- [47] E. Yamashita and K. Atsuki, “Strip line with rectangular outer conductor and three dielectric layers,” *IEEE Trans. Microw. Theory Tech.*, vol. 18, no. 5, pp. 238–244, 1970.
- [48] I. J. Bahl and P. Bhartia, “Characteristics of inhomogeneous broadside-coupled striplines,” *IEEE Trans. Microw. Theory Tech.*, vol. 28, no. 6, pp. 529–535, 1980.
- [49] P. Pramanick and P. Bhartia, “CAD Models for Millimeter-Wave Suspended Substrate Microstrip Lines and Fin-Lines,” in *Microwave Symposium Digest, 1985 IEEE MTT-S International*, 1985, pp. 453–456.
- [50] P. Jarry and E. Kerherve, “Millimeter wave filter design with suspended stripline structure (SSS),” in *ESA Workshop on Millimeter Wave Technology and Applications*, 1998, p. 1.
- [51] L. G. Maloratsky, “Reviewing the basics of microstrip,” *Microwaves RF*, vol. 39, no. March, pp. 79–88, 2000.
- [52] T. K. Ishii, *Handbook of microwave technology*. Elsevier, 1995.
- [53] E. Yamashita, B. Y. Wang, K. Atsuki, and K. R. Li, “Effects of Side-Wall Grooves on Transmission Characteristics of Suspended Striplines,” *IEEE Trans. Microw. Theory Tech.*, vol. 33, no. 12, pp. 1323–1328, 1985.
- [54] R. Levy and S. B. Cohn, “A History of Microwave Filter Research, Design, and Development,” *IEEE Trans. Microw. Theory Tech.*, vol. 32, no. 9, pp. 1055–1067, 1984.
- [55] I. Hunter, *Theory and design of microwave filters*, no. 48. let, 2001.
- [56] J. E. Dean, “Suspended substrate stripline filters for ESM applications,” in *IEE Proceedings F (Communications, Radar and Signal Processing)*, 1985, vol. 132, no. 4, pp. 257–266.
- [57] R. Corporation, “RO3000 ® Series Circuit Materials Data Sheet,” 2015.
- [58] V. L. Brekhovskikh, “Effective dielectric constant in the calculation of the second field moments in a randomly inhomogeneous medium,” *JETP*, vol. 62, no. 6, p. 1160, 1985.
- [59] Y. Y. Wang, G. L. Wang, and Y. H. Shu, “Analysis and synthesis equations for edge-coupled suspended substrate microstrip line,” in *Microwave Symposium Digest, 1989., IEEE MTT-S International*, 1989, pp. 1123–1126.

- [60] S. Awasthi, K. V. Srivastava, and A. Biswas, "Dispersion properties of four and five coupled microstrip lines in suspended substrate structure using hybrid mode formulation," in *Microwave Conference Proceedings, 2005. APMC 2005. Asia-Pacific Conference Proceedings, 2005*, vol. 2, p. 4–pp.
- [61] K.-J. Gu, Y. Wang, and Y.-H. Shu, "The analysis of the dispersion characteristics of several kinds of coupled suspended substrate microstrip lines and transmission lines with the method of lines," in *Millimeter Wave and Far-Infrared Technology, 1989. ICMWFT'89. International Conference on*, pp. 522–525.
- [62] U. Schulz and R. Pregla, "A new technique for the analysis of the dispersion characteristics of planar waveguides and its application to microstrips with tuning septums," *Radio Sci.*, vol. 16, no. 6, pp. 1173–1178, Nov. 1981.
- [63] H. Cui, J. Wang, and G. Zhang, "Design of microstrip lowpass filter with compact size and ultra-wide stopband," *Electron. Lett.*, vol. 48, no. 14, p. 856, 2012.
- [64] M. A. Sanchez-Soriano and J.-S. Hong, "Reconfigurable lowpass filter based on signal interference techniques," in *2011 IEEE MTT-S International Microwave Symposium*, 2011, no. 1, pp. 1–4.
- [65] I. V. Lindell, A. H. Sihvola, and I. Hänninen, "Realization of perfectly anisotropic impedance boundary," *Eur. Sp. Agency, (Special Publ. ESA SP*, vol. 626 SP, pp. 549–555, 2006.
- [66] C. C. Huang, N. W. Chen, H. J. Tsai, and J. Y. Chen, "A coplanar waveguide bandwidth-tunable lowpass filter with broadband rejection," *IEEE Microw. Wirel. Components Lett.*, vol. 23, no. 3, pp. 134–136, 2013.
- [67] M. Miao, J. Bu, and L. Zhao, "A bulk micromachined tunable microwave lowpass filter for 10-15GHz wireless/satellite communication," *3rd IEEE Int. Conf. Nano/Micro Eng. Mol. Syst. NEMS*, pp. 524–528, 2008.
- [68] L. Zhao, M. Miao, J. Bu, and Y. Jin, "A10-14 GHz RF MEMS tunable bandpass filter," *Int. Conf. Solid-State Integr. Circuits Technol. Proceedings, ICSICT*, pp. 2516–2519, 2008.
- [69] N. Lioutas, "Design of generalised Chebyshev suspended substrate stripline filters," ELECTRONICS RESEARCH LAB ADELAIDE (AUSTRALIA), 1986.
- [70] S. A. Alseyab, "A novel class of generalized Chebyshev low-pass prototype for

- suspended substrate stripline filters,” *IEEE Trans. Microw. Theory Tech.*, vol. 30, no. 9, pp. 1341–1347, 1982.
- [71] W. J. Getsinger, “Coupled Rectangular Bars Between Parallel Plates,” *IRE Trans. Microw. Theory Tech.*, vol. 10, no. 1, pp. 65–72, 1962.
- [72] Z. Zakaria, M. A. Mutalib, M. S. M. Isa, A. A. M. Isa, N. A. Zainuddin, and W. Y. Sam, “Design of generalized chebyshev lowpass filter with defected stripline structure (dss),” in *Wireless Technology and Applications (ISWTA), 2013 IEEE Symposium on*, 2013, pp. 230–235.
- [73] H. J. Alaqil and J. Hong, “Mechanical Tuning of a Suspended-Substrate-Stripline, Low-Pass Filter,” in *Proceedings of the Eighth Saudi Students Conference in the UK*, 2016, pp. 399–410.
- [74] W. Tang, “Planar microwave filters with electronically tunability and other novel configurations,” ,PhD dissertation, Institute of Sensors, Signals and Systems, Heriot-Watt University, Edinburgh, 2011.
- [75] R. J. Cameron, A. C. M. Kudsia, and R. R. Mansour, *Microwave Filters for Communication Systems*, vol. 43, no. 1. Hoboken, NJ, USA: John Wiley & Sons, Inc., 2007.
- [76] IEEE, “IEEE Standard Definitions of Terms for Radio Wave Propagation,” *IEEE Std 211-1997*. p. i, 1998.
- [77] H. Alaqil and J. Hong, “Combined microstrip and suspended substrate stripline combline bandpass filter with two transmission zeros,” *Mediterr. Microw. Symp.*, vol. 2016–Janua, no. c, pp. 1–4, 2016.
- [78] O. Lab, “OriginPro.” Origin Lab, Northampton, 2018.
- [79] M. Sanchez-Renedo, R. Gomez-Garcia, J. I. Alonso, and C. B. Rodriguez, “A new electronically tunable combline filter with simultaneous continuous control of central frequency and bandwidth,” *2004 IEEE MTT-S Int. Microw. Symp. Dig. (IEEE Cat. No.04CH37535)*, vol. 3, pp. 1291–1294, 2004.
- [80] H. Alaqil and J. Hong, “Tunable narrow bandwidth of a bandpass filter combined microstrip and suspended substrate stripline,” *Microw. Opt. Technol. Lett.*, vol. 60, no. 4, pp. 983–987, Apr. 2018.
- [81] A. W. R. Inc, “Microwave office user’s manual.” Inc, Applied Wave Research, 1960 E. Grand Avenue, Suite 430 El Segundo, CA 90245 USA, 2017.

- [82] Skyworks, "SMV2019 to SMV2023 Series: Hyperabrupt Junction Tuning Varactors," 2015. [Online]. Available: http://www.skyworksinc.com/uploads/documents/SMV2019_to_SMV2023_Series_200074Q.pdf. [Accessed: 18-Aug-2017].
- [83] K. C. Lee, H. T. Su, and W. S. H. Wong, "Realization of a wideband bandpass filter using cascaded lowpass to highpass filter," in *Microwave and Millimeter Wave Technology, 2008. ICMMT 2008. International Conference on*, 2008, vol. 1, pp. 14–17.
- [84] C.-W. Tang and M.-G. Chen, "A microstrip ultra-wideband bandpass filter with cascaded broadband bandpass and bandstop filters," *IEEE Trans. Microw. Theory Tech.*, vol. 55, no. 11, pp. 2412–2418, 2007.
- [85] S. Akatimagool, N. Intarawiset, and S. Inchan, "Design of waveguide bandpass filter using cascade inductive and capacitive irises," in *Antennas and Propagation (APCAP), 2016 IEEE 5th Asia-Pacific Conference on*, 2016, pp. 387–388.
- [86] Z. Zakaria, M. A. Mutalib, W. Y. Sam, and M. F. M. Fadzil, "Integrated suspended stripline structure (SSS) with J-shape defected stripline structure (DSS) To Remove Undesired Signals In Wideband Applications," in *Antennas and Propagation (EuCAP), 2015 9th European Conference on*, 2015, pp. 1–5.
- [87] H. Alaqil and J. Hong, "Cascaded Suspended Stripline Bandpass Filter," *Submitt. to Microw. Opt. Technol. Lett.*, p. 12, 2018.
- [88] J. D. Rhodes and S. A. Aloseyab, "The generalized chebyshev low-pass prototype filter," *Int. J. Circuit Theory Appl.*, vol. 8, no. 2, pp. 113–125, 1980.
- [89] J. T. Kuo and E. Shih, "Microstrip stepped impedance resonator bandpass filter with an extended optimal rejection bandwidth," *IEEE Trans. Microw. Theory Tech.*, vol. 51, no. 5, pp. 1554–1559, 2003.
- [90] M. Makimoto and S. Yamashita, "Bandpass filters using parallel coupled stripline stepped impedance resonators," *IEEE Trans. Microw. Theory Tech.*, vol. 28, no. 12, pp. 1413–1417, 1980.
- [91] H. Alaqil and J. Hong, "Mechanical Tuning of Suspended Substrate Stripline Lowpass Filter," in *Proceedings of the Eighth Saudi Students Conference in the UK*, 2016, pp. i–xxiii.

- [92] M. Sagawa, M. Makimoto, and S. Yamashita, "Geometrical structures and fundamental characteristics of microwave stepped-impedance resonators," *IEEE Trans. Microw. Theory Tech.*, vol. 45, no. 7, pp. 1078–1085, 1997.
- [93] Y. Hiroyuki, E. Haruyoshi, S. Morikazu, and M. Mitsuo, "Hairpin-shaped stripline split-ring resonators and their applications," *Electron. Commun. Japan (Part II Electron.)*, vol. 76, no. 5, pp. 45–55, May 1993.